Development of Novel Macrophage Imaging Agents

O'Neill, Alexander

Awarding institution:
King's College London

Title: Development of Novel Macrophage Imaging Agents

Author: Alexander O'Neill

Development of Novel Macrophage Imaging Agents

Alexander O'Neill

A thesis submitted in partial fulfilment for the degree of

Doctor of Philosophy

Department of Imaging Sciences

King's College London

July 2012

Declaration of Authorship

I, Alexander O'Neill, declare that this thesis title, "Development of Novel Macrophage Imaging Agents" and the work presented herein are my own.

I confirm that:

- This work was done wholly or mainly in candidature for a research degree at this university
- Where any part of this thesis has previously been submitted for a degree or any other qualification at this university or any other institution, this has been clearly stated
- Where I have consulted the published work of other, this is always clearly attributed
- Where I have quoted from the work of others, the source is always given. With the exception of such quotations, this thesis is entirely my own work
- I have acknowledged all main sources of help
- Where the thesis is based on work done by myself jointly with other, I have made clearly exactly what was done by others and what I have contributed myself

Signed:

Acknowledgements

As is the convention, I would like to thank a number of people for supporting me over the last 4 years both professionally and personally, as it would not have been possible to complete this course without them. Thank you.

Firstly, I should thank my supervisor, Greg Mullen, for securing me the Harris Studentship that led me to the department in the first place. Following that, the environment that he created allowed me to explore a project that would not have been entrusted to a chemistry graduate anywhere else! The experience has been something certainly I'll never forget and although it's delayed my start in medicine I believe I will be the better for this.

Next would be the eclectic mix that the department has attracted, and I would like to thank the academic staff that have contributed to my learning and development including Jim Ballinger, Lefteris Livieratos, Rudolfo Medina and in particular Phil Blower, Wilson Wong, Ricky Southworth, Rafael del Torres and Alberto Smith for providing invaluable feedback during my studies. Similarly I would like to thank Christine Dijkstra, Timo van den Berg and Paul Crocker who provided critical reagents and time to an otherwise complete stranger.

I'd particularly like to thank the contributions of two exceptional post-docs to my research, that being Florian Kampmeier and Richard Tavare. Even if it's all kit based, molecular biology is still beyond me however they made it far more accessible and provided the most stimulating part of my research. They have variously shown me problem solving skills and facial hair grooming which I will never forget. Following from them I am indebted to the time that other groups gave me in developing techniques, and in this way Julia Jenkins, Kat Mattock, Elisabeth Fernandes and (in particular) Kathryn Brown have all made parts of this thesis possible. On top of this Anna Wu, Kirstin Zettlitz, Felix Bergara, Jingying Xiang and Lily Wu all made my time in UCLA a hugely rewarding experience.

From the group I'd also like to thank those who have helped me out and made me laugh along the way. The light starved, over-crowded days of office suite 3 were offset by the endless banter of Koers and his commitment to keeping the lab, and particularly the fridge, supplies well stocked. In between pregnancies I recall a Dr Chia exhibiting ferocious skills of persuasion, and until the defection, Adam Badar was indeed considered a comrade, neigh brother, in arms. In keeping, Jenni Williams and Levente Meszaros assisted in some marathon imaging, as did Seckou Diocou and Putt Charoenphun, which made the intolerable tolerable and, at times, inappropriate. Thanks to Pete Williamson for the good times and for showing me the warning signs of an eloper, to Gareth Smith for his unashamed selling out, and Maite Jauregui-Osoro for exhibiting herculean stamina. A special mention must go to what can only be described as the genre defying Maggie Cooper for her setting the bar and then forgetting where

it is. Finally to Tanja Suligoj for having an absurdly mis-pronounceable last name, and to David Thakor for always returning my radiation privileges.

Outside of the lab I must thank the mighty Gareth Borer for being 100% G and for maintaining the success rate of 0% unawesomeness! Quite simply an absolute privilege and pleasure. Then those Neapolitan scoundrels Vincenzo “where’s my peptides” Abbate and Nunzianda Frascione for providing unlimited entertainment both inside and outside of fumehoods. Without those Vauxhalliers Elvis Caus, Pere Marsinach and all the members of the Chrissy P Experience, including the very Christopher Patel himself, my London experience would not have been the same, however I’d probably still have a functioning short term memory so I’m undecided upon you lot. To all of you I say, may the party continue but can we please change the soundtrack?!?

Then I would like to thank my family for their continuous support over the years, and for giving me a suitably bizarre upbringing! Both Mum and Dad have made too many sacrifices to help me along and for this I am ever grateful. And also to my sisters and grandmother for being truly irreplaceable. In particular I would like to pay tribute to the memory of my grandparents, both of whom were exceptional people.

Finally, this acknowledgement would not be complete without recognising the contribution of Sabine. Her infinite kindness and support have made the most trying of times bearable, whilst her terrifying command of the dark art of emailing has shaped virtually all of my projects and in turn the work that was generated. It simply would not have been possible or as much fun without you, so after finding Lorn Road I think that makes us even! Next up Oxford and Zurich… do we have return tickets?!

Abstract

Macrophages are an important class of cell involved in host defence and homeostasis that are able to alter their phenotype in response to their surroundings and affect a wide range of biological processes. These properties make them critical to host function in normal and disease settings, leading to their utility as targets to inform upon functional status of an organ/tissue as well as for therapeutic intervention. Thus the development of macrophage-specific imaging agents has potential clinical applications in the diagnosis and measuring response to treatment of disease.

This thesis sets forth the development of novel antibody-based nuclear imaging agents ^{99m}Tc-SER4, ^{64}Cu-NOTA-SER4, and ^{99m}Tc-ED3 targeting the antigen sialoadhesin and ^{111}In-DTPA-ED2 targeting CD163, of which both antigens are macrophage-restricted. All the agents described herein exhibit tracking to endogenous sialoadhesin-expressing macrophage populations with exceptionally fast blood clearance times. In a heterotopic cardiac transplantation model of acute rejection the tracer ^{99m}Tc-SER4 demonstrated enhanced targeting to the rejected organ, whilst following recovery to localised bone marrow radioablation preliminary data showed increased ^{64}Cu-NOTA-SER4 in the ablated bone marrow. The tracers ^{111}In-DTPA-ED2 and ^{99m}Tc-ED3 also demonstrated the feasibility of imaging distinct macrophage populations simultaneously.

In this thesis, we present sialoadhesin as a candidate target for the imaging of macrophage populations *in vivo*, with the potential for translation into the clinic.

Contents

List of Figures

List of Tables

List of Acronyms

APC	Antigen presenting cell
BFC	Bifunctional chelator
CAD	Coronary artery disease
CD	Cluster of differentiation
CNS	Central nervous system
CSF	Colony stimulating factor
CSF1R	Colony stimulating factor 1 receptor
CT	Computed tomography
DC	Dendritic cell
DMEM	Dulbecco modified eagle medium
EAE	Experimental allergic encephalitis
FBS	Fetal bovine serum
FcRn	Neonatal Fc receptor
FR	Folate receptor
HPLC	High performance liquid chromatography
HSC	Haematopoietic stem cell
IFN	Interferon
Ig	Immunoglobulin
IV	Intravenous
IL	Interleukin
ITIM	Immunoreceptor tyrosine-based inhibitory motif
ITLC	Instant thin layer chromatography
KO	Knock out
LN	Lymph node
M1	Inflammatory macrophage
M2	Anti-inflammatory macrophage
Mϕ	Macrophage

mAb	Monoclonal antibody
MDP	Methylene diphosphonate
MDSC	Myeloid derived suppressor cell
MHC	Major histocompatibility complex
MMM	Marginal metallophilic macrophage
MRI	Magnetic resonance imaging
MZM	Marginal zone macrophage
Neu5Ac	5-N acetylated-neuraminic acid
NT	Non-treated
PBS	Phosphate buffered saline
PET	Positron emission tomography
PFZM	Perifolicular zone macrophage
RBMM	Resident bone marrow macrophage
RNS	Reactive nitrogen species
ROI	Region of interest
ROS	Reactive oxygen species
sCD163	Soluble CD163
SCS	Subcapsular sinus
SDS PAGE	Sodium dodecyl sulphate polyacrylamide gel electrophoresis
SEC	Size exclusion chromatography
Siglec	Sialic acid binding Ig-like lectins
SLE	Systemic lupus erythematosus
Sn	Sialoadhesin
SPECT	Single photon emission computed tomography
SR	Scavenger receptor
TAM	Tumour associated macrophage
TGF	Transforming growth factor
$T_H1/2$	Helper T cell type 1/2

TLC	Thin layer chromatography
TNF	Tumour necrosis factor
T_{reg}	Regulatory T cell
USPIO	Ultrasmall superparamagnetic ironoxide nanoparticle
VSV	Vesicular stromatitis virus
WT	Wild type

Chapter 1:

The Macrophage Marker Sialoadhesin and Imaging

1.1 Introduction

Macrophages (Mϕ) are an important class of cell involved in host defence and homeostasis. Mϕ are able to alter their phenotype in response to their surroundings, affecting a wide range of biological processes. These properties make them critical to host function in normal and disease settings, leading to their utility as targets to inform upon functioning as well as for therapeutic intervention. The development of Mϕ-specific imaging agents has potential clinical applications in the diagnosis and measuring response to treatment of disease, in accordance with the current trend for personalised medicine. Additionally, non-invasive imaging of Mϕ populations also offers researchers a novel means of studying Mϕ behaviour *in vivo*.

1.2 An Overview of Mφ-Biology

Mϕ are present in virtually all the tissues of the body, and arise from the recruitment of circulating monocytes (Gordon and Taylor 2005). As immune cells, they are principally recognised by their function as professional phagocytes in which they remove invading pathogens via the array of germ-line encoded cell surface receptors with which they use to sense their environment. This action in innate immunity is also accompanied by their ability to secrete a variety of cytotoxic intermediates and cytokines to affect the immune response, and also to present antigenic material via major histocompatibility complex (MHC) class II to T cells. They therefore participate and form an important bridge between innate and adaptive immunity (Gordon and Taylor 2005; Pollard 2009; Geissmann, Manz et al. 2010)

Based on their anatomical location, Mϕ populations display different phenotypes and functions (Murray and Wynn 2011). For example, Kupffer cells are the most abundant

Mϕ population in the body and are responsible for clearing antigens absorbed from the gastrointestinal tract. They are also important for the maintenance of tolerance to the antigenic products of digestion, which is characterised phenotypically by a reduction in co-stimulatory molecules and functionally by the release of interleukin 10 (IL-10) in response to lipopolysaccharide (Nemeth, Baird et al. 2009). In contrast, alveolar Mϕ express high levels of pattern recognition receptors which permit the uptake of non-opsonised particles so as to manage the constant influx of particulates and pathogens that invade the airways (Taylor, Martinez-Pomares et al. 2005). However, to avoid damaging the fragile alveoli environment, alveolar Mϕ also actively suppress adaptive immunity and promote the secretion of transforming growth factor beta (TGF-β) in steady state conditions (Holt, Strickland et al. 2008). Thus, Mϕ serve not only as effectors of the immune system but also play important homeostatic and trophic roles. This latter point is exemplified by mice deficient in colony stimulating factor 1 (CSF-1), so-called CSF-1 op/op mice, which leads to the development of osteopetrosis. This disease is characterised by restricted bone marrow cavities due to the failure of osteoclast development and thus failure of bone remodelling (Stefater, Ren et al. 2011).

In vivo and *in vitro* Mϕ display considerable plasticity of phenotype, understood as an ability to continuously adapt their behaviour to the surrounding environment (Stout, Jiang et al. 2005; Murray and Wynn 2011). This feature is important as it allows Mϕ to sequentially carry out multiple, and sometimes disparate, functions. Attempts to characterise Mϕ functional status has led to the adoption of the M1/M2 paradigm. This mirrors the Th1/Th2 nomenclature where M1 Mϕ are accorded an inflammatory status (these are also sometimes known as classically activated Mϕ) typically due to exposure to cytokines such as interferon gamma (IFN-γ); while M2 Mϕ are accorded an anti-inflammatory status following exposure to mediators such as IL-4 (Sica and Mantovani 2012).

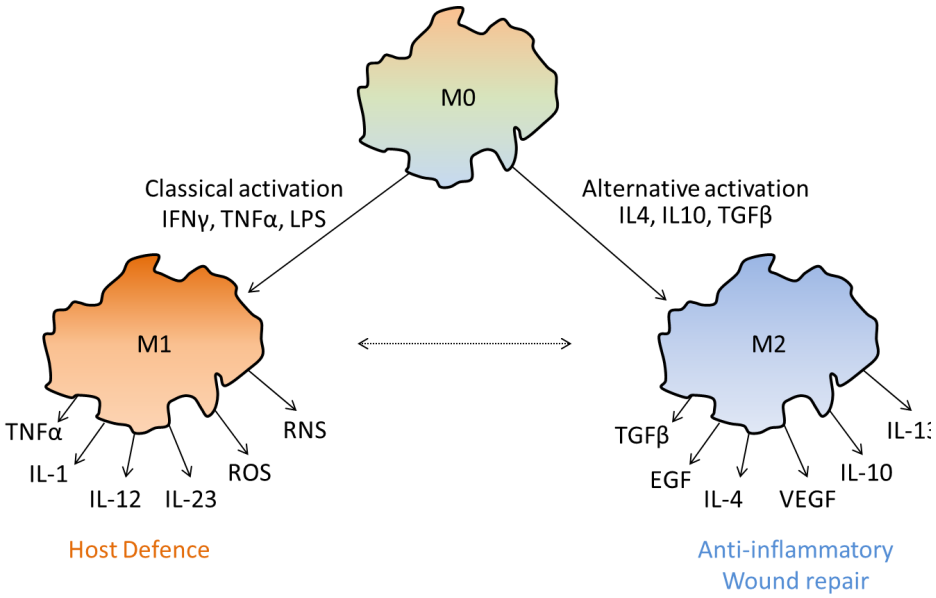

Figure 1.2.1 Mϕ Polarization. In response to inflammatory stimuli, Mϕ can adopt an M1 phenotype specialised for host defence and resulting in the release of inflammatory mediators. M2 phenotype may arise from exposure to anti-inflammatory signals, promoting processes such as wound repair during the resolution of inflammation. GF epidermanl growth factor, RNS/ROS reactive nitrogen/oxygen species, TNFα tumor necrosis factor α, VEGF vascular endothelial growth factor, TGF β transforming growth factor β. Figure adapted from (Laskin, Sunil et al. 2011)

The M2 phenotype has since become a general pooling ground for any phenotype that isn't inflammatory, leading to the grouping of behaviours that aren't well related, such as anti-inflammatory behaviour with wound remodelling behaviour. It is now commonly acknowledged that Mϕ do not adopt strict phenotypes, but instead exist within a spectrum of phenotypes, permitting them to subtly alter their actions(Mosser and Edwards 2008). However, M1/M2 is still a convenient tool for understanding immunological function, and conveys an important phenomenon that it is the balance between Mϕ phenotypes rather than Mϕ burden that correlates with function/dysfunction. The development of cancer is often cited in this respect, where the initiation of a tumour is the result of inflammatory Mϕ promoting an abnormal environment. Tumour progression is caused by the switch from inflammatory M1 phenotype to anti-inflammatory M2 phenotype, which provides and immunosuppressive environment that enables the tumour to evade the immune system (see Figure 1.2) (Mantovani and Sica 2010). In a converse scenario, the progress of atherosclerosis is dependent upon Mϕ recruitment where plaque

maturation is marked by an increase of M1 relative to M2 Mϕ numbers (Pello, Silvestre et al. 2011).

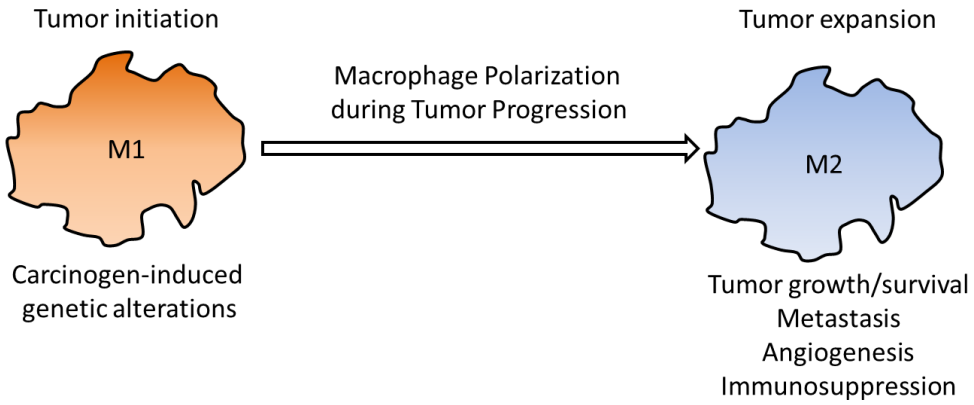

Figure 1.2.2 Mϕ polarization during tumor progression. Hypothesised role for inflammatory M1 Mϕ in tumor initiation, which undergo phenotypic switch to anti-inflammatory M2 phenotype which promotes tumour expansion. Figure adapted from (Mantovani and Sica 2010)

1.3 Mφ Markers

There are a variety of antigens used in the *ex vivo* identification of human Mϕ and of these the markers CD64, CD68 (Macrosialin), CD163, CD169 (Sialoadhesin (Sn)) and CD204 (Mϕ Scavenger Receptor A) represent the set of trans-species pan-Mϕ markers (Zola, Swart et al. 2007). Due to the significant plasticity of Mϕ phenotype, producing a single Mϕ marker has eluded researchers and none is uniquely expressed on Mϕ. CD64 is expressed on monocytes and subsets of germinal and blood dendritic cells (DCs); CD68 on various leukocytes; CD163 on monocytes; CD169 on monocytes; CD204 on monocytes and DCs. CD68 is Mϕ-restricted, however it is an intracellular antigen and thus not suitable for non-invasive imaging due to restricted access. Of the remaining markers, CD163 and sialoadhesin (Sn, CD169 or Siglec 1) represent the most Mϕ-restricted of these markers, however because of significant levels of soluble CD163 (Van Gorp, Delputte et al. 2010), access to cell-bound CD163 is compromised, and therefore Sn is a more suitable marker for Mϕ-targeting, albeit of sub-populations, *in vivo*.

1.4 Siaoladhesin and the Siglec Family

The family of cell surface proteins known as the Siglecs (sialic acid binding Ig-like lectins) are characterised by the presence of an extracellular sialic acid-binding N-terminal domain followed by up to 16 further immunoglobulin-like (Ig-like) domains. Although no broad activities/functions of this family have been identified, conservation in the cytoplasmic tails of Siglecs coupled with the recurring presence immunoreceptor tyrosine-based inhibitory motifs (ITIMs) in a majority of the Siglec family has suggested an immunoregulatory role for these structures (Crocker, Paulson et al. 2007; Crocker and Redelinghuys 2008; von Gunten and Bochner 2008). As one of the first members of this group (Kelm, Pelz et al. 1994), the receptor Sn was originally identified on a subset of Mϕ that were able to bind, but not phagocytose, sheep red blood cells in a sialic acid-dependent manner (Crocker and Gordon 1985; Crocker and Gordon 1986). Sequence analysis of mouse and human Sn has shown relatively less similarity in the cytoplasmic domain (32% similarity with human Sn) as compared to the extracellular region (72% similarity) ((Klaas and Crocker 2012)). This observation, coupled to the lack of an ITIM (Crocker, Mucklow et al. 1994; Crocker and Redelinghuys 2008) has led to the speculation that Sn primarily serves extracellular functions, such as cell-cell and cell-matrix interactions (Hartnell, Steel et al. 2001).

Sn is a 185kDa protein (Crocker, Kelm et al. 1991) with an extracellular region containing 17 Ig-like domains (Crocker, Mucklow et al. 1994) – by far the highest number of domains of the known Siglecs. As with all Siglecs, sialic acid binding is mediated by the V-set terminal Ig-like domain which is necessary and sufficient for sialic acid binding (Nath, Vandermerwe et al. 1995; May, Robinson et al. 1998) and shows a preference for 5-N acetylated-neuraminic acid (Neu5Ac) which is α(2,3)-linked to preceding carbohydrates (Crocker, Mucklow et al. 1994; Kelm, Schauer et al. 1994). Sn displays low affinity for monovalent ligands (k_D in the range of 1 mM) (Blixt, Collins et al. 2003), and it is thought that simultaneous multivalent low-affinity associations create sufficient high avidity which lead to biologically meaningful interactions of Sn. This is in-line with *in vitro* data demonstrating increased binding capacity of Sn with increasing saccharide content (Hashimoto, Suzuki et al. 1998).

It has been postulated that the extracellular region of Sn may function to extend the V-set domain away from the glycocalyx so as to enable interaction with ligands in a *trans* fashion (see Figure 1.3) (Crocker, Hartnell et al. 1997). A comparison of Sn activity in rat splenic and lymph node (LN) Mϕ has indicated that splenic Mϕ are masked considerably by endogenous sialylglycoconjugates through *cis*-type interactions which can be ablated by sialidase treatment, whilst LN Mϕ are relatively unaffected by masking (Nakamura, Yamaji et al. 2002). In this way, cell expression of sialic acids may be used to modulate functional Sn levels on cells, in effect fine tuning expression.

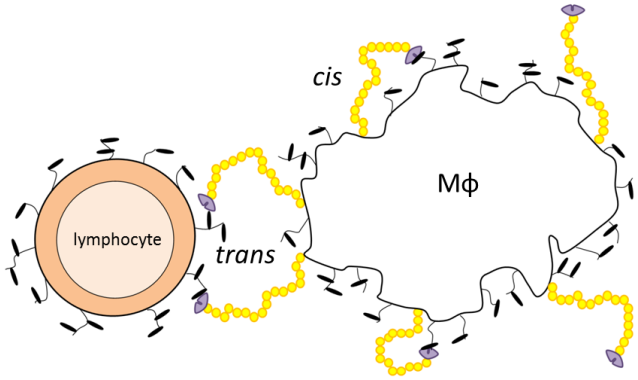

Figure 1.2.3 Cis and Trans Sn binding. *Cartoon of Sn extending beyond glycocalyx to interact with neighbouring lymphocyte sialic acids (trans-interaction) as well binding to self sialic acids (cis-interaction)*

1.5 Sialoadhesin Expression

Of the species studied so far (human (Hartnell, Steel et al. 2001), mouse (Crocker and Gordon 1989), rat (Dijkstra, Dopp et al. 1985) and pig (Revilla, Poderoso et al. 2009; Poderoso, Martinez et al. 2011) Sn has been found to be most abundantly expressed by Mϕ subsets occupying secondary lymphoid tissue (see Table 1.1).

Sn Expression in Secondary Lymphoid Tissue				
Tissue/Cell Type	**Rat**	**Human**	**Mouse**	**Pig**
MMM	+	n/a	+	/
MZM	+	-	+/-	+
PALS	+/-	-	-	/
Splenic PFZM	n/a	+	n/a	n/a
PAMS	n/a	+	n/a	+[B]
Red Pulp	+/-	+/-	+/-	-
LN Supcapsular Sinus	+	+[A]	+	+
LN Medulla	+	+[A]	+	+

Table 1.1 Sn expression in Secondary Lymphoid Tissue. Key: n/a not applicable / undetermined, - undetected, +/- low expression, + expression. PFZM:perifollicular zone Mϕ, PAMS:periartiolar-associated Mϕ, LN: lymph node, MMM: marginal metallophilic Mϕ, MZM marginal zone Mϕ, PALS periarteriolar lymphoid sheath. [A] sinusoidal expression throughout LN[53], [B] ellipsoidal vessels associated with Sn expression, possibly equivalent to PAMS (Revilla, Poderoso et al. 2009).

In all species studied, Mϕ lining the subcapsular sinus (SCS) as well as the medulla of the LN highly express Sn, whereas splenic distribution varies between species (see Figure 1.4). Marginal metallophilic Mϕ (MMM), a population that lines the marginal sinus at the periphery of the white pulp in rodents, express high levels of Sn. In rats marginal zone Mϕ (MZM) exhibit similar Sn levels to MMM, whereas in mice MZM expression is relatively lower. Both species demonstrate low levels of Sn expression in red pulp Mϕ. With differing splenic architecture in primates (Mebius and Kraal 2005) sialoadhesin positive (Sn+) Mϕ are located in a compartment found between the red pulp and marginal zone identified as the perifollicular zone (Steiniger, Barth et al. 1997; Brinkman-Van der Linden, Sjoberg et al. 2000).

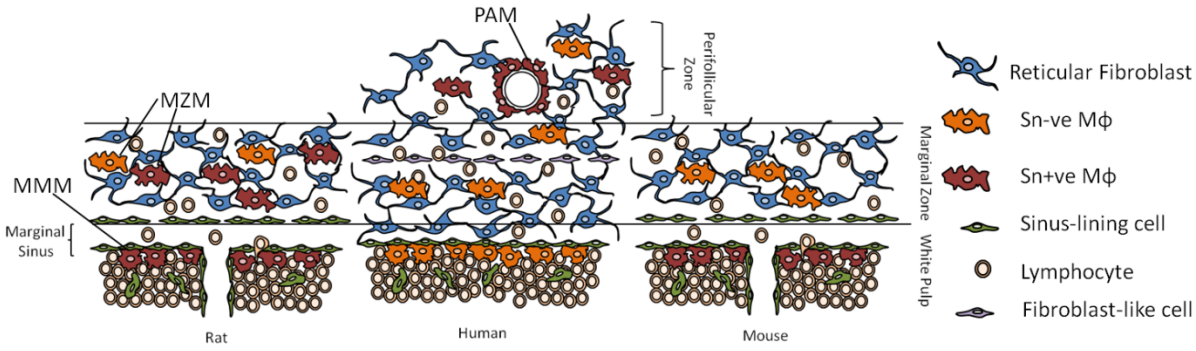

Figure 1.2.4 Comparison of the distribution of Sn+ Mϕ in the splenic microenvironment. A framework of reticular fibroblasts (blue) forms the basis of the marginal zone and is continuous with the reticular fibroblasts in the red pulp and the sinus-lining cells (green) of the marginal sinus. In all species, Sn+ Mϕ (red) are observed as a line of cells at the internal border of the white pulp (the so called marginal metallophilic Mϕ (MMM)). In rodents, the white pulp is separated from the marginal zone (MZ) by a marginal sinus, and in the case of the rat spleen, Sn+ Mϕ are observed in the marginal zone. In humans, the marginal zone is absent of Sn+ Mϕ, but the unique structure known as the perifollicular zone contains Sn+ Mϕ both sporadically and clustered around arteriolae (known as periartiolar-associated Mϕ (PAM)). Figure adapted from (Mebius and Kraal 2005).

In the absence of a marginal sinus and MMM in primate spleens, the Mϕ sheaths that line capillaries of the perifollicular zone are speculated to be equivocal to MMM found in rodents (Steiniger, Barth et al. 1997). By immunohistochemistry, higher expression levels of Sn have been reported in human versus chimpanzee spleens. The origin of this remains to be elucidated, but could be the result of increased expression of Sn-ligand (Neu5Ac) in humans or increased *cis*-inhibition due to sialic acid differences in chimpanzees (Brinkman-Van der Linden, Sjoberg et al. 2000). In pigs, splenic Sn expression is observed in the marginal zone and elliptical vessels (Revilla, Poderoso et al. 2009) which may be comparable to the periarterial Mϕ sheaths observed in humans.

The LNs and the white pulp area of the spleen function as focal centres where microbial particles, antigen presenting cell (APCs) (which may carry antigen from the periphery or acquire antigen locally) and their corresponding antigen-specific lymphocytes engage and initiate adaptive immune responses. The splenic marginal zone/perifollicular region and the LN SCS are both transitional areas where cells and molecules enter the white pulp or LN parenchyma (see Figure 1.5). MMM lining the marginal sinus of the spleen, where the blood enters the tissue, can be considered

anatomically analogous position to Mϕ that form a rim under the LN SCS. Here, the afferent lymph enters the tissue, which is consistent with the idea that these cells and their Sn have a role in antigen capture/processing and in cell-cell communication (Kraal and Mebius 2006). This conserved positioning of Sn+ Mϕ at the borders of lymphoid tissue and circulating fluids strongly suggests a function as a mediator of adaptive immunity.

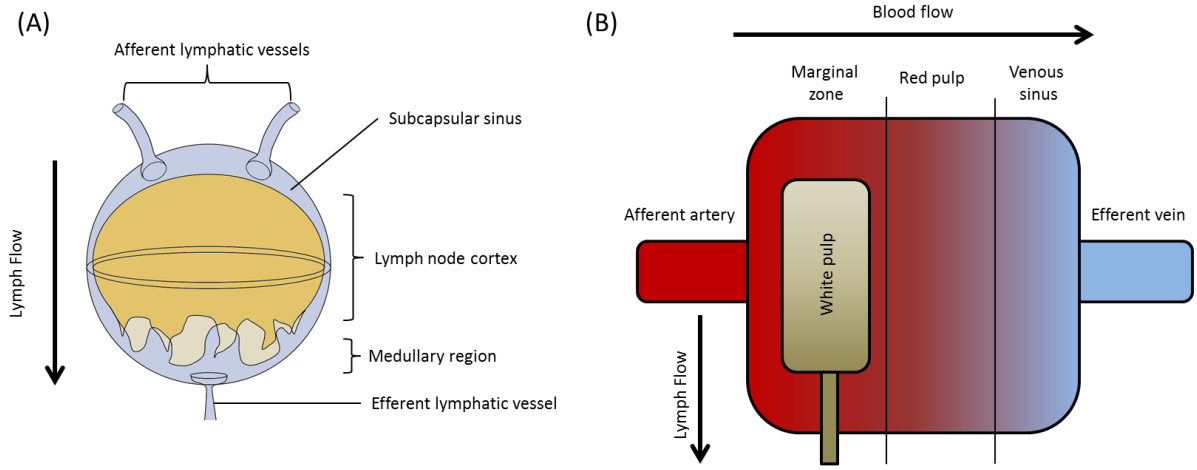

Figure 1.2.5 Diagram of Lymph Node and Schematic of Spleen. (A) The lymph node is composed of a capsule into which afferent lymphatic vessels drain, and within resides the lymph node cortex (containing all the immunological machinery) which is separated from the capsule by the subcapsular and medullary sinuses. The lymph node is then drained via an efferent lymphatic vessel. (B) On entry into the spleen, blood flow passes from the afferent artery into the marginal zone where it comes into close contact with the white pulp. From here, blood drains sequentially into the red pulp, the venous sinuses and exits the spleen through the efferent veins.

Lower levels of Sn expression can be found on Mϕ in tissues other than lymphoid, with varying degrees of *cis*-masking shown to obscure apparent Sn levels (Nakamura, Yamaji et al. 2002; Ducreux, Crocker et al. 2009). Both mice and humans express relatively high levels of Sn on resident bone marrow Mϕ (RBMM), whereas in rats Sn is absent from this population.

1.6 Sialoadhesin Regulation

It has been shown that Sn induction on PBMC and various Mϕ subsets isolated from humans (Hartnell, Steel et al. 2001; York, Nagai et al. 2007; Rempel, Calosing et al.

2008), rats (Gessl, Boltznitulescu et al. 1989; vandenBerg, vanDie et al. 1996) and pigs (Delputte, Van Breedam et al. 2007) can be achieved by incubation with either type I or II IFN. The exception to this has been mice, which despite being the most extensively studied species for Sn, inducing factors have yet to be identified (Crocker, Hill et al. 1988; McWilliam, Tree et al. 1992). Rat (Gessl, Boltznitulescu et al. 1989; vandenBerg, vanDie et al. 1996) and human Sn induction (Hartnell, Steel et al. 2001) has also been shown following tumour necrosis factor alpha (TNF-α) exposure, and additionally ligation of human TLRs involved in viral and bacterial sensing (York, Nagai et al. 2007) (which also induce IFN-α secretion) have been observed to increase expression.

In the case of both mice and pigs an unidentified component of autologous serum has been shown to induce expression (Crocker, Hill et al. 1988; Delputte, Van Breedam et al. 2007). This dependence of expression upon circulating factors may well explain the observed changes in Sn expression on Mϕ populations following disruption of the blood-brain barrier (Perry, Crocker et al. 1992) and afferent lymphatics (Mebius, Hendriks et al. 1990). The factors negatively regulating Sn aren't as unified. T_H2 cytokines in mice (McWilliam, Tree et al. 1992) and both viral and bacterial-sensing TLRs in humans (York, Nagai et al. 2007) have been shown to down-regulate expression, whilst IL-2 and IFN-γ demonstrated some inhibitory effect in rats (Damoiseaux, Dopp et al. 1989).

1.7 Function(s) of Sialoadhesin Positive Mφ

To date, the functional roles of Sn expressing Mϕ in the LN have been best characterised. SCS Mϕ border the lymphocyte-rich LN and flowing lymph, leading to the speculation that these resident cells perform a gate-keeping role, restricting access of lymphatic components including pathogens and soluble material to the LN. SCS Mϕ capture and secretion of IFN-α in response to neurotropic viral infection, and subsequent prevention of viral access to the central nervous system (CNS) exemplifies this behaviour (Iannacone, Moseman et al. 2010). As cells of the innate immune system, Mϕ routinely perform this scavenging and inflammatory cytokine secreting

activity, however further data illustrates Sn Mϕ direct action in supporting the adaptive immune response. Following subcutaneous injection of viral particles, SCS Mϕ have been shown to prevent the systemic dissemination of virus through its capture followed by initiation of adaptive immunity directly by presentation of antigen to B cells (Junt, Moseman et al. 2007). Similarly, SCS Mϕ-mediated capture, processing and presentation of antigenic material to invariant natural killer T cells (Barral, Polzella et al. 2010), CD8 T cells (Asano, Nabeyama et al. 2011) and B cells (Phan, Green et al. 2009) has demonstrated this connection between a classical scavenging role and engaging adaptive immunity.

This close relationship between sialoadhesin expressing Mϕ and lymphocytes presents a potential opportunity for pathogen transmission which has been exploited. SCS Mϕ capture of *Toxoplasma gondii* results in T cell recruitment and subsequent transfer of parasite from Mϕ to T cell, which then promotes host invasion of the pathogen by trafficking (Chtanova, Han et al. 2009).

The spleen similarly locates sialoadhesin positive Mϕ in the vicinity of lymphocyte-rich tissue and flowing fluid (in this case blood rather than lymph). Due to the difficulty of isolation or selected depletion of either marginal metallophilic Mϕ and marginal zone Mϕ subsets (the splenic Mϕ populations that express high Sn depending upon species) identifying specific roles for these subsets has so far proven troublesome (den Haan and Kraal 2012). Depletion of MZ Mϕ (MMM + MZM) via clondronate liposomes (McGaha, Chen et al. 2011) or use of transgenics (Miyake, Asano et al. 2007) and exposure to apoptotic cells has revealed the importance of MZ Mϕ debris clearance and maintenance of tolerance, with their absence leading to autoimmunity. MZ Mϕ presence was also required in generating CD8 T cell response to intravenous (IV) viral infection (Backer, Schwandt et al. 2010). This study showed that targeting of antigen specifically to Sn+ Mϕ promoted CD8 T cell response, involving cross presentation with DCs but not eliminating a possible direct activation role for Sn+ Mϕ. More recently, an effective humoral response to vesicular stromatitis virus (VSV) was shown to involve Sn+ Mϕ capture and subsequent enforced replication, thought to enrich antigen load and enhance immunity (Honke, Shaabani et al. 2012). SCS Mϕ were similarly observed

as repositories for viral replication in a response to VSV challenge in the LN which is thought to enhance immunity (Iannacone, Moseman et al. 2010). These data all point to the specialised role that Sn+ Mϕ play as scavengers and enforcers of adaptive immunity.

Analysis of Sn knock-out (KO) mice has revealed decreased soluble IgM levels as well as subtle alteration in CD8 T cell and various B cell populations, furthering the notion of Sn supporting immunoregulatory functions (Oetke, Vinson et al. 2006). During experimental allergic encephalitis (EAE), Sn KO mice have shown reduced disease severity along with reduced numbers of infiltrating T_H1 and T_H17 cell in the CNS. Additionally higher numbers of regulatory T cells (T_{reg}) were observed in the CNS. *In vitro* proliferation of CD4 T cells using either Sn KO or wildtype (WT) CNS-infiltrating Mϕ as APCs showed lower T_{reg} proliferation using WT Mϕ which could be ameliorated by blocking of Sn (Wu, Rauch et al. 2009). This was the first *in vitro* account of Sn Mϕ directly regulating T cell behaviour, opening the possibility that this proinflammatory effect of Sn is corroborated by other autoimmune studies in which Sn KO mice have exhibited reduced disease severity (Jiang, Hwenda et al. 2006; Ip, Kroner et al. 2007). In a somewhat more artificial model of disease, Sn+ Mϕ in the liver have been observed to form clusters with CD4 and CD8 T cells during a successful Graft-versus-Leukaemia response. Following infusion of anti-Sn antibody, Mϕ-T cell cluster formation, along with survival rate, were reduced. Additionally, isolated Sn Mϕ were shown to present MHC I and MHC II restricted peptides to CD8 and CD4 T cells, respectively (Rocha, Umansky et al. 1997; Muerkoster, Rocha et al. 1999). Altogether these data show that Sn directly mediates effects of the immune system that can be broadly classified as inflammatory. However, the exact nature of this effect, its mechanism and whether it is affected centrally (i.e. in lymphoid structures) or peripherally has yet to be determined.

In vitro Sn has been shown to mediate binding to a variety of pathogens in a sialic acid-dependent manner (Jones, Virji et al. 2003; Vanderheijden, Delputte et al. 2003; Monteiro, Lobato et al. 2005; Heikema, Bergman et al. 2010). This has led to the speculation that Sn primary function is to identify such structures and remove them

from the lymph/blood using accessory receptors (the exception being porcine Sn which exhibits endocytosis (Delputte, Van Gorp et al. 2011)). In line with this, type I IFN regulation of Sn may serve to increase recognition of sialic acid-displaying pathogens during infection. Based on the observation that Sn is non-phagocytotic and possesses an extensive, highly conserved extracellular domain that experiences considerably less *cis*-masking than other Siglecs, another hypothesis is that Sn mediates cell-cell interactions (Crocker, Paulson et al. 2007). In line with this, Sn has shown to display binding to various cell populations (Hartnell 2001; Crocker 1995; van den Berg 1992) with one study recording differential binding according to T cell maturity in which authors reasoned this assisted in T cell homing to lymphoid tissue (Vandenberg, Breve et al. 1992). During EAE (see above) it was noted that T_{reg} in the afflicted tissue displayed increased Sn ligand. *In vitro*, isolated T_{reg} were then shown to proliferate in the absence/blocking of Sn expression on Mϕ which were acting as APC, establishing the link between Sn-mediated interaction and lymphocyte behaviour (Wu, Rauch et al. 2009). Counter receptors for Sn including CD43 (van den Berg, Nath et al. 2001), MUC-1 (Nath, Hartnell et al. 1999), Mϕ galactose c-type lectin 1 (Martinez-Pomares, Crocker et al. 1999) and chimeric mannose receptor binding protein (Kumamoto, Higashi et al. 2004) contribute to our understanding that Sn can mediate interactions with various cell surface proteins. It has been speculated that to meet this requirement in identifying self-structures, Sn expression in humans is significantly higher than in primates. The reasoning for this is based on the increase burden of the Sn ligand Neu5Ac in humans due to loss of Neu5Gc synthesis, leading to increased Sn expression in order to maintain efficient screening for self (Brinkman-Van der Linden, Sjoberg et al. 2000).

From the finding that MZM and SCS Mϕ participate in the induction of an adaptive immune response, targeting antigen to Sn+ Mϕ has been explored as a means of inducing immunity. Delivery of antigen to Sn using a monoclonal antibody (mAb) has been shown to strongly inhibit tumour growth in mice (Backer, Schwandt et al. 2010) whilst a humoral response and increased reactivity of PBMC was observed in pigs (Poderoso, Martinez et al. 2011). Without specifically targeting Sn+ Mϕ, an efficient anti-tumour response was mounted following subcutaneous of necrotic tumour cells.

This effect was abolished by selective depletion of Sn+ Mϕ in LN, illustrating the importance of this subset in vaccination (Asano, Nabeyama et al. 2011). Coupled to the data concerning that MZ Mϕ maintain self-tolerance following exposure to apoptotic material, it is clear that Sn+ Mϕ represent important links in the induction of tolerance and in-tolerance (i.e. vaccination).

1.8 Sialoadhesin in Disease Settings

Sialoadhesin positive Mϕ have been identified in a variety of disease settings, and the following collates the known data in separate models.

1.8.1 Cancer

Mϕ play an important role in the pathophysiology of cancer, displaying both pro- and anti-tumorcidal behaviours (Mantovani, Allavena et al. 2008). Clinically, increased Sn expression has been recorded in splenic marginal cell lymphoma (Marmey, Boix et al. 2006) as well as identification of Sn positive Mϕ infiltrates in MUC-1 positive breast carcinoma (Nath, Hartnell et al. 1999).

In mice, splenic and liver Sn expression has been shown to correlate with lymphoma stasis/regression in a model of Graft-versus-Leukaemia reactivity (Umansky, Beckhove et al. 1996; Rocha, Umansky et al. 1997; Muerkoster, Wachowski et al. 1998). Following adoptive immunotherapy in this model, donor lymphocytes were shown to cluster with Sn+ Mϕ and isolated Mϕ were able act as a professional APC by presenting antigen to CD4 and CD8 T cells (Rocha, Umansky et al. 1997; Muerkoster, Wachowski et al. 1998). Furthermore, *in vivo* administration of a non-depleting anti-Sn mAb resulted in reduced accumulation of CD8 T cells and cluster formation, as well as reduced survival rates. *In vitro* Sn blocking showed reduced proliferation of cytotoxic T lymphocytes in the presence of Sn+ Mϕ pulsed with antigen (Muerkoster, Rocha et al. 1999). These Sn+ Mϕ were later shown to express increased levels of CD40, a receptor which is involved in T cell priming, activation and differentiation as well as in the mediation of Mϕ effector functions suggesting that Sn+ Mϕ activate recruited T cells and hence promote a tumoricidal response (Muerkoster, Laman et al. 2000). Altogether, these data point to immunologically active role for Sn in promoting tumour rejection mediated by a T cell response.

Analysis of rat tumours has shown Sn+ Mϕ to be present in hepatic metastatic carcinoma (Heuff, Vanderende et al. 1993), adenocarcinoma of the prostate (Landstrom and Funa 1997) and transplanted xenografts (Yamashiro, Takeya et al. 1994; Yamashiro, Takeya et al. 1998). In prostate adenocarcinoma the number of Sn+ Mϕ has shown a strong positive correlation with tumour apoptosis and negative correlation with tumour growth. As with mice, rat Sn expression was found to be concomitant with lymphocyte recruitment.

1.8.2 Arthritis

As inflammatory cells, Mϕ constitute a significant proportion of the cellular infiltrate during rheumatoid arthritis and contribute to both tissue destruction and remodelling during disease progression (Kinne, Stuhlmueller et al. 2007). In keeping with this, Sn positive Mϕ have been identified in the joints of RA patients (Hartnell, Steel et al. 2001).

In the rat, accumulation of Sn+ Mϕ into the arthritic synovium and joint space has been shown to occur within a day following induction and along with lymphocyte influx (Dijkstra, Dopp et al. 1987; Verschure, Vannoorden et al. 1989; Kool, Gerritsboeye et al. 1992). Following arthritic induction, increased Sn expression in the LN SCS, splenic MZ and red pulp has been found which may be a reflection of the increased serum levels of relevant inflammatory cytokines (Carol, Pelegri et al. 2000) (see Section 1.8). Similarly a systemic increase in TNF-α has been observed after arthritis induced by intraperitoneal (IP) injection with streptococcal cell wall fragments in which elevated Sn expression was found on isolated peritoneal Mϕ (Chou, Dong et al. 1998). Treatment with clodronate-laden small unilamellar vesicles (SUVc) has been shown to reduce overall Mϕ burden (including Sn+ Mϕ) and arthritic severity (Richards, Williams et al. 1999), although whether this effect resulted specifically from the Sn+ Mϕ subset was undetermined. The sum of this data strongly correlates inflammation with the presence of Sn positive, furthering the notion of Sn as a marker of inflammatory Mϕ.

1.8.3 Glomerulonephritis

Glomerulonephritis is an inflammatory renal disease in which Mϕ accumulation is a prominent feature, and where increased burden correlates to poorer clinical prognosis (Nikolic-Paterson and Atkins 2001). Analysis of kidney tissue from patients with glomerulonephritis has shown that Sn+ Mϕ accumulation correlated with glomerular injury and following glucocorticoid therapy Sn expressing Mϕ numbers dropped (Ikezumi, Suzuki et al. 2005). Sn expressing Mϕ have been widely studied in rodent models of glomerulonephritis, principally as an indicator of Mϕ maturity/activation during nephritis (Lan, Nikolicpaterson et al. 1993; Lan, Nikolicpaterson et al. 1995; Erwig and Rees 1999; Lai, Cook et al. 2001; Kluth, Erwig et al. 2004; Yamate, Machida et al. 2004; Ricardo, van Goor et al. 2008). As with humans, anti-inflammatory treatment (IL-4 (Cook, Singh et al. 1999), IL-6 (Karkar, Smith et al. 1997), IL-11 (Lai, Cook et al. 2001), has resulted in depletion of Sn Mϕ recruitment and amelioration of disease severity.

1.8.4 CNS Inflammation

The recent development of Sn KO mice has allowed the study of these Mϕ in various autoimmune settings, which has provided further evidence of an immunoregulatory role. Sn KO mice display reduced disease severity in experimental autoimmune uveoretinitis (EAU) (Jiang, Hwenda et al. 2006), and myelin degeneration models (Kobsar, Oetke et al. 2006; Ip, Kroner et al. 2007) in which reduced lymphocyte invasion was observed in KO strains. During EAE increased T_{reg} and decreased effector T cell numbers were detected in the CNS of KO compared to wild type (WT) mice, with i*n vitro* data showing Sn expression to directly influence T_{reg} proliferative responses (see Section 1.6) (Wu, Rauch et al. 2009).

Monocytes cultured from rat strains which are more susceptible to experimental autoimmune disease induction have demonstrated higher levels of Sn expression than less susceptible strains (Damoiseaux, Huitinga et al. 1992). This mirrors KO data from mice, insofar as Sn expression correlates with disease severity. Also similar to mice, induction of experimental allergic encephalomyelitis resulted in the recruitment of Sn+ Mϕ throughout the CNS parenchyma and meninges (Polman, Dijkstra et al. 1986).

Once again lymphocyte recruitment was positively correlated with increased Sn however no causal relationship was shown. Taken together, these data point towards the presence of Sn strongly associates with an adaptive immune response.

1.9 Expression of Sn in other Myeloid-lineage cells

Under homeostatic conditions, Sn expression is restricted to mature Mϕ populations, although there is evidence that a subset of DC in the LN may perhaps also express Sn (Crocker and Gordon 1989; Berney, Herren et al. 1999; den Haan and Kraal 2012). However, under pathological circumstances expression has also been shown to be elevated on circulating monocytes in a variety of clinical conditions including coronary artery disease (CAD) (Xiong, Zhou et al. 2009), Systemic Lupus Erythematosus (SLE) (Biesen, Demir et al. 2008), HIV (Pulliam, Sun et al. 2004) and systemic sclerosis patients (York, Nagai et al. 2007). For CAD and SLE, expression of Sn on monocytes was correlated to disease severity. Additionally in SLE, Sn levels were strongly correlated with IFN-α, indicating the dependence of expression upon inflammatory stimuli, which is consistent with *in vitro* type I IFN regulation of Sn (see Section 1.6). Whether expression is a factor in disease progression or is simply symptomatic is unresolved, with some speculating on a role in monocyte recruitment to sites of inflammation (Xiong, Zhou et al. 2009). An interesting observation has been in HIV upregulation of Sn on circulating monocytes, in which Sn may offer a means for HIV to gain access to the CNS. In this scenario, it has been speculated that the increased infection of Sn+ monocytes serves to promote HIV-associated dementia (Rempel, Calosing et al. 2008). When considering the expression of Sn on DC, it has been shown *in vitro* that Sn can be induced following exposure to human rhinovirus and that potent T cell anergy can be affected in mixed leukocyte reaction coculture experiments (Kirchberger, Majdic et al. 2005). It was speculated that synapse formation during T cell activation could be inhibited by Sn liganding to CD43, and later on shown that the inhibitory factor was IL-35 specifically released from CD4+ and CD8+ T effector cells (Seyer, Kirchberger et al. 2010), which once again illustrates the immunoregulatory role of Sn expression.

1.10 Molecular Imaging

Molecular imaging has been described as the visual representation, characterisation and quantification of biological processes at the cellular and subcellular level in a living host (Massoud and Gambhir 2003). This technology relies on the use of molecular probes in conjunction with various imaging modalities (e.g. positron emission tomography (PET), magnetic resonance imaging (MRI), etc.) to non-invasively detect biological events. For research purposes, the value of molecular imaging is in the analysis of intact living subjects. This permits repeated studies on the same subject (reducing both subject numbers and variability from using multiple subjects), analysis of processes in an *in vivo* setting (more biologically meaningful than an *in vitro* setting), as well as whole body visualisation of processes rather than sampled regions (such as with histological approaches). In clinical terms, molecular imaging represents a significant technological advance as earlier techniques have relied upon detection of morphological and structural changes in order to infer diagnose and monitor pathology. As such changes typically occur during the advanced stages of disease, molecular imaging allows for earlier detection (and with it earlier medical intervention) as well as inform upon a patients response to treatment. Additionally, molecular imaging can assist in the prediction of a patients response to therapy (e.g. a radio-labelled therapeutic can inform upon whether the therapeutic will target the site of disease in an individual sufficiently) and is also used in radio-immunotherapy for dosing calculations, which are critical for optimising treatment (James and Gambhir 2012).

1.10.1 Nuclear Imaging

Nuclear imaging is the process of detecting an administered radioactive compound in order to non-invasively visualise physiological processes (in both disease and homeostasis). This technique relies upon the inclusion of a radioactive nuclide into a targeting vector which shows specificity for a desired structure/process as well as instrumentation able to detect the appropriate source of radiation.

The two technologies used for detecting an administered radiotracer both depend upon the detection of γ radiation but with each arising from a different process. These

systems are single photon emission computed tomography (SPECT) and PET. SPECT involves the detection of γ radiation released from the nuclear rearrangement of a radionuclide. This is driven by a radioisotope changing its nuclear structure from a higher energy configuration to a lower, more stable one, with the difference in energy between these states released as γ radiation Rather than detecting γ radiation released from nuclear rearrangement, PET detects radiation released from the annihilation of a positron with an electron, which produces two photons at 180° to one another. The origin of the positron is a radioisotope with an overabundance of protons in its nucleus which achieves greater stability through the decay of a proton into a neutron and a positron (and a neutrino) (see Figure 1.6).

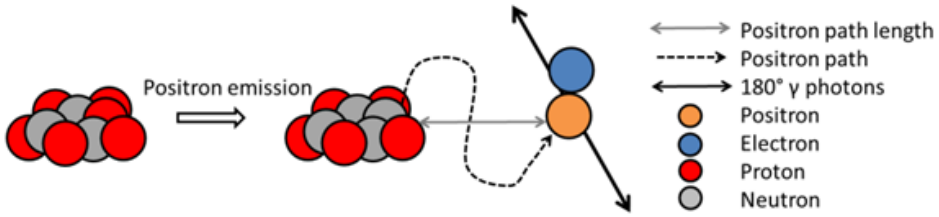

Figure 1.2.6 Positron Annihilation. Atoms with an overabundance of protons can achieve greater stability by the conversion of a proton into a neutron along with the release of a positron. An annihilation event results from a positron encountering an electron which results in the release of two photons with a fixed energy (511 KeV) at 180° from each other. PET systems are designed to detect these events.

These two different sources of γ radiation result in slightly different scanners designed for their detection. Both designs include a basic γ camera that is composed of a scintillator, which fluoresces in response to incoming γ radiation, coupled to a photomultiplier, which amplifies and digitises this fluorescent signal. The systems then diverge in terms of how they collect incident radiation. SPECT scanners typically use a rotating set of cameras which include collimators to eliminate photons that are not perpendicular to the scintillator. A series of planar images are then made from multiple angles which are then reconstructed into a 3D image of activity distribution. PET systems instead utilise a 360° arrangement of cameras which only detect 180° photons that arrive within a short time of one another (these being photons produced from positron annihilation). The origin of radiation can then be derived from the trajectories of detected annihilation events (see Figure 1.7).

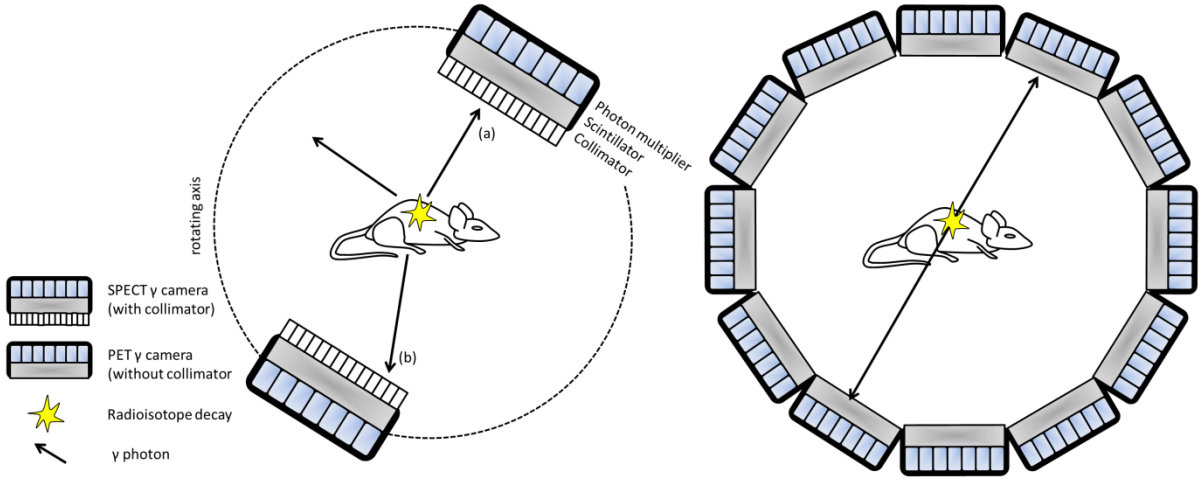

Figure 1.2.7 Schematic of SPECT and PET scanners. A) SPECT scanners employ γ cameras on a rotating axis which collect photons that arrive perpendicular to the camera's scintillator (a) to produce a series of planar images that are reconstructed into a 3D image of activity distribution. Non-perpendicular photons are eliminated by the presence of a collimator (b). B) PET scanners contain a 360° ring of cameras which identify annihilation events by detecting the near simultaneous arrival of 180° photons. PET scanners dispense with collimators hence have greater sensitivity as compared to SPECT systems.

As PET systems do not require collimators, far more incident radiation reaches the scintillator compared to SPECT hence PET is a more sensitive technique. Additionally, attenuation correction (the process of correcting for signal loss due to interaction with the matter it passes through, i.e. the patient) is much simplified in PET than SPECT which improves image quality (Garcia 2012). The reliance on positron annihilation for PET results in an inherent limit to accuracy as the origin of radiationis the location of the annihilation event, which can be in excess of a 1mm from the tracer (which is radioisotope dependent). Also as the radiation released from annihilation is always the same wavelength, distinctions between radionuclides cannot be made in PET whereas in SPECT different nuclides emitting different wavelength radiation permit multiple tracers to be administered and detected simultaneously. The high cost of producing PET nuclides in cyclotrons as compared to generator produced SPECT isotopes has also provided economic obstacles to PET development. However, the greater availability of non-metallic PET radioisotopes (alongside metallic PET isotopes) permits the synthesis of biological analogues which aren't available with the mainly metallic SPECT isotopes.

1.10.2 Imaging Mφ

To date *in vivo* imaging of Mϕ has largely focussed upon either exploiting their phagocytotic activity by engulfment of particulate agents (such as ultrasmall superparamagnetic ironoxide nanoparticles (USPIOs) (Tang, Muller et al. 2009; de Roos 2012) and perfluorocarbon emulsions (Temme, Boenner et al. 2012)) or by the targeting of structures (such as vascular cellular adhesion protein-1) and products (such as reactive oxygen species) which are not exclusive to this cell type (Quillard, Croce et al. 2011). The widespread use of nanoparticle-based imaging agents is as much an exploitation of Mϕ phagocytotic activity as it is a response to a lack of Mϕ -restricted antigens, this being a consequence of their considerable plasticity. The lack of specificity of nanoparticles is observed in USPIOs uptake where despite the significant role that Mϕ scavenger receptor A plays (Lunov, Zablotskii et al. 2011) USPIOs uptake is also seen in rapidly proliferating cells (Moore, Weissleder et al. 1997). Furthermore the presence of Mϕ is not necessarily indicative of disease prognosis as it is often the balance of Mϕ phenotypes that determines outcome (see 1.1) and so agents that can reveal this are desirable.

The targeting of Mϕ scavenger receptors through peptide motifs is increasingly being explored for imaging applications, particularly in the field of atherosclerosis research (Cormode, Chandrasekar et al. 2009; Segers, Yu et al. 2012). Additionally, folate receptor (FR) targeting is currently under clinical trials as a means of imaging and therapeutic delivery of M1 Mϕ (Low, Henne et al. 2008), and has seen successful in visualising a variety of Mϕ -mediated disease settings, including arthritis (Xia, Hilgenbrink et al. 2009), atherosclerosis (Ayala-Lopez, Xia et al. 2010) and infection (Henne, Rothenbuhler et al. 2012). This promising tracer is also used for imaging cancer as tumours have been shown to upregulate FR (see Chapter 4), which does confound its Mϕ specificity, and also present imaging formulations are based on small molecule folate analogues which result in high kidney uptake, prohibiting imaging of glomerular disease.

1.11 Rational for this study

Mϕ are a critical cell type in a variety of homeostatic and pathological processes, such that the ability to non-invasively detect their presence or absence can inform upon proper and improper host functioning. Furthermore, the ability to identify specific Mϕ subclasses is more informative as Mϕ phenotype is often the determinant of disease outcome.

The sialic acid receptor Sn is expressed on Mϕ in disease settings and is conserved between humans and preclinical models. We hypothesise that Sn represents a putative candidate target for the imaging of a Mϕ subpopulation in disease, and have investigated its feasibility using radiolabelled monoclonal antibodies by SPECT and PET modalities.

1.12 Aims

The aims of this project were to develop imaging systems that would allow the detection of Sn-expressing Mϕ in disease conditions.

1. To produce and evaluate, *in vitro*, a mouse Sn specific imaging agent for SPECT using the mAb SER-4
2. To validate the use of the SPECT tracer *in vivo* and in an acute transplant rejection model in the mouse
3. To produce and validate an anti-Sn PET radio-immunoconjugate using a murine radioablation model
4. To evaluate the utility of two radiolabelled antibodies against CD163 and Sn in imaging endogenous Mϕ in the rat

Radiotracers were evaluated in wild type animals and, with time permitting, in disease models. The disease models included an acute transplant rejection model in which macrophage recruitment was analysed following heterotopic transplantation of matched and mis-matched donor hearts using a SPECT tracer. Additionally, a model of localised bone marrow radioablation was also selected where macrophage recruitment following regional irradiation was analysed with the influence of signalling and tumour presence studied.

Chapter 2:

Expression, Purification and *in vitro* Characterisation of ^{99m}Tc-SER-4

2.1 Introduction

Monoclonal antibodies have revolutionised medical science by virtue of their exquisite specificity in recognising molecular structures. Their ability to bind unique cellular markers has long-since been combined with radioactive nuclides to afford compounds that demonstrate high binding selectively and which are detectable at minute concentrations. Such technology has found increasing utility in the field of diagnostic medicine, and in particular imaging. However of all the cellular targets chosen none so far have been directed to Mϕ, a critical cell type in a variety of homeostatic and pathological processes. In this chapter we aim to produce a novel radiotracer based on the mAb SER-4 (raised to the Mϕ marker Sn) with the potential to bind Mϕ populations.

2.1.1 Antibodies

Antibodies are a class of protein which are secreted by a subset of immune cells in order to recognise and remove/neutralise pathological processes or pathogens. They are produced by the pairing of two different proteins (denoted heavy and light chains) which in turn associate with other paired chains depending upon the isotype of antibody (IgA, IgG, IgD, IgE, IgM represent the five known isotypes). In the circulation, the most abundant antibody type is denoted IgG (or immunoglobulin-gamma) which accounts for approximately 70% of circulating antibodies. IgG is a molecule formed from the association of two heavy and light chain pairs. The heavy and light chains of IgG are formed from 4 domains and 2 domains for the heavy and light chain, respectively) of which the N terminal domain contains the sequence which determines binding specificity of the antibody and is known as the variable region. The C terminal domains define the effector functions of the antibody, such as recruitment of immune effector cells (see Figure 2.1).

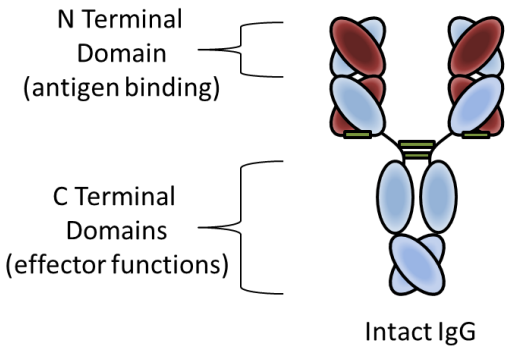

Figure 2.1 Schematic domain structure of IgG. Intact IgG is a 150kDa tetramer composed of an identical light (purple) and heavy (blue) chain pair connected by disulfides (green bar). The N terminal domain of both heavy and light chains defines antigen binding (including so-called variable region) whilst the C terminal domains of the heavy chain define the antibody's effector functions.

2.1.2 Hybridoma Technology

Much early research involving antibodies relied upon the handling of sera from immunised animals containing antibodies raised to different epitopes of the same immunogen (termed *polyclonal* antibodies) as well as irrelevant antibodies already present in the circulation (see Section 2.1.3). The ability to fuse an antibody secreting B cell with a myeloma cell to produce an immortal cell line secreting antibodies with the same specificity (a *monoclonal* antibody or mAb) was introduced in the late 1970's and is known as hybridoma technology (Kohler and Milstein 1975). This technology marked a revolution in the use of antibodies as they could now be generated in large quantities with precise specificity (see Figure 2.2).

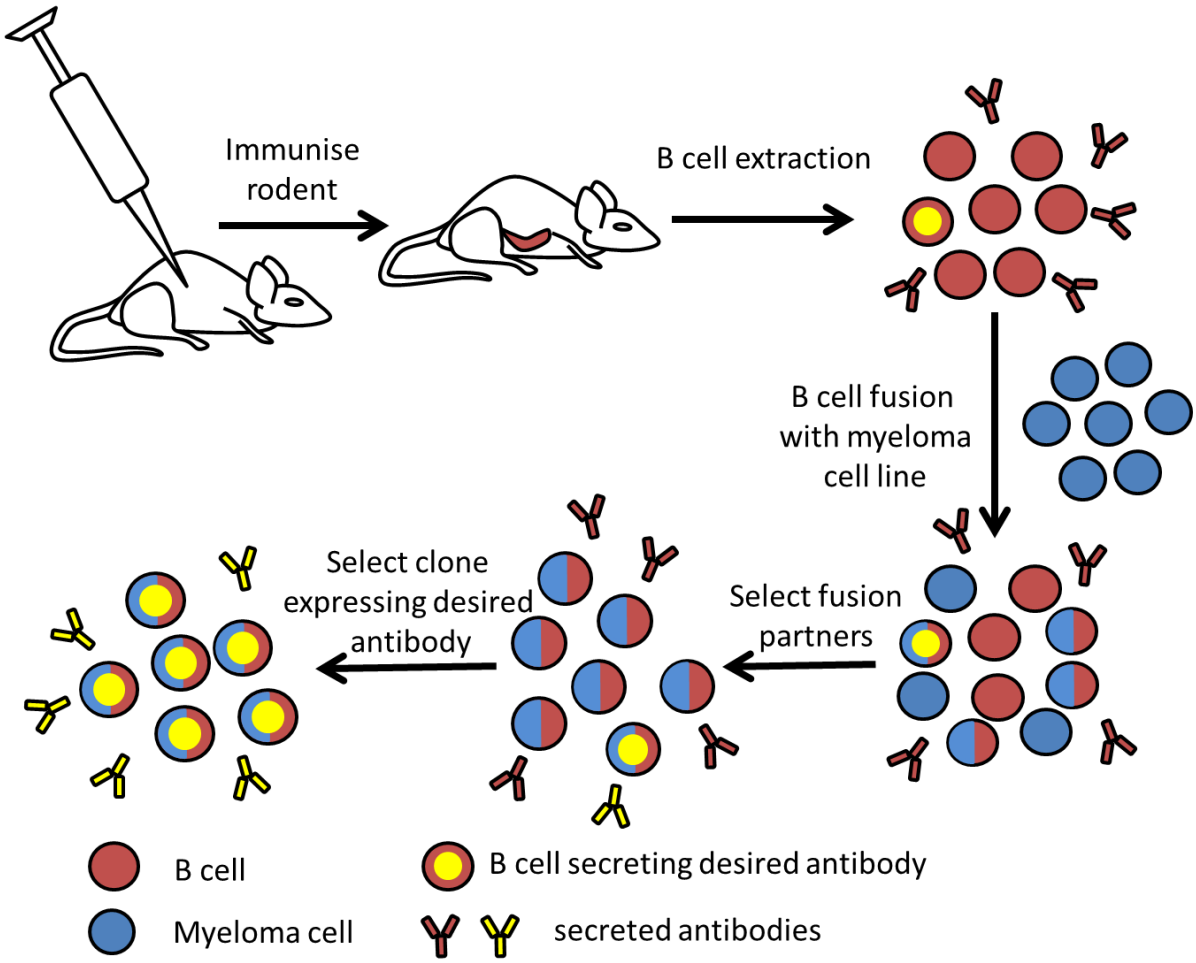

Figure 2.2 Preparation of a hybridoma. B cells are extracted from a mouse immunised with an antigen. Harvested B cells are then fused with a myeloma cell line and the successful partners selected for in selective media. The clone expressing the desired antibody is identified and expanded. Figure adapted from Molecular Biology of the Cell, p509, 2008.

2.1.3 Radiolabelled Antibodies

Antibodies have long been of interest as research tools to scientists. By combining antibody specificity with the ability to sensitively detect radioactivity, the labelling of antibodies with radioisotopes has been pursued since the 1940's (Pressman and Keighley 1948). The application of radiolabelled antibodies for non-invasive imaging was originally published separately by two groups in 1974, both utilising polyclonal radiolabelled antibodies to image tumour growth in mice (Goldenberg, Preston et al. 1974; Mach, Carrel et al. 1974). However the contribution of polyclonal, or "inert radiolabelled proteins", had a marked effect on increasing uptake at tumour sites

(Goldenberg, Preston et al. 1974). Upon the advent of mAb production, researchers were quick to realise their application to imaging. During the first such study, authors noted that both greater specificity and greater reproducibility over anti-sera led to lower doses for administration (Ballou, Levine et al. 1979).

Monoclonal antibodies are now routinely used therapeutically for the management of a variety of diseases, and increasingly their radiolabelled forms (known as radioimmunoconjugates) are becoming important in both diagnosis and therapy (Boswell and Brechbiel 2007) (see Table 2.1).

Generic Name	Trade Name	Agent/target
Rituximab	Rituxan	Chimeric anti-CD20 IgG_1
Trastuzumab	Herceptin	Humanized anti-HER2 IgG_1
Alemtuzumab	CamPath	Humanized anti-CD52
Cetuximab	Erbitux	Chimeric anti-EGFR
Bevacizumab	Avastin	Chimeric anti-VEGF
Sulesomab	Leukoscan	[^{99m}Tc] Murine anti-NCA-90 Fab
Arcitumomab	CEA-Scan	[^{99m}Tc] Murine anti-CEA Fab
Capromab pendetide	Prosta-Scint	[^{111}In] Murine anti-PSMA
Tositumomab "anti-B1"	Bexxar	[^{131}I] Murine anti-CD20 IgG + unlabeled tositumomab
Ibritumomab tiuxetan	Zevalin	[^{90}Y] Murine anti-CD20 IgG + rituximab

Table 2.1 Selected list of commercial FDA-approved antibodies for detection and treatment of cancer. Taken from (Boswell and Brechbiel 2007).

2.1.4 Radiolabelling Approaches

The selection of a radionuclide depends upon the kinetics of the radiotracer and on its intended application (i.e. diagnostic or therapeutic). In general, intact antibodies display relatively long blood half-lives (of the order of days to weeks) due to their size exceeding renal cut off and also neonatal Fc receptor (FcRn)-mediated recycling of internalised antibodies (see Figure 2.3). For this reason long-lived isotopes are favoured when imaging with IgG, such as ^{89}Zr for PET and ^{111}In for SPECT, as sufficient time must be allowed after administering a radiolabelled antibody to allow it to clear the blood, which prohibits the use of short lived isotopes.

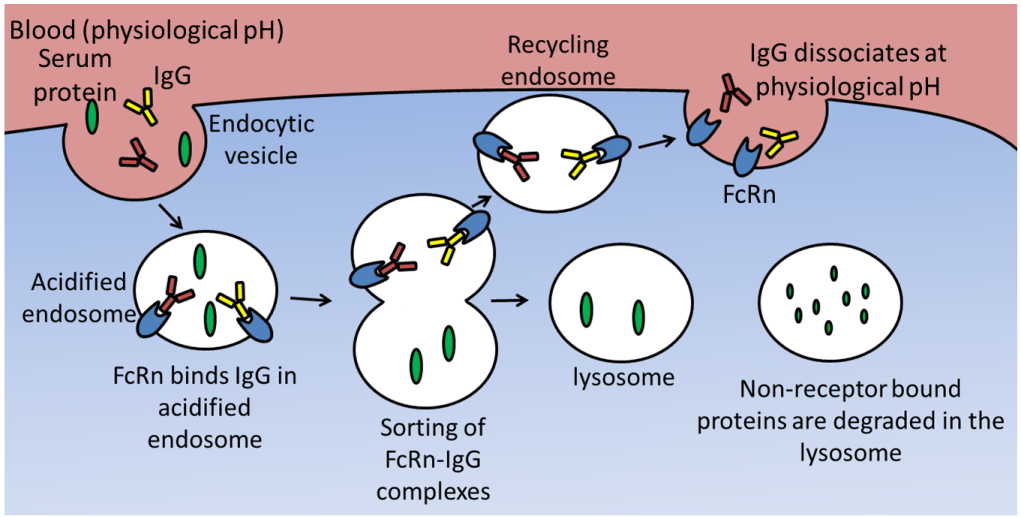

Figure 2.3 FcRn-mediated recycling of IgG. The neonatal Fc receptor for IgG (FcRn) is expressed on endothelial cells and circulating monocytes. These cells internalise serum IgG which binds to FcRn under acidic endosomal conditions FcRn then recycles IgG back into the circulation, extending its serum half-life. Serum proteins without an Fc region are subjected to lysosomal degradation. Figure adapted from (Roopenian and Akilesh 2007).

Another practical factor to consider when selecting a radioisotope is availability. The majority of PET isotopes are cyclotron produced and, relative to SPECT isotopes, possess short half-lives. This limits their use to centres with access to cyclotron production facilities. SPECT isotopes are more readily available in part due to their longer half-lives permitting transport between production sites and end users, but also because of the availability of in-house generators. This is particularly relevant for the isotope ^{99m}Tc, for which the presence of a generator coupled with its favourable half-life (6 h) permits radiotracer preparation and SPECT scanning whilst minimising patient exposure) and its ideal emission properties (143 KeV γ-photon, complementing clinical γ detectors), has led to its use accounting for over 70% of diagnostic scans in the US during 2007 (Liu 2008).

Although the half-life of 6 h prohibits longitudinal studies with ^{99m}Tc it is frequently used for in vivo imaging of intact antibodies. In this case it is not just the aforementioned favourable imaging properties that make ^{99m}Tc attractive but also the simplicity with which antibodies can be radiolabelled with it. Traditionally when preparing a radiopharmaceutical using a metallic radionuclide, the structure of the pharmaceutical must be altered so as to include groups that can co-ordinate and thus

bind to the radioisotope. Often this is achieved by the introduction of a bifunctional chelator (BFC), a reagent that possesses a metal chelating site as well as a site capable of covalently bonding to a targeting molecule. With a variety of BFC available the ability to introduce radiometals into a host of different structures is possible. However introduction of a BFC onto an antibody is a delicate process as antibody affinity must be maintained by ensuring biologically relevant sites are not modified whilst at the same time incorporating enough chelating sites to be able to prepare a radiopharmaceutical with a high specific activity. This is known as indirect labelling. A BFC-independent strategy of radiolabelling antibodies with ^{99m}Tc is also possible and this is afforded by the exposing of internal cysteines by mildly reducing an antibody and using these as intrinsic chelators for ^{99m}Tc (see Figure 2.4). This process is known as direct labelling and its advantages over indirect labelling are that modification is restricted largely to the hinge region of the antibody, thus removed from the binding domains, and also it requires no BFC handling which reduces the overall complexity of the labelling process.

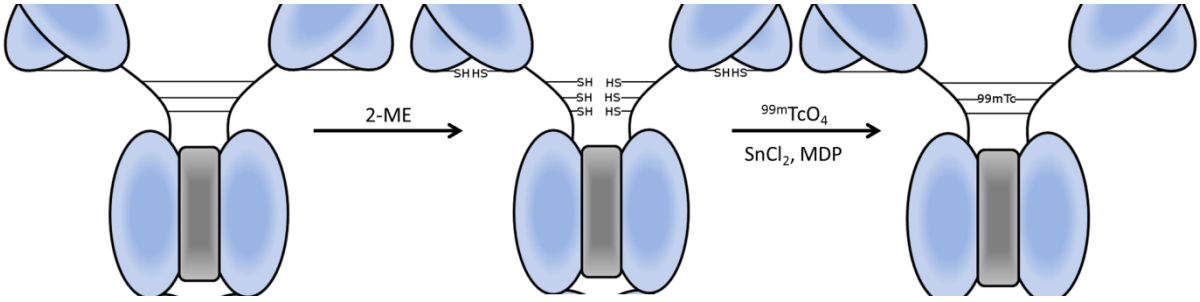

Figure 2.4 Direct labelling of IgG. Disulfides reduced by 2-mercaptoethanol followed by pertechnetate in the presence of a reducing agent ($SnCl_2$) and MDP. Free cysteines co-ordinate with reduced ^{99m}Tc(V) and disulphides reform.

2.1.5 Monoclonal Antibody SER-4

The mAb SER-4 recognises the antigen sialoadhesin (Sn), a Mϕ-restricted cell surface marker (Crocker and Gordon 1989; Crocker, Kelm et al. 1991). Sn is a member of the sialic acid IgG-like lectin family of proteins which are characterised by affinity for specific sialic acid ligands (Kelm, Pelz et al. 1994), and so far has been identified in humans (Hartnell, Steel et al. 2001), mice (Crocker and Gordon 1989), rats (Dijkstra, Dopp et al. 1985), pigs (Revilla, Poderoso et al. 2009) and chimpanzees (Brinkman-Van

der Linden, Sjoberg et al. 2000). Endogenously, the highest levels of Sn expression are found in Mϕ populations located in the LNs and spleen, typically bordering lymphoid tissue and transiting fluid. Sn induction is broadly related to type I and II interferons (vandenBerg, vanDie et al. 1996; Hartnell, Steel et al. 2001; Delputte, Van Breedam et al. 2007), and Sn positive Mϕ exhibit immunoregulatory behaviour both *in vivo* and *in vitro* (Oetke, Vinson et al. 2006; Ip, Kroner et al. 2007; Wu, Rauch et al. 2009). Targeting of antigens to Sn positive Mϕ has been shown to be an efficient means of evoking an immune response (Backer, Schwandt et al. 2010; Poderoso, Martinez et al. 2011), whilst deletion of this subset can enhance autoimmunity (Miyake, Asano et al. 2007; McGaha, Chen et al. 2011). However knock down of Sn has been shown to reduce disease severity in various autoimmune models (Jiang, Hwenda et al. 2006; Ip, Kroner et al. 2007; Wu, Rauch et al. 2009), which altogether illustrates an immunoregulatory role. Sn positive Mϕ have been detected in various preclinical disease models and in clinical settings including tumour infiltrates (Nath, Hartnell et al. 1999), glomerular nephritis (Ikezumi, Suzuki et al. 2005) and rheumatoid arthritis (Hartnell, Steel et al. 2001). Hence non-invasive imaging of Sn positive Mϕ may inform upon an important class of immunologically active cells.

2.2 Materials and Methods

2.2.1 SER-4 Hybridoma

Anti-mouse Sn SER-4 antibody was isolated as previously described using the SER-4 hybridoma (Crocker PR, 1989) which was kindly provided by Dr. Paul Crocker (University of Dundee, Dundee, UK)). Cells were grown in 1640 RPMI (Sigma, Poole, UK) supplemented with pen/strep (Invitrogen) and IgG depleted FBS (Source Bioscience UK Ltd, Nottingham, UK). 8 x 10^6 cells were suspended in 5 mL then transferred to a Celline CL350 flask (Figure 2.4; Integra Biosciences AG). Cells were pelleted every 7 days, and the supernatant harvested with the pellet resuspended 1:4 in media and returned to the CL350 flask.

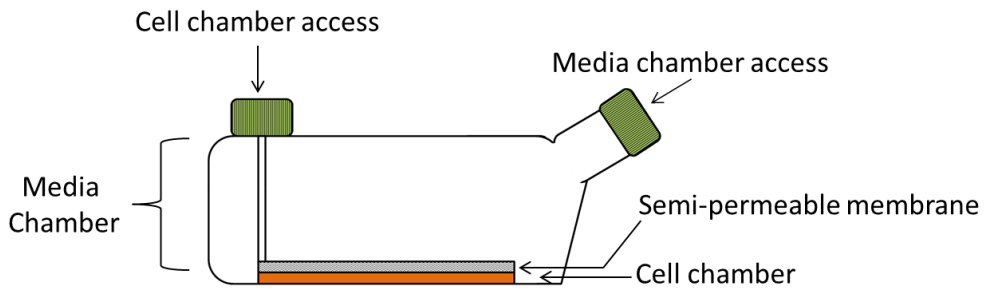

Figure 2.5 Celline CL350 design. Celline CL350 permits high densities of hybridoma cells to be cultured by continuous exchange of fresh nutrients and media from media chamber through semipermeable membrane into the cell chamber by diffusion. 10 kDa molecular weight cut-off for semipermeable membrane results in retention of serum proteins and antibody in the cell chamber, facilitating purification as well as decreasing FBS consumption as media chamber can be used with unsupplemented media.

2.2.2 SER-4 Purification

5 mL of supernatant from SER-4 hybridoma (Crocker and Gordon 1989) was diluted in 5 mL binding buffer (20 mM sodium phosphate, pH 7.0) and passed through a 0.22 µm filter. Filtrate was loaded on to a 5 mL HiTrap Protein G HP column (GE, Chalfont St. Giles, UK) then washed with 10 column volumes of binding buffer. Antibody was eluted with 0.1 M glycine-HCl, pH 2.7, collected in 2.5 mL fractions and neutralised with 200 µL of 1 M Tris.HCl, pH 9.0. Protein concentration was determined by measuring OD_{280} using a Biophotometer (Eppendorf, Cambridge, UK). Protein fractions were transferred to dialysis cassettes (Thermofisher, Loughborough, UK) and dialysed in phosphate buffered saline (PBS) with 3 buffer exchanges. Antibody was then concentrated using Vivaspin columns (Sartorius Stedim, Epsom, UK) to 10 mg/mL. Protein fractions were then analysed by reduced and non-reduced SDS PAGE (200 V, 120 A, 50 min). Gels were then stained with SimplyBlue Safe Stain (Invitrogen, Paisley, UK) for 45 minutes followed by 3 washes with deionised water.

2.2.3 Immunohistochemistry

Spleens from 8 week old male C57BL/6 mice were harvested, embedded in OCT (RA Lamb Ltd, Eastbourne, UK) and snap frozen in liquid nitrogen. Tissues were then cut 5 µm (Bright Instruments, Huntingdon, UK) and mounted onto polylysine slides

(Thermofisher, Loughborough, UK). Sections were air dried overnight, transferred to 50 mL Falcon tubes (BD Biosciences) and then stored at -80°C.

For staining, sections were left at room temperature for 10 min before removing from the falcon tube. Sections were immersed in chilled acetone for 5 min. and then left to air dry for 15 min. Sections were incubated in 0.3% H_2O_2 in PBS (BDH) for 30 min followed by avidin/biotin blocking (Vector Laboratories, Burlingame, USA). Sections were incubated overnight with SER-4 (1 µg/mL), followed by incubation with biotinylated goat anti-rat secondary (10 µg/mL, BD), and finally streptavidin-horse radish peroxidase (undiluted, Pharmingen, San Diego, USA). Samples were visualised using the Vector NovaRed Substrate kit (Vector Labs) and counter stained with haematoxylin (RA Lamb Ltd, Eastbourne, UK), followed by washing, dehydration and mounting in DPX mountant (BDH). Images were captured using a Leica Leitz DMRB research microscope and Micro-Publisher 3.3 RTV camera. Images were analysed with Image-Pro Plus 7.0 from Media Cybernetics software and Photoshop.

2.2.4 Preparation of ^{99m}Tc-SER-4

200 µL of purified SER-4 (10 mg/mL, PBS) was incubated with 2 µL of 2-mercaptoethanol (14.3 M, Sigma Aldrich, Poole, UK) for 30 min at 21°C. The solution was transferred to a PD MiniTrap G-10 column (GE Healthcare, Chalfont St. Giles, UK) and eluted with degassed PBS. 0.5 mL fractions were collected and OD_{280} determined using a BioPhotometer (Eppendorf, Cambridge, UK). Fractions with an OD_{280} corresponding to antibody concentrations of >1 mg/mL were pooled, aliquoted into 20 µL fractions, snap-frozen in liquid nitrogen and stored at -80^{o} C until further use.

To establish the influence of methylene diphosphonate (MDP) kit volume on radiolabelling efficiency, radiolabelling was initially performed using X µL (X = 0, 5, 7.5, 15, 20) of a reconstituted MDP kit (Medronate Draximage, Draxis, USA) added to 20 µL of freshly thawed reduced SER-4, followed by 200 MBq of sodium pertechnetate Tc-99m in a volume of 20 to 40 µL saline (kindly provided by Department of Nuclear Medicine at Guys Hospital UK) then incubated at room temperature for 30 min.

Labelling efficiency measured using instant thin layer chromatography-SA (ITLC-SA) strips (Varian Medical Systems UK, Ltd., Crawley, UK) using a mobile phase of 0.1 M citrate buffer, pH 5, and analysed using a gamma ray thin layer chromatography (TLC) scanner (Lablogic, UK). Labelling efficiency was assessed also by high performance liquid chromatography-size exclusion chromatography (HPLC-SEC) using a BioSep SEC-300 column (Phenomenex, Macclesfield, UK) with an isocratic mobile phase of 100 mM phosphate buffer pH 7.0 at a flow rate of 1 mL/min and in-line gamma detector (Lablogic, UK). Mouse IgG2a isotype (AbD Serotec, Oxon, UK) control IgG was prepared as described above.

2.2.5 ^{99m}Tc-SER-4 Serum Stability

50 MBq of ^{99m}Tc labelled SER-4 or isotype control IgG were added to AB type human serum (Sigma) or 0.1 M PBS (Gibco) at 1:4 v/v and incubated at 37 °C for 20 h. Samples were analysed at 0, 4, 6 and 20 h by HPLC-SEC using a BioSep SEC-300 column (Phenomenex, Macclesfield, UK) with an isocratic mobile phase of 100 mM phosphate buffer, pH 7.0, at a flow rate of 1 mL/min. Serum stability was calculated as the area under the ^{99m}Tc-SER-4 peak (retention time = 8 min 25 sec) as a fraction of total activity.

2.2.6 *In vitro* ^{99m}Tc-SER-4 Binding Assay

0.1 µg of labelled antibody (0.1 µg/µL) was added to 0.2 µg of recombinant sialoadhesin-Fc fusion protein (Sn-Fc, 6.7 µg/mL) (Kelm, Pelz et al. 1994) (kindly provided by Dr. Paul Crocker (University of Dundee, UK) and incubated at 37 °C. Binding to Sn-Fc was measured by HPLC-SEC using a BioSep SEC-300 column (Phenomenex, Macclesfield, UK) with an isocratic mobile phase of 100 mM phosphate buffer, pH 7.0 at a flow rate of 1 mL/min and compared to the ^{99m}Tc-IgG isotype binding. Specificity was shown by comparison with the binding of isotype ^{99m}Tc-IgG and by blocking with a 10-fold excess of cold SER-4.

2.3 Results

2.3.1 SER-4 Purification

SER-4 antibody was purified from the supernatant of SER-4 hybridoma grown in IgG depleted media using Protein G purification. Yields of between 9 – 12 mg/L of unsupplemented media were recovered. Hybridoma supernatant displayed the presence of SER-4 by protein band at approx. 150 kDa, which approximates to the size of an intact IgG (lane 1 – see Figure 2.6). The absence of this band in the loading fraction indicates the successful extraction of SER-4 antibody from the hybridoma supernatant (lane 2). Similarly the wash fraction displayed no IgG contamination (lane 3). Protein collected from the elution fraction indicated the presence of IgG (lane 4) with reduction resulting in the disappearance of intact IgG band and emergence of heavy and light chain protein bands at c.25 and 50kDa mass (lane 5).

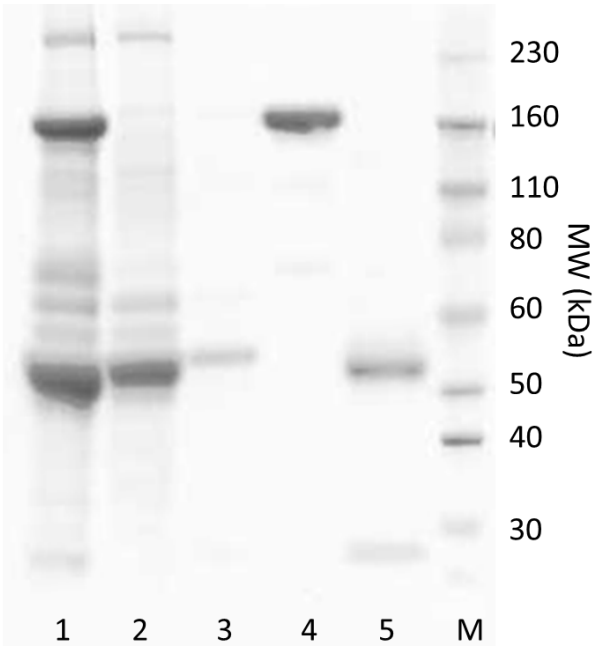

Figure 2.6 Protein G purification of SER-4. SER-4 hybridoma supernatant (lane 1) was loaded on to a Protein G column (unbound loading fraction – lane 2) which was then washed (wash fraction - lane 3). SER-4 antibody was then eluted (lane 4). A sample of SER-4 was then reduced (lane 5). Fractions were run on SDS-PAGE and stained with SimplyBlue.

2.3.2 Immunohistochemistry

Frozen spleen sections were incubated overnight with SER-4, followed by biotinylated secondary and streptavidin-HRP with VectorRed substrate for staining. Nuclei were counter-stained with haemotoxylin. In the absence of SER-4, white pulp can be observed as patches of heavy nuclear staining encapsulated by less nucleated red pulp (see Figure 2.7 A). Incubation with SER-4 reveals elliptical rings of SER-4 staining delineating the border between the white and red pulp regions of the spleen. Sporadic staining is also observed in the red pulp region (see Figure 2.7 B).

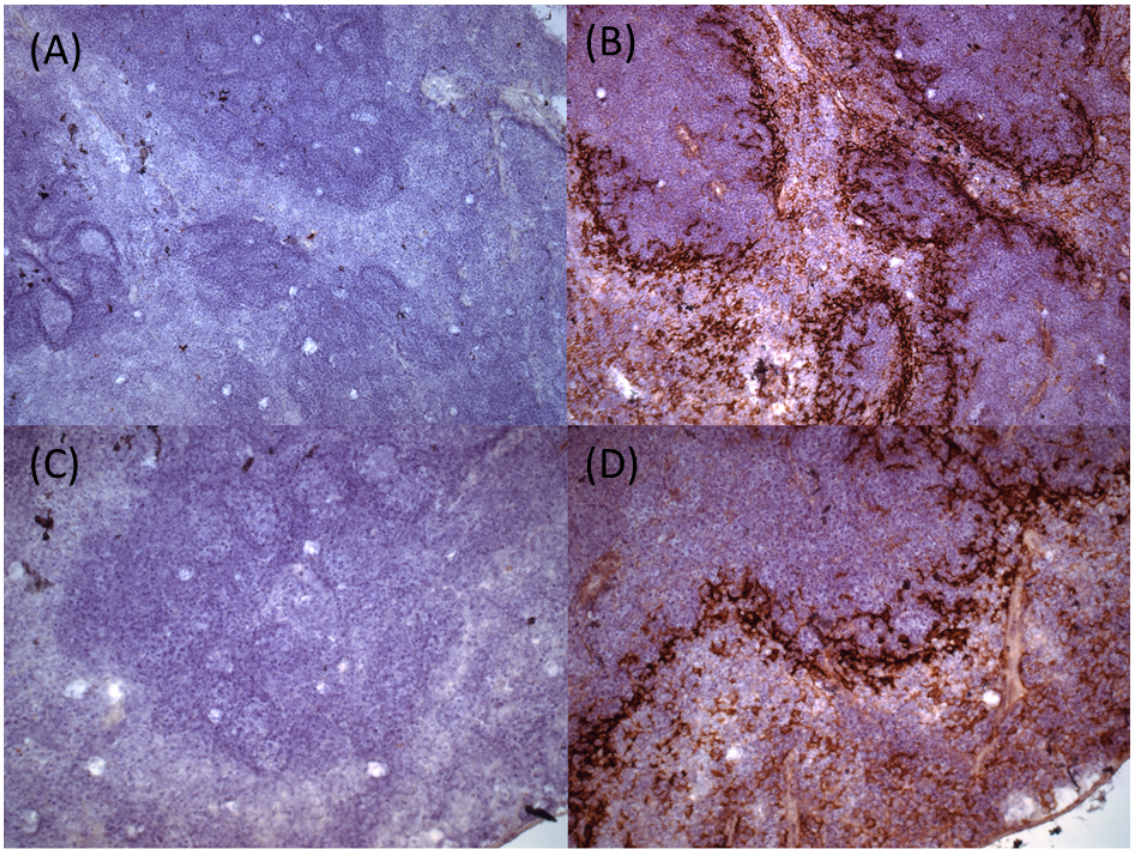

Figure 2.7 SER-4 staining of spleen. Mouse spleens were incubated with PBS (A + C) or SER-4 (B + D) overnight, followed by appropriate secondary/substrate and counter stained with haemotoxylin. Regions of increased nuclear staining identify the white pulp characterised by abundant lymphocyte populations, whilst sparser nuclear stain corresponds to red pulp composed of a loosely populated, sinusoidal structure. Perimeter between white and red pulp containing MMMs stains strongly for SER-4, with sporadic staining observed in the red pulp. Top row: magnification x 100, bottom row: magnification x 200.

2.3.3 Preparation of ^{99m}Tc-SER-4

SER-4 was partially reduced by incubation with 2-mercaptoethanol, purified and stored in frozen aliquots then radiolabelling performed by addition of pertechnetate with freshly reconstituted MDP kit. Radiochemical purity and yield were assessed by SEC radioHPLC with PBS as eluent and ITLC using citrate buffer (pH 5, 0.1 M), respectively. SEC radioHPLC showed two peaks with > 99% of activity eluted at 8 min 25 sec, corresponding to antibody fraction, and a negligible proportion (< 1%) eluted at 17 min 45 sec, corresponding to free pertechnetate (see Figure 2.8 A). ITLC shows presence of protein-associated activity (Rf = 0) with an absence of free Tc-99m *pertechnetate* (Rf = 1) (see Figure 2.8 B).

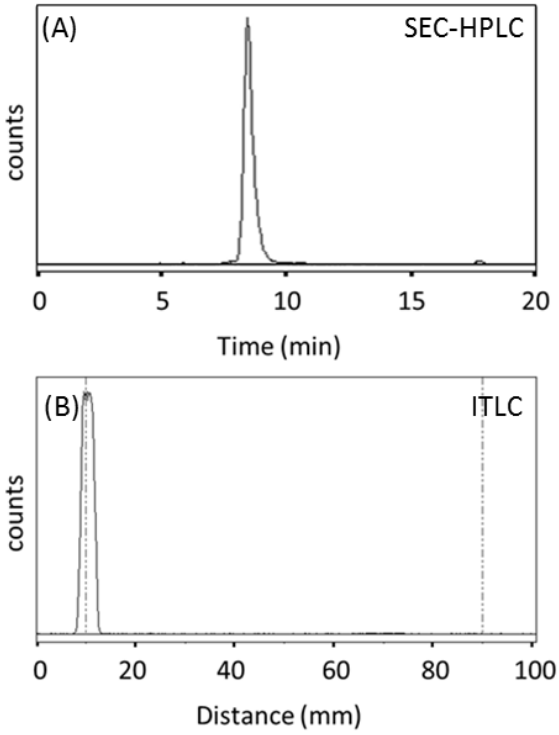

Figure 2.8 Direct labelling of SER-4. Following disulphide reduction, SER-4 was labelled with ^{99m}Tc. (A) Samples were injected on SEC radioHPLC showing elution of majority activity with the antibody (t = 8 min 20 sec, > 99%) and a minor peak (t = 17 min 45 sec, < 1%). (B) ITLC showed the presence of radiolabelled protein (Rf = 0, 100%) and no free pertechnetate (Rf=1, 0%).

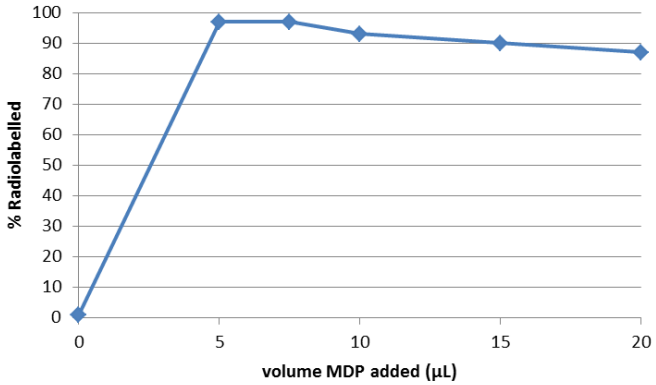

Figure 2.9 % Radiolabelling with respect to MDP kit volume added. In the absence of MDP, only small amounts of antibody are labelled (1%). Addition of intermediate amounts of MDP kit (5 and 10 µL) achieves 97% radiolabelling, whilst further increases in MDP kit addition diminish % radiolabelling.

The influence of MDP kit volume on % radiolabelling was established by addition of various amounts of kit to constant amounts of antibody and activity. With no MDP present, radiolabelling is 1%, whilst addition of both 5 and 10 µL of MDP kit achieved 97% labelling, which dropped with increasing amounts of kit (see Figure 2.9)

2.3.4 ^{99m}Tc-SER-4 and Isotype Serum Stability

^{99m}Tc-SER-4 was incubated in the presence of serum or PBS and stability assessed by SEC radioHPLC at the time points 0, 4, 6 and 20 h. In the presence of PBS alone, % radiolabelling decreases over 20 h (see Table 2.2) whilst in the presence of serum the speciation of activity remains unchanged. In serum at 20 h, 98% activity is associated with antibody (elution time 8 min 25 sec) with 2 % released as free pertechnetate (elution time 17 min 45 sec). In PBS the values change to 92 % and 8 % for antibody bound and free pertechnetate peaks, respectively (see Figure 2.8). Similarly the isotype demonstrates greater stability in serum (97 % antibody radiolabelled at 20 h) than in PBS (89 % antibody radiolabelled at 20 h) (see Figure 2.10).

	Time (hr)	0	4	8	20
SER-4	Serum (% bound)	98	98	98	98
	PBS	99	96	94	92
Isotype	Serum	100	100	98	97
	PBS	100	98	95	89

Table 2.2 Serum stability of ^{99m}Tc labelled SER-4 and Isotype. Antibodies were labelled according to 2.3.3, incubated in either mouse serum or PBS and stability assessed by SEC radioHPLC. Percentage bound was assessed by comparison of bound activity to that of free activity peaks.

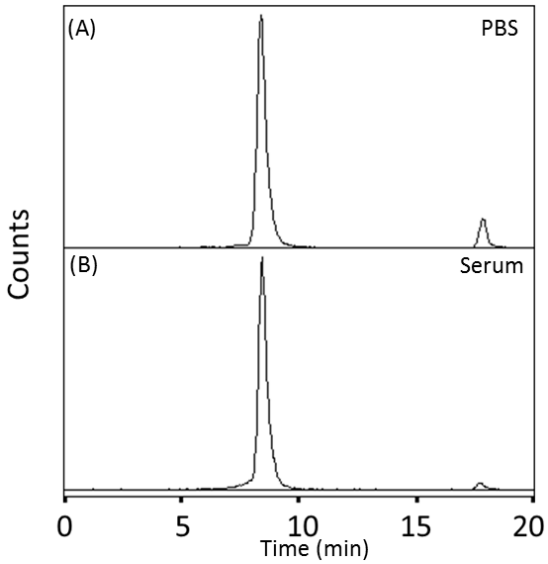

Figure 2.10 SEC radioHPLC analysis of ^{99m}Tc-SER-4 stability at 20 hr. ^{99m}Tc-SER-4 was incubated in the presence of PBS (A) or serum (B) for 20 hr at 37°C then injected into SEC radioHPLC system. Percentage bound was assessed by comparison of bound activity (integral of 8 min 25 sec peak) to that of free activity (integral of 17 min 45 sec peak).

2.3.5 In vitro ^{99m}Tc-SER-4 Binding Assay

Binding of ^{99m}Tc-SER-4 was semi-quantitatively assessed by binding to recombinant Sn-Fc fusion protein using SEC radioHPLC. Binding was observed by a shift in retention time of the gamma signal owing to increased mass of ^{99m}Tc-SER-4+Sn-Fc as compared to free ^{99m}Tc-SER-4. Free ^{99m}Tc-SER-4 eluted with a retention time of 8 min 35 sec (see Figure 2.11 A) whereas ^{99m}Tc-SER-4 in the presence of Sn-Fc eluted at 7 min 20 sec (see Figure 2.11 B), with 82% activity associated this peak. A proportion of unbound ^{99m}Tc-SER-4 (2% of total activity) was also detected at 12 min 45 sec. The binding of ^{99m}Tc-SER-4 to Sn-Fc was completely abrogated by the presence of 10 fold excess unlabelled SER-4 (see Figure 2.11 C). Isotype control ^{99m}Tc-IgG had a retention time of 8 min 30 sec and did not bind Sn-Fc (see Figure 2.11 D)

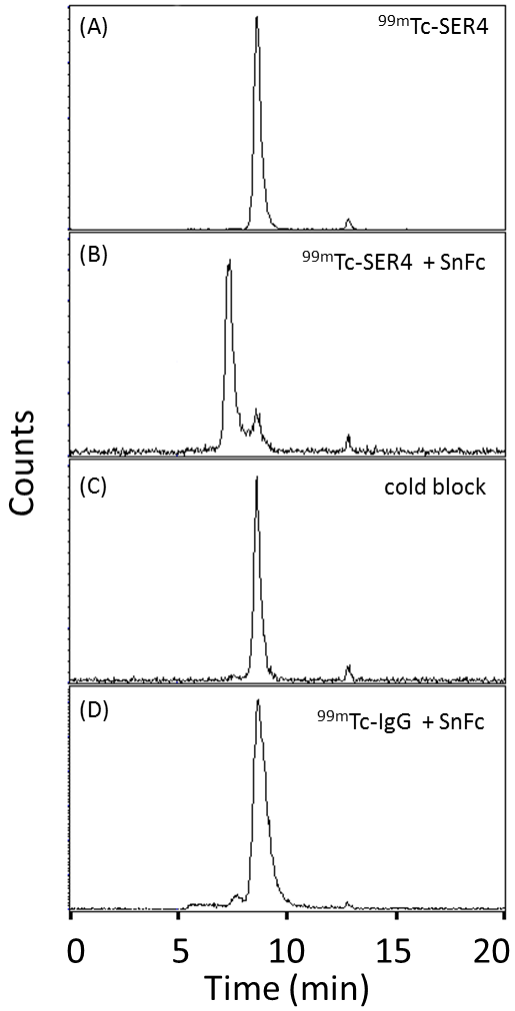

Figure 2.11 SEC radioHPLC analysis of ^{99m}Tc-SER-4 binding. Binding of ^{99m}Tc-SER-4 to recombinant Sn-Fc protein was assessed by SEC radioHPLC. Unbound ^{99m}Tc-SER-4 eluted with a retention time of 8 min 35 sec (A) whilst ^{99m}Tc-SER-4 in the presence of Sn-Fc showed a shift in retention time to 7 min 20 sec corresponding to ^{99m}Tc-SER-4+Sn-Fc complex along with some unbound ^{99m}Tc-SER-4 (B). Binding to Sn-Fc was completely abrogated by incubation with 10 fold excess of cold SER-4 (C) whilst ^{99m}Tc-IgG showed no binding to recombinant Sn-Fc (D).

2.4 Discussion

SER-4 hybridoma was grown using the Celline CL350 system in order to minimise the quantity of media supplements required as compared to using a traditional T75 flask procedure. This was especially relevant with regards to the consumption of IgG-depleted FBS, an expensive media supplement essential for the purification of mAb free from contaminating IgG. In this system approximately 4 mL supernatant was recovered per week, from which between 3 – 4 mg of SER antibody could be retrieved at the expense of 350 mL unsupplemented media. Thus a recovery of 9 – 12 mg per

litre was produced, making the Celline system an efficient means of producing SER-4 antibody.

The purification of hybridoma supernatant using Protein G resulted in a protein band corresponding to the expected mass of an intact mononclonal IgG antibody (approx. 150 kDa). Reduction of the purified protein resulted in the characteristic bands at 25 and 50kDa corresponding to the light and heavy chain repsectively (see Figure 2.4). Confirmation of SER-4 binding to endogenous Sn was demonstrated by staining frozen mouse spleen sections SER-4. Incubation with SER-4 revealed elliptical staining pattern characteristic of marginal metallophilic Mϕ forming boundaries between the red and white pulp regions of the spleen (see Figure 2.5) (Crocker, Hill et al. 1988).

SER-4 was was radiolabelled with ^{99m}Tc using the direct labelling method described by Mather and Ellison (Mather and Ellison 1990). The selection of radioisotope and the method employed were complementary: direct labelling is a fast and convenient means of labelling antibodies, and is used clinically (hence reliable, robust and reproducible). Direct radiolabelling involves partial reduction of disulphide bonds concentrated in the hinge region of the intact antibody such that the overall structure is preserved. Pertechnetate is then reduced by $SnCl_2$ and weakly chelated to the ligand MDP in the presence of the partially reduced antibody. Weak chelation of Tc(V) results in transfer of ^{99m}Tc to only sites with higher affinity than MDP, thus decreasing occupancy of low affinity sites from which ^{99m}Tc could be stripped easily *in vivo*. Once transferred to reduced disulphide it is speculated that the bridge is reformed with ^{99m}Tc linking the cysteines. Mather and Ellison also reported that the presence of contaminating 2-mercaptoethanol from the reduction step in the radiolabelling step was desirable for optimal radiolabelling. They reasoned that contamination possibly prevents the rapid reoxidation of reduced disulphides as well as maybe participating in chelation with ^{99m}Tc (Mather and Ellison 1990).

With the variables of MDP volume, amount of activity and antibody concentration during radioabelling it was decided in order to conserve antibody stocks that the amount of activity used would be based upon clinically administered activites. Clinically direct labelling of antibodies routinely achieves 1 – 5 MBq/µg antibody

(Gmeiner Stopar, Fettich et al. 2008; Malviya, de Vries et al. 2011) and so a value of 2 MBq/µg of SER-4 was selected. MDP kit addition was then varied to establish what volume would achieve the greatest labelling efficiency for 200 MBq $^{99m}TcO_4$ added to 100 µg SER-4. Addition of 5 µL of reconstituted MDP kit (approx 10% total volume) achieved a maximum labelling efficiency, whereas addition of >10 µL saw a decrease in % radiolabelling. This was probably due to excess MDP competing with reduced disulphides for binding to ^{99m}Tc. Absence of MDP kit resulted in negligible labelling (1%) as $SnCl_2$ reagent is required for reduction of Tc to permit bonding with free cysteines.

SER-4 was reduced in batch, then aliquoted and snap frozen in order to provide a stock of reduced antibody for labelling. This was done for convenience as well as to reduce variation in radiolabelling. Aliquots were radiolabelled then quality control was performed via radioTLC and SEC-radioHPLC. These techniques are complimentary as radioTLC is a reliable method of assaying total bound and unbound activity (radiochemical yield) whilst radioHPLC is able to resolve labelled proteins (radiochemical purity). By ITLC a high radiochemical yield was routinely achieved, however the quantity of contaminating colloidal pertechnetate was not established (see Figure 2.6 A). SEC radioHPLC showed a high radiochemical purity and gamma counter detection of the guard column inidcated an absence of trapped colloidal pertechnetate. Using these techniques, antibody radiolabelling >99% was consistently achieved.

Serum stability of ^{99m}Tc-SER-4 was assayed by incubation of the radiotacer in serum or PBS and sampling performed at 0, 4, 6 and 20 hr time points. Radiolabelled antibody in the presence of PBS exhibited higher instability than in serum. The observed degradation in the absence of serum could be the result of radiolysis, a process in which it is thought free radicals generated during radioactive decay can lyse chemical bonds and lead to loss of a radioisotope from its parent radiopharmaceutical. Thus it is speculated that the presence of free radical scavengers, such as bovine serum albumin, can mitigate this effect (Chakrabarti, Le et al. 1996).

The immunoreactive fraction of ^{99m}Tc-SER-4 was determined by binding to recombinant Sn-Fc protein followed by analysis using radioHPLC in conjunction with a SEC. Recombinant Sn-Fc contains the first 4 N-terminal domains of Sn fused to the Fc-portion of human IgG, resulting in a dimer with approximate mass of 150kDa (Crocker, Freeman et al. 1995). Binding of ^{99m}Tc-SER-4 to at least one epitope per dimer would result in a mass increase of approximately double the native antibody, significant enough to alter the retention time of the antigen-antibody complex relative to the free antibody by size exclusion chromatography.

However, resolution of the antigen-antibody and antibody peaks was incomplete, which prevented affinity from being calculated reliably as peak integrals could only be approximated. For this assay, the lowest detectable ^{99m}Tc-SER-4 concentration by radioHPLC was determined and then incubated with an excess of recombinant Sn-Fc protein for 30 min. The resulting binding trace was used to determine the minimum immunoreactive fraction, calculated at 82%. Specificity of binding was shown by blocking in the presence of 10 fold excess of cold SER-4 as well as by absence of antigen-antibody complex in the after incubation of Sn-Fc with control ^{99m}Tc-IgG.

2.5 Summary

A novel radiopharmaceutical for Mϕ imaging, ^{99m}Tc-SER-4, has been prepared and evaluated *in vitro*. It binds to the cell membrane marker Sn in marginal metallophilic Mϕ found in splenic tissue section as well as to soluble antigen in solution. An efficient Tc-99m labelling procedure has been developed with specific activities that will allow for *in vivo* imaging. The directly-labelled antibody SER-4 displays both serum stability and affinity for the target antigen, making it suitable for *in vivo* imaging of Sn positive Mϕ.

Chapter 3:

In vivo SPECT Imaging of ^{99m}Tc-SER-4

3.1 Introduction

Radiolabelled antibodies are increasingly important as a means of visualising pathology, finding utility in the diagnosis of disease and following its response to treatment. In the instance of chronic ailments, such as with maintenance of transplant tolerance, patient treatment relies on the early identification of rejection events so as to manage exposure to otherwise deleterious drug regimens whilst prolonging transplant viability. Approaches to identifying pathological processes involve detecting the cellular or molecular effectors of disease, or their by-products, using a suitable sensor. One such cellular effector is the Mϕ, an important cell type in homeostasis but also critical to pathogenesis in various disease settings. A notable feature of Mϕ is their considerable phenotypic variability, where often it is their activation state and not just presence that determines the outcome of disease. In this chapter we aim to evaluate the *in vivo* behaviour of the putative SPECT imaging agent ^{99m}Tc-SER4 in detecting endogenous Mϕ populations as well as recruited inflammatory Mϕs during acute transplant rejection.

3.1.1 Antibody Imaging

The clinical imaging of radiolabelled antibodies is now routinely performed for both diagnostic and dosimetry purposes. The use of a radiolabelled mAb in diagnosis can reveal the presence of pathology, the suitability of a given therapy (e.g.using the unconjugated antibody) and also allow monitoring of a subjects response to treatment. Alternatively dosimetry studies can be performed prior to radioimmunotherapy with a conjugated mAb which allows the calculation of the maximum administered dose whilst minimising undesirable effects, such as myeloablation (Goldsmith and Signore 2010). For these reasons numerous mAbs have been radiolabelled and their in vivo properties assessed, of which the selected targets can be divided into one of three classes. These are: 1) antibodies that target structures

unique to specific cell types, such as T and B cells (Malviya, Galli et al. 2010), in order to track the immune response during pathology; 2) antibodies directed to cancer cell-associated antigens which permits the direct identification of malignant cell types; 3) antibodies which target secretory products/signalling molecules associated with a pathological process (Glaudemans, Dierckx et al. 2010).

3.1.2 Transplant Rejection

During transplant rejection, the donor organ promotes an immune response in the recipient in which T cells play a central role. By recognising mismatches in the donor MHC or other donor polymorphic cellular proteins, host T cells will either eliminate donor cells directly, via CD8 effector cells, or by driving the expansion of B cells directing antibody to the grafted organ. Additionally, T_{reg} cells are thought to be important for the maintenance of tolerance to a transplanted organ. Aside from T cells, components of innate immunity also play a variety of roles during transplant rejection and tolerance. In this setting the presence of Mϕ is generally associated with graft rejection and/or resistance to tolerance induction (Li 2010). The significance of this cell type is underlined by depletion of Mϕ in a murine cardiac transplant model resulting in a 70% decrease cardiac allograft vasculopathy (CAV), a hallmark of chronic rejection (Kitchens, Chase et al. 2007).

Despite advances in the median survival rate of cardiac transplant recipients (from 8.3 years in the 1980's to 10.4 years in the 1990's), long term survival has not significantly altered in the last 20 years (Stehlik, Edwards et al. 2010) Post transplantation patients receive immunosuppressive therapy to help maintain tolerance to the transplanted organ with the complication that immune compromised individuals are more likely to develop malignancy or infection. Hence transplant recipients receive on going immune monitoring in order to predict acute events but also to determining an individual's immune response so as to minimise these toxic immunosuppression regimens (Sawitzki, Schlickeiser et al. 2011).

3.1.3 Imaging Transplant Rejection

Despite the development of non-invasive techniques to identify acute cellular rejection in cardiac transplants, none so far have replaced the surveillance biopsies due to failure to validate the preliminary findings of these studies. With its invasive nature and associated risk coupled with non-representative sampling, there is a clinical need to replace biopsy sampling with non-invasive monitoring of rejection (Labarrere and Jaeger 2012). In the instance of cardiac transplant rejection, the requirement for molecular imaging is outlined by morphological/functional imaging techniques such as echocardiogram being insufficiently sensitive to detect early rejection events, and leading to diagnosis only after irreparable damage to the transplanted organ has occurred (Christen, Shimizu et al. 2010). Despite this need, only preliminary studies have been performed using molecular imaging to monitor transplant status. Thus far, only radiolabelled annexin-V (which targets exposed phosphatidylserine on apoptotic cells) has been used clinically to study transplant rejection, and has shown a correlation between rejection severity and tracer uptake (Narula, Acio et al. 2001).

Preclinically, Mϕ-targeting iron oxide nanoparticles (see Chapter 1) have been shown to image both renal and cardiac transplant rejection and to be able to detect the response to immune suppressive therapy (Wu, Ye et al. 2011). More recently, the ^{19}F MRI has been examined to monitor acute transplant rejection, offering the advantage over iron oxide nanoparticles as the signal detected is unique to the tracer rather than emerging from the water. This makes detecting the tracer far less ambiguous, although suffers from the drawback that is even less sensitive than ^{1}H nanoparticle MRI (Hitchens, Ye et al. 2011). The utility of Mϕ imaging has been shown by recruitment monitored during chronic renal rejection using USPIOs to show improved sensitivity of early detection over routinely used biochemical markers (Beckmann, Cannet et al. 2006).

3.2 Materials and Methods

3.2.1 Standard Biodistribution

Syringes (25G X 16mm, Terumo) were weighed before and after injection, and serial dilutions of 1:4 were performed with a starting 50 µL stock solution. Animals were injected via tail vein with approximately 20 MBq of ^{99m}Tc-SER4 in PBS (100 µL at 100 µg/ml). After culling according to schedule 1, the animals were dissected and the following organs collected: intestines, stomach, spleen, liver, kidney, heart, lungs, blood (20 µL), muscle, bone and tail. The tissue samples were weighed and radioactivity counted using a gamma counter (LKB Wallac, Finland). Injected dose was calculated from total activity in each injected syringe minus activity counted in tail, and presented as the percentage of injected dose per gram (%ID/g) of each tissue sample.

3.2.2 *In vivo* SPECT/CT Imaging

Imaging was performed using a nanoSPECT/CT small animal scanner (Bioscan Inc., Washington, USA) SPECT images were obtained using a 4-head scanner with 1 mm pinhole collimators. Helical acquisitions were performed with 24 projections with the time per projection adjusted so as to make overall scan time of 30 min. CT images were obtained using 45 KVp X-ray source, set with a 500 ms exposure time in 180 projections lasting approximately 10 min. Images were reconstructed using proprietary BioScan InVivoScope (IVS) software.

Adult male mice (C57BL/6, 8 – 10 weeks) were injected IV under anaesthesia (isoflurane, VetOne, UK) with approximately 20 MBq ^{99m}Tc-SER4 in 100 µL (100 µg/ml; n = 9). After injection, one mouse was transferred to nanoSPECT/CT and imaged continuously for 6 h. Non-imaged mice were recovered and culled at 1 h, 3 h and 6 h post injection (n = 3 per time point) after which standard biodistributions were performed.

8 week old C57BL/6 and C57BL/6 $Sn^{-/-}$ (Sn KO) male mice were injected IV under anaesthesia (isoflurane, VetOne, UK) with approximately 20 MBq ^{99m}Tc-SER4 or ^{99m}Tc-IgG in 100 µL (100 µg/ml; n = 3). Mice were recovered, then anaesthetised and imaged at 3 h. Mice were culled at 4 h post-injection followed by standard biodistribution.

3.2.3 Heart Transplant Rejection Model

Transplants were performed by L Meader, K Brown and W Wong. 8 week old allogeneic (BALB/c) and syngeneic (C57Bl/6) hearts were transplanted in to adult male mice (C57Bl/6) (Corry RJ, Primarily vascularized allografts of hearts in mice. The role of H-2D, H-2K, and non-H-2 antigens in rejection, 1973). Briefly, superior and inferior vena cava and pulmonary veins of the donor heart were ligated. The donor aorta was then anastomosed to the recipient aorta and the donor pulmonary artery anastomosed to the inferior vena cava in the recipient abdomen. The transplanted heart was perfused via the coronary arteries, resulting in a fully vascularised heterotopic transplant (see Figure 3.1).

7 days post transplantation mice were injected IV with approximately 20 MBq ^{99m}Tc-SER4 (1 mg/mL; n = 5 and 4 for allogeneic and syngeneic, respectively) or ^{99m}Tc-IgG in 100 µL (n = 5). Mice were imaged at 3 h and culled 4 h post-injection. Standard biodistributions were performed and additionally the donor hearts were collected, washed outside in PBS then divided in two approximately equal portions. One portion was weighed and gamma counted with the other collected tissues. The second portion was embedded in optimum cutting temperature (OCT) matrix (RA Lamb, Thermo Fischer Scientific), snap frozen in liquid nitrogen then stored at – 80°C for immunohistochemistry.

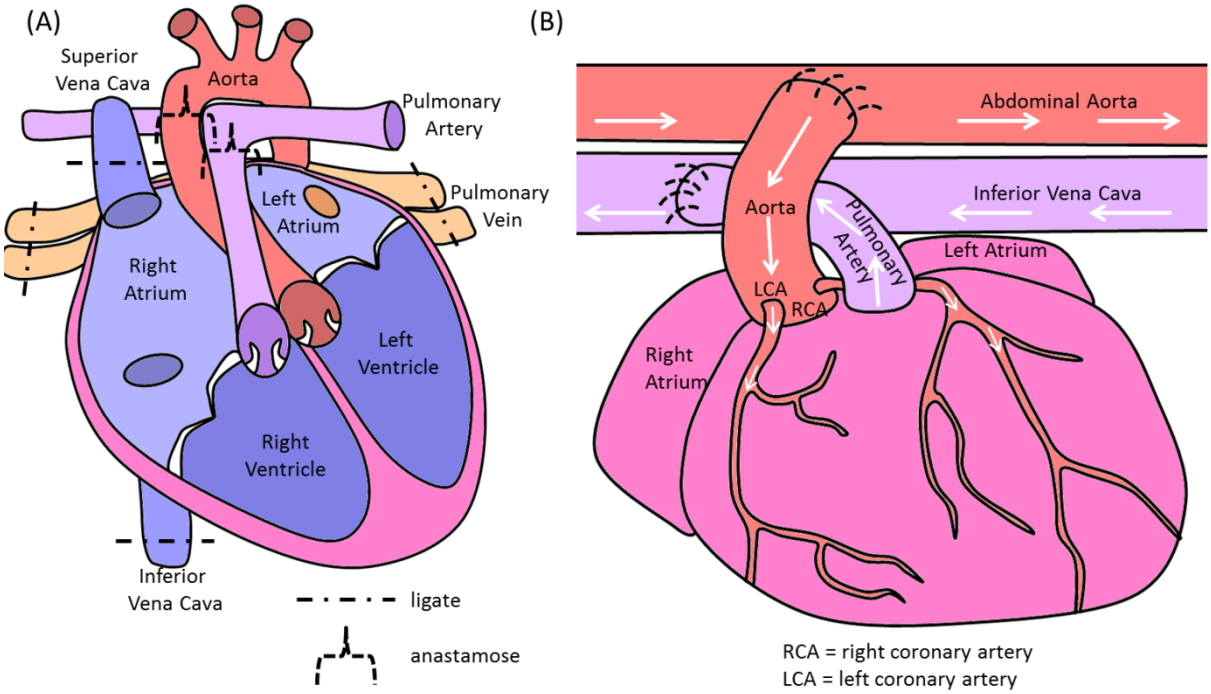

Figure 3.1 Schematic of Heart before and after transplantation. (A) The superior and inferior vena cava as well as the pulmonary vein is ligated in the pretransplanted heart, while the aorta and pulmonary artery are prepared for anastomosis. (B) The transplanted heart is placed in the recipient's abdominal cavity with donor aorta and pulmonary artery anastomosed to abdominal aorta and inferior vena cava. Perfusion of the transplanted heart takes place via the coronary arteries.

3.2.4 Statistical Analysis

All of the data are given as means ± SD of *n* independent measurements. Statistical analysis of experiments was performed with a Student T test using GraphPad Prism (GraphPad Software). Statistical significance was assigned for P values < 0.05.

3.2.5 Immunohistochemistry

OCT embedded tissues were cut at 5 µm using a Brightwater Cryostat (Bright Instruments, Huntingdon, UK) and mounted onto polylysine slides (Thermofisher, Loughborough, UK). Sections were air dried overnight, transferred to 50 ml falcon tubes (BD Biosciences) then stored at – 80°C until staining. For staining, sections were taken from freezer and left at room temperature for 10 min before removing from falcon tube. Sections were immersed in chilled acetone for 5 min and then left to air dry for 15 min. Sections were incubated in 0.3% H_2O_2 in PBS for (BDH) for 30 min

followed by avidin/biotin blocking (Vector Laboratories, Burlingame, USA). Sections were incubated overnight with SER4 (1 μg/mL), followed by incubation with biotinylated goat anti-rat secondary (10 μg/ml, BD), and finally streptavidin-horse radish peroxidase (Pharmingen, San Diego, USA). Samples were visualised using the Vector NovaRed Substrate kie (Vector Labs) and counter stained with haematoxylin (RA Lamb Ltd, Eastbourne, UK), followed by washing, dehydration and mounting in DPX mountant (BDH). Images were captured using a Lecia Leitz DMRB research microscope and Micro-Publisher 3.3 RTV camera. Images were analysed with Image-Pro Plus 7.0 from Media Cybernetics software and Photoshop.

3.3 Results

3.3.1 Biodistribution of ^{99m}Tc-SER4

Mice were injected with ^{99m}Tc-SER4 and one mouse scanned continuously for 6 hr post injection using nanoSPECT/CT (see Figure 3.2). Whole body imaging showed rapid accumulation of ^{99m}Tc in the spleen, liver and bone marrow, with a gradual drop in blood pool as seen in the observed heart signal along with a concomitant accumulation in the bladder. Imaging also revealed the uptake of ^{99m}Tc-SER4 in the intestines. Superior to the heart, and within the thoracic cage a signal was detected in the majority of mice. The origin of this uptake was not identified.

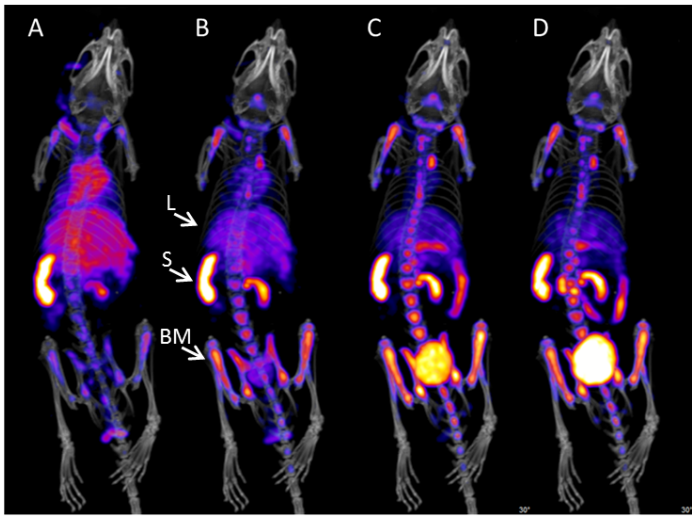

Figure 3.2 Static nanoSPECT/CT imaging of ^{99m}Tc-SER4 in wild type mouse. Mouse injected IV with ~20 MBq of ^{99m}Tc-SER4 and imaged over time. **A-D:** Static SPECT acquisitions at 30, 60, 180 and 360 min post-injection, respectively, overlayed on CT acquired 10 min post injection. Arrows indicate liver (L), spleen (S) and bone marrow (BM). Images normalised by application of same arbitrary threshold limits.

Alongside scanning, biodistributions were performed by weighing and measuring radioactivity of tissues removed from culled mice at 1 h, 3 h and 6 h post injection (n = 3 per time point - see Figure 3.3). Rapid accumulation of ^{99m}Tc-SER4 within an hour post injection was observed in the spleen, liver and bone marrow with 313, 87 and 22 %ID/g values recorded an hour post injection, respectively. Blood levels drop progressively from 39 %ID/g at 1 h, to 25 %ID/g at 3 h and 15 %ID/g at 6 h post injection.

A:

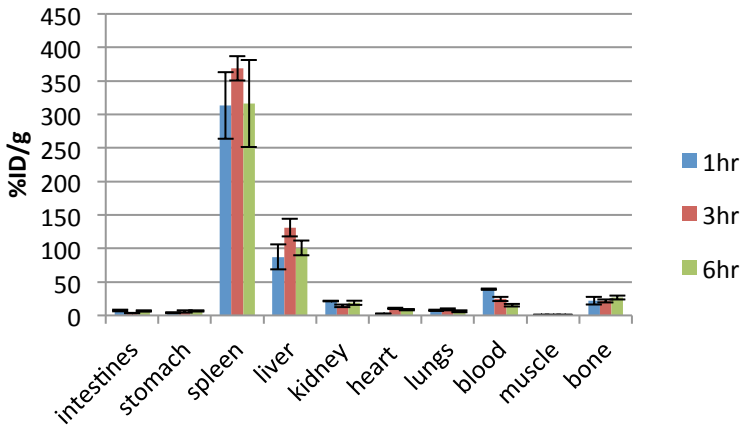

B:

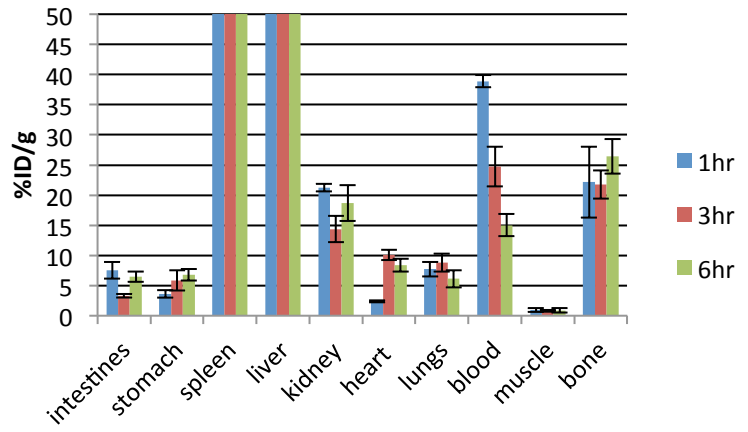

Figure 3.3 Biodistribution of ^{99m}Tc-SER4 in C57Bl/68 week old mice (n=3 per time point). Mice were injected IV into the tail vein with ~20MBq of 99mTc-SER4. After 1 h, 3 h and 6 h mice were culled and organs harvested, weighed and gamma counted. Radioactive uptake in organs is presented as the percentage-injected dose per gram per organ. **A:** Full biodistribution. **B:** Rescaled to a max of 50 %ID/g of A to see biodistribution of lower activity organs (error represents a standard deviation of n = 3)

3.3.2 Comparison of ^{99m}Tc-SER4/IgG in Wild Type and Sn KO mice

C57BL/6 Sn mice were injected with either ^{99m}Tc-SER4 or ^{99m}Tc-IgG and C57BL/6 $Sn^{-/-}$ mice injected with ^{99m}Tc-SER4. Mice were imaged at 3 h post injection and culled at 4 h. Whole body imaging showed absence of characteristic splenic and bone marrow uptake of ^{99m}Tc-IgG in wild type mice (Figure 3.4 A) as well ^{99m}Tc-SER4 in Sn KO mice (Figure 3.4 C), as compared to ^{99m}Tc-SER4 in wildtype mice (Figure 3.4 B). Both control

groups demonstrated significant blood pool (as observed by heart and carotid artery visualisation) as well as increased abdominal signal. In all three groups, bladder accumulation was observed.

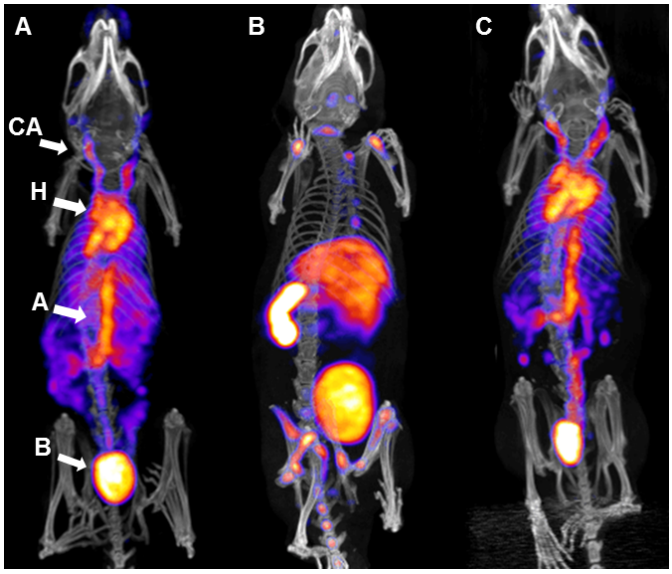

Figure 3.4 nanoSPECT/CT imaging of ^{99m}Tc-SER4 and ^{99m}Tc-IgG in wild type and Sn knockout mice. Wild type mice were injected IV with ~20 MBq of either ^{99m}Tc-IgG (A) or ^{99m}Tc-SER4 (B) and Sn knockout mice with ^{99m}Tc-SER4 (C) and imaged 3 hours later. Arrows indicate signal arising from carotid arteries (CA), heart (H), aorta (A) and bladder (B).

Biodistribution data records elevated splenic (207 %ID/g) and bone marrow (40 %ID/g) uptake of ^{99m}Tc-SER4 in wild type versus KO mice (8 and 4 %ID/g for spleen and bone marrow, respectively) as well as enhanced uptake compared to control ^{99m}Tc-IgG in wild type mice (17 and 9 %ID/g for spleen and bone marrow, respectively). Liver uptake was also higher for ^{99m}Tc-SER4 in wild type mice (38 %ID/g) as compared to in the KO (10 %ID/g) and ^{99m}Tc-IgG in wild type mice (26 %ID/g) (see Figure 3.5). The presence of contaminating blood pool signal is significant (especially when considering highly vascularised organs such as the heart and liver). Tissue-to-blood ratios attempt to correct for the influence of blood pool signal from specific uptake for each tissue, with spleen, liver and bone marrow showing on average 28, 4 and 10 times higher tissue-to-blood ratio, respectively, in wild type mice injected with ^{99m}Tc-SER4 as compared to the control groups (^{99m}Tc-IgG in wild type mice plus ^{99m}Tc-SER4 in Sn KO mice) (see Figure 3.6).

A:

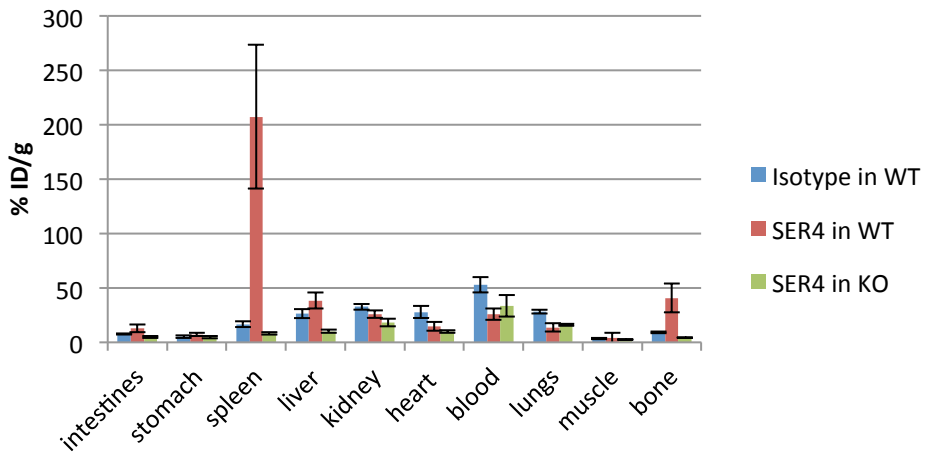

B:

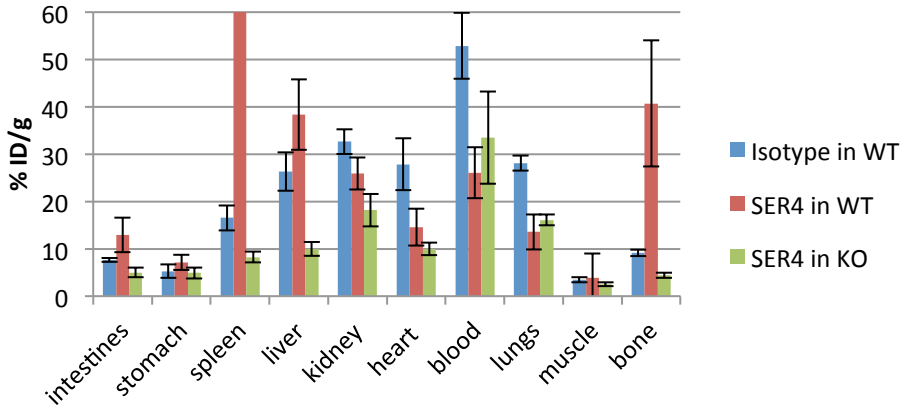

Figure 3.5 Biodistribution of ^{99m}Tc-SER4 and ^{99m}Tc-IgG in wild type and Sn knockout mice (n=3). Wild type mice were injected IV with ~20 MBq of either 99mTc-IgG (blue) or ^{99m}Tc-SER4 (red) and Sn knockout mice with ^{99m}Tc-SER4 (green) and imaged 3 hours later. After 3 h organs were harvested, weighed and then counted for radioactivity using a gamma counter. Uptake into organs is presented as the percent-injected dose per gram organ. **A:** Full biodistribution. **B:** Zoom of A to see distribution in low activity organs.

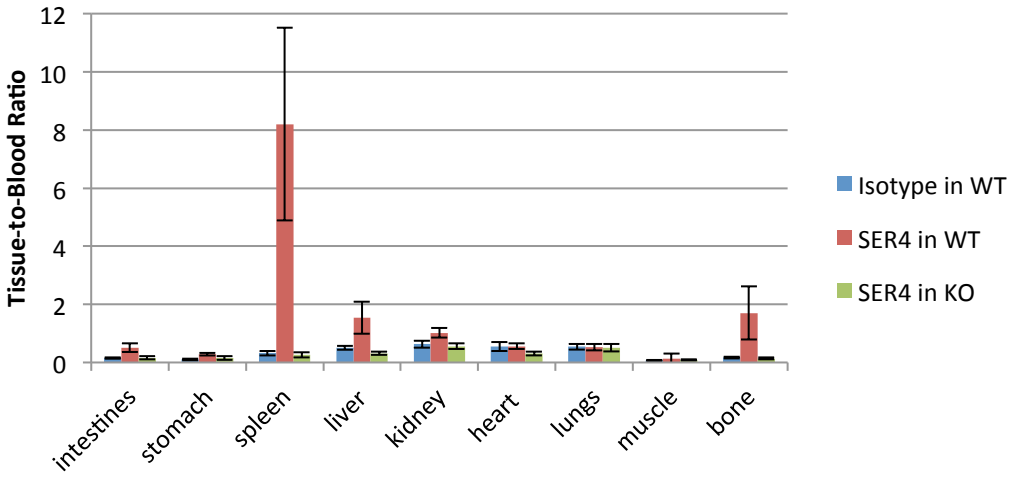

Figure 3.6 Tissue-to-blood ratio of ^{99m}Tc-SER4 and ^{99m}Tc-IgG in wild type and Sn knockout mice (n=3). Representation of biodistribution data from figure 4.7 as tissue-to-blood ratio.

3.3.3 Heart Transplant Rejection Model

Heterotopic cardiac transplants were performed using syngeneic (donor and recipient from same background) and allogeneic (donor and recipient from different backgrounds) donor hearts transplanted into the recipient abdominal cavity. Mice were recovered and imaging performed 7 days post transplantation. Whole body nanoSPECT/CT imaging revealed characteristic ^{99m}Tc-SER4 uptake to the spleen, liver and bone marrow in both transplant groups (Figure 3.7 A and B). Analysis orthogonal slices taken from the abdominal cavity reveals emergence of signal corresponding to soft tissue from the site of transplantation (and not a bowel loop) in the allogeneic transplants (Figure 3.7 C to H).

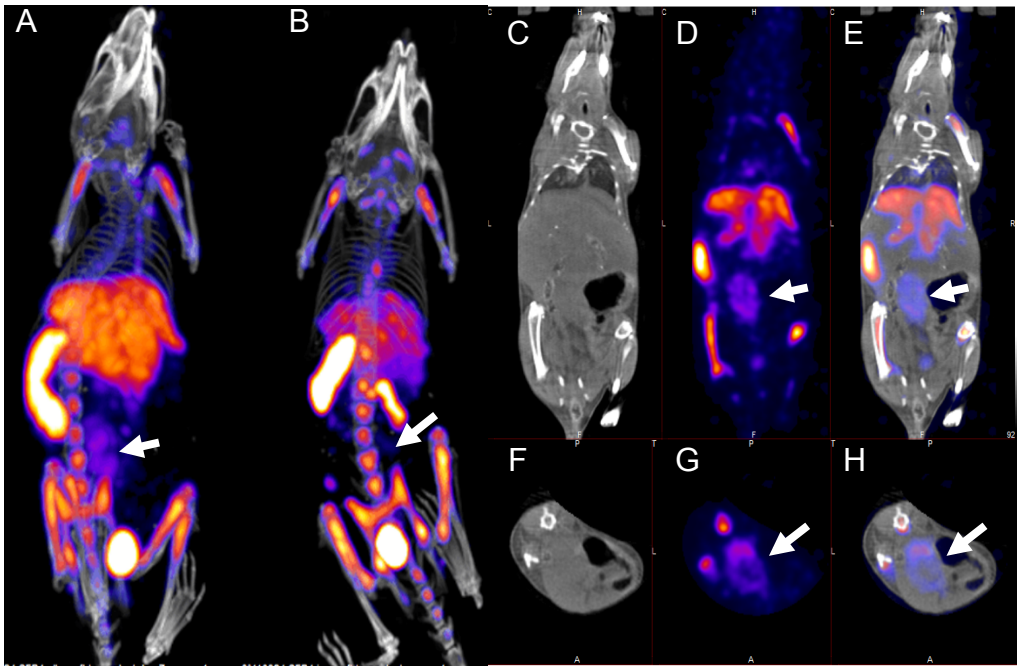

Figure 3.7 nanoSPECT/CT imaging of 99mTc-SER4 in heterotopic transplant model. Representative nanoSPECT/CT images of recipients with either a) allogeneic or b) syngeneic donor heart imaged 3 hrs post injection with 99mTc-SER4. CT, SPECT and fused images from coronal (c, d, e, respectively) and transversal (f, g, h, respectively) planes of an allogeneic recipient are shown. Arrows indicate site of abdominal cardiac transplant with uptake of tracer in allogeneic donor heart absent in the syngeneic donor heart..

Biodistribution data shows ^{99m}Tc-SER4 uptake in allogeneic transplants (8.40 %ID/g ± 1.78 %ID/g) to be significantly higher than ^{99m}Tc-SER4 uptake in syngeneic transplants (3.00 %ID/g ± 1.63 %ID/g; p = 0.0023) or ^{99m}Tc-IgG uptake in allogeneic transplants (5.93 %ID/g ± 0.57 %ID/g; p = 0.0336) (see Figure 3.10). Likewise, target-to-blood ratios illustrate higher uptake in allogeneic ^{99m}Tc-SER4 uptake versus ^{99m}Tc-IgG and ^{99m}Tc-SER4 in allogeneic and syngeneic transplants, respectively. Approximately an 8-fold higher ^{99m}Tc-SER4 uptake in allogeneic donor heart versus the ^{99m}Tc-SER4 syngeneic donor heart and ^{99m}Tc-IgG allogeneic donor heart groups was observed (Figure 3.9).

A:

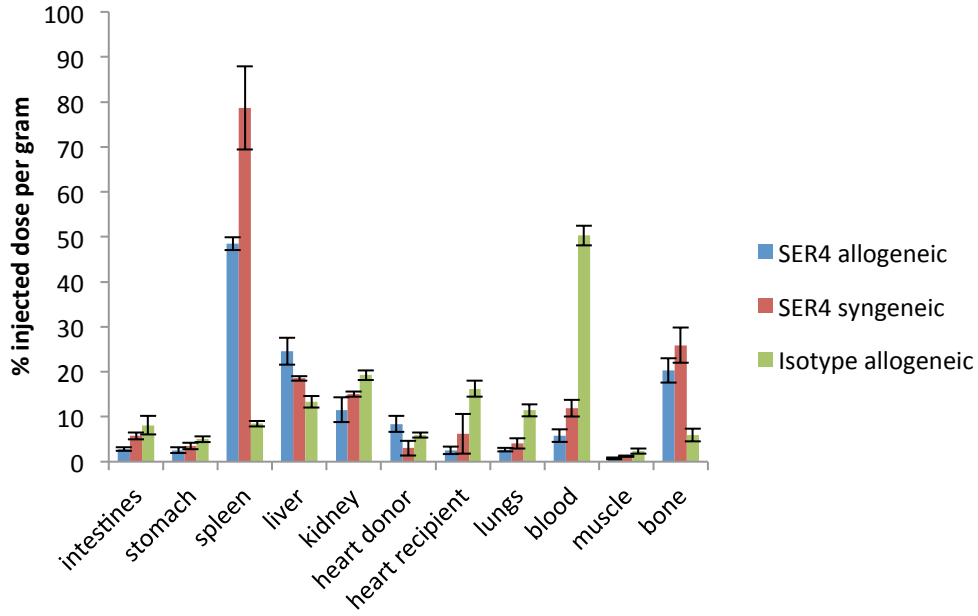

B:

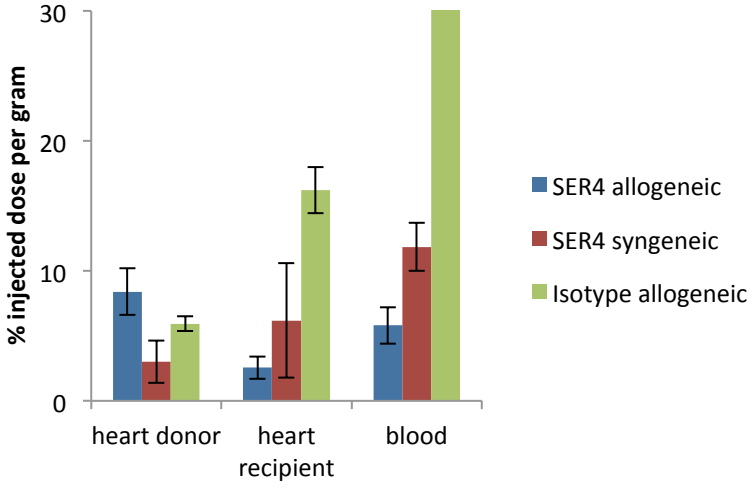

Figure 3.8 Biodistribution of 99mTc-SER4 in allogeneic and syngeneic heart grafts (n= 4 to 5). 8 week old C57Bl/6 mice receiving either allogeneic BALB/c heart grafts were injected with ~20 MBq ^{99m}Tc-SER4 (blue) or ^{99m}Tc-IgG (green) and syngeneic C57Bl/6 heart grafts were injected IV with ^{99m}Tc-SER4 (red) 7 days post transplantation. After 4 h organs were harvested, weighed and then counted for radioactivity using a gamma counter. Uptake into organs is presented as the percent-injected dose per gram organ. **A:** Full biodistribution. **B:** Donor heart, recipient heart and blood.

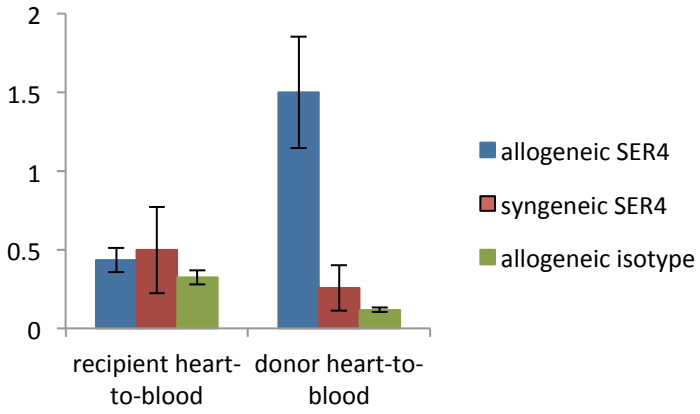

Figure 3.9 Ratio of % injected dose per gram of syngeneic and allogeneic donor/recipient hearts to blood. %ID/g data from recipient and donor hearts (allogeneic and syngeneic) were expressed as a factor of blood %ID/g.

3.3.4 Transplant Immunohistochemistry

Donor and recipient hearts from day 7 post transplantation were snap frozen and stained for Sn expression. Allogeneic donor transplants exhibit high expression of Sn (see Figure 3.10 A) as compared to syngeneic donor transplants (see Figure 3.10 B). Of interest, recipient (i.e. native) hearts exhibit an endogenous population of Sn positive cells (see Figures 3.10 C and D).

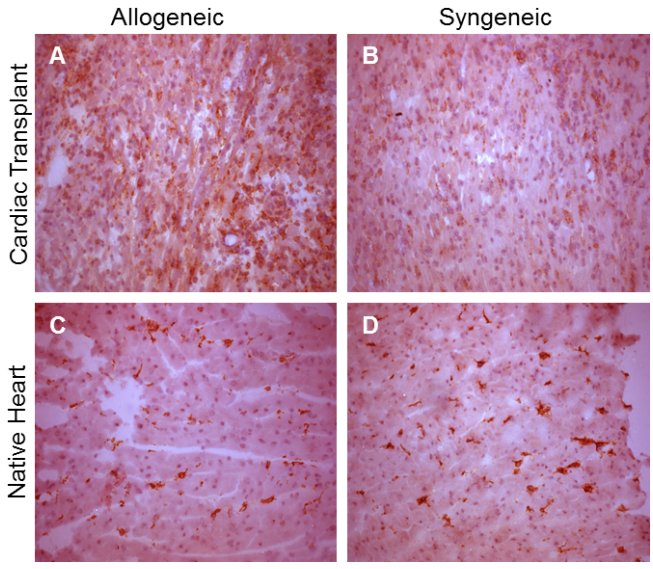

Figure 3.1010 Recipient and donor hearts stained for Sn expression. 5 µm sections from donor ((A) allogeneic, (B) syngeneic) and recipient ((C) allogeneic, (D) syngeneic) were stained for Sn (brown) and counter-stained with haematoxylin. For donor transplants, allogeneic (A) heart shows substantially higher Sn expression as compared to syngeneic (B) heart. Recipients hearts both exhibit endogenous sialaodhesin expression ((C) and (D)). Magnification 200x.

3.4 Discussion

Intact antibodies can display serum half-lives of the order of days to weeks, which is a function of their molecular mass exceeding the renal cut off (typically 150 kDa for full length IgG versus 50 kDa cut off) and of neonatal FcR-mediated recycling of IgG (Carter 2006). ^{99m}Tc-SER4 exhibits uniquely rapid blood extravasation due to high expression of endogenous antigen principally in the spleen. From one comparison of a radiolabelled antibody and its engineered fragments, the blood clearance of ^{99m}Tc-SER4 resembles that of a diabody rather than an IgG (with half-lives of 170 min and 330 min, respectively) (Jain, Venkatraman et al. 2007). Mϕ populations expressing the highest levels of Sn are typically found in border regions between flowing lymph/blood and lymphoid tissue, implying a function as sentinel cell types (see Chapter 1). This property seems to be critical in the rapid extravasation of ^{99m}Tc-SER4 from the blood, uniquely offering imaging time points far earlier than for any known intact IgG. The specificity of this effect was confirmed by the ^{99m}Tc-SER4's distribution in Sn KO mice, in which blood retention of ^{99m}Tc-SER4 was similar to that of untargeted isotype control in wild type mice.

The distribution characteristics of radiolabelled SER4 are in accordance with the data concerning Sn expression in mice, and in line with this %ID/g values reflect the relative expression levels as determined by IHC between tissues. In descending levels of expression, spleen, liver and bone marrow represent the set of vascularised tissues expressing Sn (avascular LNs contain the highest expressing Sn cells in the body located in the SCS) and thus the expected locations of ^{99m}Tc-SER4 uptake. A complicating matter for the determination of activity of a given tissue is the contribution that residual blood makes to the overall gamma counts. This is particularly evident in the liver (and to some extent the bone marrow), where only after representing the data as tissue-to-blood ratio is it clear that enhanced uptake in the liver is a consequence of targeting to Sn. This effect would be reduced by washing of removed organs with saline (as was performed in transplanted hearts) or by culling by exsanguination. This latter technique was performed in later studies (see Chapter 4).

The differential uptake observed in the bone (highest in femur and vertebrae) may represent enhanced uptake in regions with larger cavities (i.e. greater bone marrow mass). Alternatively this may relate to heterogenous Sn expression across bone marrow reservoirs, which could be examined by histological analysis. As Sn positive Mϕ are implicated in haematopoieitic stem cell (HSC) retention in the bone marrow (Chow, Lucas et al. 2011), heterogenous Sn expression may inform upon different HSC niches localised in different bone marrow regions. Progressive accumulation in the intestines observed by whole body imaging may represent specific uptake mediated by Sn positive Mϕ resident in the lamina propria and Peyer's patches (Crocker and Gordon 1989), or possibly non-specific metabolism. The absence of progressive accumulation represented in the biodistribution data may represent any localised specific uptake being masked by the considerable size of the intestines, in effect normalising the intestinal %ID/g data. This may be avoided by assessing intestinal activity on sections of intestine rather than counting the intact organ.

From the biodistribution there are still significant amounts of ^{99m}Tc-SER4 in the circulation at 6 hr. Imaging at a later time point would permit greater clearance of antibody and thus drop the contribution blood pool would make to the collected samples. However with the isotope ^{99m}Tc, imaging at greater than 24 h would equate to 4 half-lives and thus drastically affect the quality of image. An alternative would be to use a longer lived isotope, such as ^{111}In, which would allow imaging at later time points without significant drop in the achieved image quality. The reason for using ^{99m}Tc in this study was its ready availability as compared to longer lived isotopes and the ease with which the radiolabelled compound (^{99m}Tc-SER4) could be prepared. The selection of imaging at 3 h post-injection was decided upon qualitatively using the imaging data in which the blood pool significantly dropped over the first 60 min, whilst between hours 3 and 6 substantial changes in blood pool visualisation weren't observed. Also imaging at earlier time points provides a more dynamic picture of radiotracer uptake and hence disease processes. This is lost when imaging using slow clearing agents, such as with USPIOs which are imaged approximately 36 h post injection (Quillard, Croce et al. 2011).

The progressive accumulation of activity in the bladder has been attributed to transchelation of ^{99m}Tc from the IgG disulphides to free sulfhydryls presented by cysteine and glutathione (Hnatowich, Mardirossian et al. 1993). This effect has been considered favourable for earlier imaging as blood pool activity is significantly lower than indirectly labelled antibodies. Some authors have speculated that in vivo, the extracellular concentration of sulfhydryls isn't sufficient for transchelation to take place, and instead speculate elevated excretion of directly labelled antibodies represents internalisation followed by transchelation in the lysozyme, after which chelated ^{99m}Tc is transported and excreted (Karacay, Ong et al. 1998). Whether the rapid accumulation of ^{99m}Tc in urine following ^{99m}Tc-SER4 administration can be explained by an internalising process is debatable given the short time frame between injection and imaging.

In vivo specificity of ^{99m}Tc-SER4 in wild type mice was confirmed by comparison with ^{99m}Tc-IgG and ^{99m}Tc-SER4 in wild type and Sn KO mice, respectively. Whole body imaging at 3 hr post injection showed high splenic uptake as well as distinct liver and bone marrow uptake in the case of ^{99m}Tc-SER4 administered to wild type mice. This distribution was absent in both of the control groups, where instead high blood pool was observed (indicated by visualisation of the heart and the carotid arteries).This accords with endogenous Sn expression promoting extravasation of radiotracer whereas the absence of this sink in the control groups leads to much higher blood retention. A diffuse peritoneal signal was seen in the control mice that may be attributed to the longer blood half live of radiotracer in these control groups affording greater access to metabolic processing and excretion. Alternatively, although all images were adjusted to the same threshold, the intense signal provided by the spleen in the targeted group may obstruct detection of a weaker peritoneal signal. Across all groups similar bladder uptake was observed, implicating the role of transchelation. Also an absence of any thyroid or stomach signal indicates the stability of the radiotracer regarding release of free pertechnetate which would target hNIS positive tissues in these organs.

Biodistribution data corroborates with whole body imaging by showing greatly elevated uptake for the spleen and the bone marrow in the targeted group versus the

control groups. Although this effect is observed in the liver it is to some extent masked by the contaminating blood signal owing to perfusion effects. Thus higher blood activity in control groups results in an increased non-specific liver uptake (due to blood perfusion) as compared to the non-specific uptake in the targeted group. This non-specific effect offsets the specific uptake of ^{99m}Tc-SER4 to Sn positive Mϕ in the liver and so to account for this data was represented as a tissue-to-blood ratio. This representation shows enhanced uptake in spleen, bone marrow and liver and hence indicates the specificity of the ^{99m}Tc-SER4 tracer. The increased uptake observed in the intestine of ^{99m}TC-SER4 treated WT mice (as compared to control groups) may correspond to specific uptake by Sn positive Mϕ populations found in the lamina propria and Peyer's patches (Crocker and Gordon 1989).

Targeting of Sn positive Mϕ during disease was performed using allogeneic and syngeneic cardiac heterotopic heart transplants at day 7 post transplantation. Whole body imaging at 3 hr post radiotracer injection revealed characteristic uptake to spleen, bone marrow and liver. Additionally, ^{99m}Tc-SER4 showed increased uptake in the abdominal cavity for the allogeneic compared to syngeneic transplant. This is expected as the allogeneic response is far more aggressive compared to syngeneic and in turn leads to greater Mϕ recruitment (Mannon 2012).

Biodistributions were performed at 4 hr post injection and reproduce the imaging data, with specificity indicated by elevated ^{99m}Tc-SER4 uptake compared to control ^{99m}Tc-IgG for both spleen and bone marrow. Blood pool activity was recorded highest in the isotype control group followed by the SER4 syngeneic then allogeneic groups. In the SER4 groups, blood activity corresponded to splenic uptake, with the allogeneic transplanted mice showing the least uptake.This may be a result of increased uptake in the allogeneic donor heart compared to the syngeneic reducing the overall blood load.

The presence of Sn positive Mϕ was confirmed by immunohistochemistry. Comparison of staining from allogeneic and syngeneic donor hearts confirmed increased Sn expression along with the allogeneic response. Interestingly, staining of recipient heart revealed the presence of Sn positive Mϕ which represents the presence of an as yet unidentified murine Sn positive Mϕ population in the heart.

3.5 Summary

In this chapter, the *in vivo* functioning of the novel Mϕ imaging agent ^{99m}Tc-SER4 was assessed. ^{99m}Tc-SER4 exhibited unique clearance kinetics for an intact antibody, with endogenous Sn expression (principally in the spleen) permitting earlier imaging as compared to control antibodies. Specificity of ^{99m}Tc-SER4 was confirmed by comparison with untargeted isotype antibody as well use of ^{99m}Tc-SER4 in Sn KO mice. A proof-of-principle imaging experiment was performed using a cardiac model of transplant rejection to elicit Mϕ recruitment. ^{99m}Tc-SER4 displayed increased uptake corresponding to increased Sn positive Mϕ burden as compared to non-specific control antibody, illustrating ^{99m}Tc-SER4 suitability as a Mϕ targeting imaging agent.

Chapter 4

In vivo PET Imaging of ^{64}Cu-SER464Cu-SER4

4.1 Introduction

Mϕs are a highly adaptable cell type able to alter their behaviour drastically in order to manipulate their environment. For this reason endogenous tissue residing Mϕ populations are invaluable for their ability to display varied responses in order to maintain homeostasis. One such little understood population are bone marrow Mϕs which play an important role in the regulation of the haematopoietic environment, and may have important implications for transplantation. Similarly, tumour associated Mϕs (TAMs) are critical to the regulation of the tumoural environment and are shown to assist in tumour progression and present as potential therapeutic targets. In this chapter we aim to produce a novel PET radiotracer using the anti-Sn antibody SER-4 and perform preliminary imaging studies to examine its Mϕ targeting properties of resident bone marrow subpopulation response to irradiation as well as Sn Mϕ recruitment to tumours. In particular, we examine the influence of the cytokine colony stimulating factor 1 (CSF-1) upon Mϕ recruitment and the relationship of Sn expression to the heterogenous cell population known as myeloid-derived suppressor cells (MDSC). The data presented here is collected from a 3 month residence in the laboratories of Prof Anna Wu, Department of Molecular Imaging, Crumps Institute, UCLA and supported by the MEC Luminary Fund.

4.1.1 Bone Marrow Mφ and Radioablation

In the carefully regulated environment of the bone marrow, HSCs - the source of all the blood cell types including lymphoid, myeloid and erythroid lines - are found in specialized niches which support their renewal and maturation down committed cell lineages Within this specialised environment it is speculated that Mϕ maintain homeostasis via classical phagocyte activity alongside performance of trophic functions such as participation in erythrocyte development (so-called erythroblast islands) (Chasis and Mohandas 2008) and in the retention of HSCs (Winkler, Sims et al. 2010).

Due to the presence of highly proliferating immature cells, the bone marrow is considered one of the most radiosensitive organs, which permits its selective ablation using levels of irradiation that leave other cell populations unharmed (Dainiak 2002; Fliedner, Graessle et al. 2002). This phenomenon is used to replace a host's bone marrow with that of a donor, and has found extensive use preclinically for the study of cell behaviour (Aparicio-Vergara, Shiri-Sverdlov et al. 2010) and clinically for the treatment of haematological disease (Copelan 2006). The effects of acute localised irradiation to the regenerative capacity of the bone marrow have long been investigated, with exposure causing rapid depletion in cellularity which then fails to regain haematopoietic function (Knospe, Blom et al. 1966). In the case of whole body irradiation and HSC transfer, HSC homing to the depleted bone marrow results in the restoration of haematopoiesis (Srour, Jetmore et al. 2001).

Following localised irradiation, bone marrow cellularity is observed to decrease, while erythrocytes extravasate, sinusoids dilate/collapse, blood flow and vascular permeability increase, and progenitor and inflammatory cells infiltrate (Higashi, Fisher et al. 2000). MRI has been used to track the processes of oedema formation and the emergence of adipose tissue which gradually reforms into marrow following irradiation (Daldrup-Link, Henning et al. 2007). However there is a striking lack of immunohistochemical data regarding this process (Lerouxel, Moreau et al. 2009) and so the involvement of cellular subsets and their spatial interplay during recovery to irradiation is under represented.

4.1.2 Tumour Associated Mφ, MDSC and CSF-1

Cancer is a systemic disease, altering the immune response to evade eradication as well as promoting trophic activities that enable metastasis. Tumours modulate their local environment as well as the regional environment in order to achieve this. For instance, both infiltrating and sentinel LN lymphocytes which directly drain a primary tumour show immune supressed activity. In this way tumours can be considered organs containing transformed and untransformed cells characterised by complex

interplay to sustain and promote tumour growth (Cochran, Huang et al. 2006; Pollard 2009; Laoui, Van Overmeire et al. 2011).

Mϕ are key components of the tumoural environment and are considered important for initiation through to metastasis. Clinically, the increased presence of Mϕ (or TAMs) is correlated with poorer prognosis (Bingle, Brown et al. 2002) and thought to be attributed to their immunoregulatory and trophic functions. For instance, TAM accumulation is associated with the angiogenic switch, causing tumour vascularisation and increasing malignancy, whilst release of cytokines such as TGF-β and IL-10 suppress the immune response (Pollard 2009). It has been speculated that this immune suppressive activity can be regarded as normal trophic behaviour whereby in response to tissue damage (caused by tumour development) TAMs propagate an anti-inflammatory environment in order to not stimulate autoimmunity to self-antigens (Qualls and Murray 2010).

Another population of cells recognised for their pro-tumoural effects are MDSC, a heterogeneous population of immature myeloid cells noted for their immunosuppressive effects and first identified in the circulation of cancer patients and tumour-bearing mice (Gabrilovich and Nagaraj 2009). They are acknowledged to participate in disease settings by impairing cytotoxic T cell and NK cell activity, as well promoting T_{reg} cells, leading to their therapeutic targeting. Inhibition/elimination of MDSC so as to ablate their pro-tumour activity is currently being explored, whilst stimulation of MDSC is being examined for promoting tolerance in transplant recipients (Ochando and Chen 2012). However, MDSC also display a functional plasticity commonly associated with Mϕ, where a recent evaluation has shown them to possess both immuno-suppressive and immuno-stimulating properties (Pastula and Marcinkiewicz 2011).

An important mediator of Mϕ behaviour is CSF-1 (also known as Mϕ colony stimulating factor), a cytokine that promotes myeloid differentiation and Mϕ function, survival and migration (Hamilton 2011; Hume and MacDonald 2012). *In vivo*, administration of CSF1 and soluble CSF1 receptor (CSF1R) has been shown to elevate and diminish Mϕ, respectively, in the lymphoid tissue (Hashimoto, Chow et al. 2011).

Inhibition of CSF1R has variously been shown to downregulate Mϕ recruitment to tumours (MacDonald, Palmer et al. 2010; Coniglio, Eugenin et al. 2012) and experimentally-induced inflammation (Lenzo, Turner et al. 2012).

4.1.3 Tumour Imaging with PET/CT

A discussion of nuclear imaging is presented in Chapter 1. The clinical use of PET/CT has resulted in significant advances in the diagnosis, as well as the staging and management, of cancer. In the field of oncology there is an array of tracers that have been employed to identify tumours and to define their functional status. ^{18}F-Fluorodeoxyglucose is at present one of the most widely used tracers, and functions as a glucose analogue resulting in accumulation in highly metabolic cells that often characterises cancerous tissues. ^{18}F-Fluorodeixy-L-thymidine is another small molecule tracer, and behaving as an analogue of thymidine it is incorporated into proliferating cells, which can often correlate with the response to treatment characteristics of a tumour. In addition, tracers based upon integrin binding (the RGD peptides) which identify neovascularisation, somatostatin receptors that characterise certain neuroendocrine tumours and bone scintigraphy agents (such as NaF) are all used routinely for oncological imaging (Histed, Lindenberg et al. 2012). The use of radiolabelled antibodies against antigens over-expressed on tumour cells is also steadily rising as a specific way of identifying tumours and their metastasis, and to predict response to therapeutic antibodies as well as perform dosimetry measurements (Kaur, Venktaraman et al. 2012).

Preclinically, various strategies are being examined for targeting of Mϕs in tumours. The use of USPIOs that exploit Mϕ phagocytosis (Daldrup-Link, Golovko et al. 2011; Shih, Hsu et al. 2011) is being explored due to the clinical availability of USPIOs (see Chapter 1). Additionally, targeting of the FR which is expressed by some Mϕ subsets is being examined, however as the FR is not restricted to Mϕs and is also expressed by certain tumours, this is not a cell specific approach (Mueller and Schibli 2011; Fischer, Mueller et al. 2012). Considering that both Mϕ presence and phenotype are implicated

in pathogenesis of tumours, there is clearly a clinical imperative in being able to identify specific Mϕ populations via imaging.

4.2 Materials and Methods

4.2.1 Cell Culture

Ras+myc-transformed RM-1 prostate tumour cells (kind gifts from Dr. Timothy C. Thompson, Baylor College of Medicine) were cultured in Dulbecco modified Eagle medium (DMEM) containing 10% fetal bovine serum (FBS), 100 U/mL penicillin, and 15mM HEPES at 37°C with 5% CO2.

4.2.2 Tumour Models

Tumor implantation was performed by Dr Jingying Xu, UCLA. RM-1 (2.5×10^5 cells) were implanted subcutaneously in the thigh of C57BL6 male mice (6-10 weeks old, Jackson Laboratory, Bar Habor), and treatment started when the tumours reach 4 mm in diameter. All animal experiments were approved by the Animal Research Committee of the University of California Los Angeles. Tumour size was measured by digital callipers daily or every two days depending on the model. Mice were sacrificed and tissues were excised at the ethical tumour size limit of 1.5 cm in diameter.

4.2.3 Localised Irradiation

Localised irradiation was performed by Dr Jingying Xu, UCLA. Localised irradiation was performed from a linear accelerator (DMCO X-irradiator, Precision X Ray, CT) with a dose rate of 1.84 Gy/min and a 1.5 cm bolus on the surface (300kV, 10mA). When tumours reached 4-5 mm in diameter, mice were anesthetized (30 µL, 4:1 xylazine) and radiated with a single dose of 10 Gy to the tumour area with the rest of body shielded. Non-tumour bearing and tumour bearing mice were both irradiated on the right femur. Following irradiation, mice were divided into 6 groups receiving either no treatment (NT group) or soluble CSF1R inhibitor PLX3397 (CSF1R group) in their diet (Plexxikon, CA), and recovering from localised irradiation by 2 days, 7 days or 7 days with implanted tumour (See Figure 4.1 for schematic). 3 mice per group were

prepared, however most groups experienced mortality during irradiation procedure resulting in group sizes of n = 2 and n = 3.

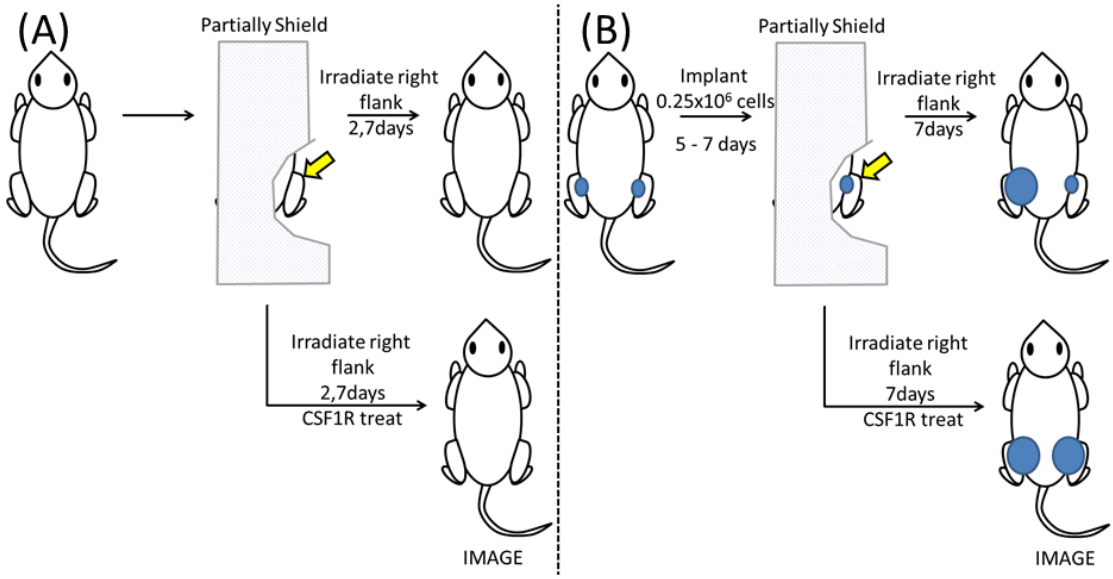

Figure 4.1 Schematic of Localised Irradiation and Tumour Model. Non-tumour bearing mice (A) were partially shielded and exposed to localised radiation on the right flank. Mice then received either no treatment or CSF1R inhibitor treatment. Both groups were allowed to recover for 2 or 7 days, whereupon they were imaged with ^{64}Cu-SER4. (B) Tumours were initiated and left for 5-7 days before mice received partial irradiation. Mice received either CSF1R treatment or no treatment and at day 7 post-irradiation were imaged with ^{64}Cu-SER4. 3 mice per group were prepared, however most groups experienced mortality during irradiation procedure resulting in group sizes of n = 2 and n = 3.

4.2.4 Preparation of SER4-NOTA

2.8 µL of S-2-(4-Isothiocyanatobenzyl)-1,4,7-triazacyclononane-1,4,7-triacetic acid (pSCN-Bn-NOTA, Macrocyclics, TX) in ethanol (2 mg / 100 µL) was added to SER4 antibody (200 µL, 10 mg/mL) in PBS (approx. 40:1 excess chelator) and adjusted to pH 8.0 using concentrated sodium hydroxide. The reaction proceeded at room temperature and after 2 hr was transferred to a PD10 column pre-equilibrated with PBS. Eluted fractions were assayed for protein content using NanoDrop 2000 (ThermoFisher) and protein fractions pooled (total volume 1 mL). Final solution concentration was 1.4 mg/mL.

4.2.5 Radiolabelling of SER4-NOTA

$^{64}CuCl_2$ in 0.1M HCl (Mallinckrodt Institute, Washington School of Medicine, MO) was added to SER4-NOTA and incubated at 43 °C for 40 min. Weakly bound Cu was challenged by addition of 10 mM EDTA in ammonium acetate (100 mM, pH 6.0) and incubated at room temperature for 5 min. The reaction was then transferred to a Micro BioRad Spin Column 6 (BioRad, CA) pre-equilibrated in ammonium acetate (100 mM, pH 6) and eluted (1000 RCF, 2 min). Radiolabelling was assayed using Monoclonal Antibody ITLC Strips Kit (Biodex Medical Systems, NY) with PBS as eluent, the strips cut in half and activity measured using a Wallac WIZARD automatic gamma counter (PerkinElmer, MA). Serum stability and recombinant antigen binding were not performed due to time constraints of the project.

4.2.6 Standard Biodistribution

Syringes (25 G X 16 mm, Terumo) containing approximately 3.5 MBq of ^{64}Cu-SER4 in 200 µL saline (50 µg/mL) were gamma counted (Capintec, NJ) before injection. Mice were injected via the tail vain under isoflurane (Anaquest, WI) and after imaging were culled immediately by exsanguination. The animals were then dissected and the following organs collected: intestines, stomach, spleen, liver, kidney, heart, lungs, left femur, right femur, blood (c. 1 mL), muscle and tail. The tissue samples were weighed and radioactivity counted using a Wallac WIZARD automatic gamma counter (PerkinElmer, MA). Injected dose was calculated from total activity in each injected syringe as determined by a 1% standard minus activity counted in tail, and presented as the percentage of injected dose per gram (%ID/g) of each tissue sample. Relative uptake values for the irradiated to non-irradiated femur were determined as the ratio of their respective tracer uptake (%ID/g)

4.2.7 *In vivo* PET and CT Imaging

Dynamic imaging was performed using a Genisys^4 scanner (Sofiebiosciences, CA), acquired over 2 hr and reconstructed using a 3D ML-EM algorithm. Static imaging was

performed using Inveon PET (Siemens, WA), with 10 min acquisition and reconstructed using filtered back projection. CT imaging was performed using MicroCat II Scanner (Concorde Microsystems, TN) using 45 KVp X-ray source, set with a 500 ms exposure time in 180 projections lasting approximately 10 min. Images were reconstructed and displayed using AMIDE (Loening and Gambhir 2003). Percentage injected dose per gram (% ID / g) values during dynamic imaging study were calculated using mean activity per unit volume data from regions of interests (ROIs) defining target organs/tissues. Mean activity per volume values were translated into activity per mass by assuming the average density of tissue to be 1 g per cm^3, and these values compared to total activity defined by the scanner field of view to produce %ID/g values. ROIs defining the irradiated and non-irradiated femur cavities were used to define relative uptake between irradiated and non-irradiated femurs. The ratio of their mean activity per volume of the irradiated to non-irradiated femur determined the relative uptake value.

Adult male mice (C57BL6, 6 – 10 weeks) were injected IV under anaesthesia (isoflurane, VetOne, UK) with approximately 3.5 MBq ^{64}Cu-SER4 in 200 µL (50 µg/mL). For dynamic imaging, 1 cannulated mouse was injected whilst in the scanner and image acquisition begun immediately. For static imaging, mice were allowed to recover, then anaesthetised and imaged at 4 hr post injection. Mice were culled immediately after static imaging and biodistributions performed.

4.2.8 Flow Cytometry Analysis

Flow cytometry was performed by Dr Jingying Xu, UCLA. For bone marrow collection, femurs were excised and flushed with PBS and cell numbers counted. Tumours were dissected into approximately 1- to 3-mm^3 fragments and digested with 80 U/mL collagenase (Invitrogen) in DMEM containing 10% FBS for 1.5 hours at 37°C while shaking. Single-cell suspensions were filtered and incubated for 30 min on ice with the following: APC, PerCP-Cy5.5, APC-e780-conjugated antibodies (CD11b, Gr-1 and F4/80, respectively) were purchased from eBioscience (1:200). SER4-FITC was prepared using FluoReporter FITC Labelling Kit (Invitrogen, 1:200).

Cells were washed twice before analysis by flow cytometry (BD LSR-II, Beckman Coulter, CA). Data was analysed with FlowJo software (TreeStar).

4.3 Results

The following results are representative of a pilot study. As such the data is from limited group sizes (six groups n = 2 or n = 3), which has restricted the majority of analysis to descriptive rather than statistical. When sufficient group size permits, 2-way unpaired Student's T test is used, with significance ascribed to p values < 0.05.

4.3.1 Preparation of ^{64}Cu-SER4

The recorded recovery of SER4-NOTA from A_{280} measurements was 70% (1.4 mg from 2.0 mg starting material). Radiolabelling followed by EDTA challenge resulted in radiolabelling purity > 99% as assessed by ITLC, and specific activities of approx. 3.5 MBq / 10 μg were recorded.

4.3.2 Dynamic Scanning of ^{64}Cu-SER4

A naïve mouse was injected via a tail vein cannula with ^{64}Cu-SER4 and a dynamic scan was performed. The scan was initiated immediately prior to injection and recorded automatically once activity was detected in the field of view. At T = 0 min (see Figure 4.2 A), ^{64}Cu-SER4 was observed in the vasculature, as indicated by the detection of the inferior vena cava which received the injected dose. The signal from the heart was highest in this image relative to the later time points which also points to the presence of probe throughout the vasculature. At T = 5 min (see Figure 4.2 B), the carotid arteries and heart are delineated, as is the liver. By T = 5 min, both the femur and the pelvis can also start to be visualised, which progressively become more defined (C to F). The spleen is observed as a lower right hand lobe associated with the liver (corresponding to the left hand side of the mouse) which gradually increases in intensity throughout the study. From T = 0 min to T = 60 min (A to E), changes in the redistribution of radionuclide are observed, however between 60 min and 120 min (E to F) no apparent redistribution occurs.

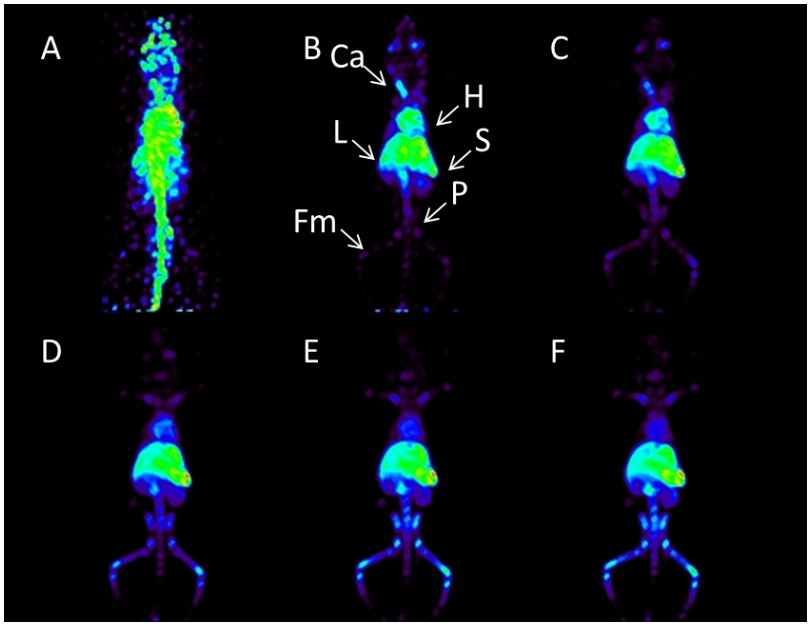

Figure 4.2 Genesys[4] dynamic imaging of ^{64}Cu-SER4.

Mouse injected IV via a tail vein cannula with ~3.5 MBq ^{64}Cu-SER4 and imaged continuously over 2 hr. Images represent whole body acquisitions at (A) 0 min, (B) 5 min, (C) 10 min, (D) 30 min, I 60 min and (F) 120 min post injection. Arrows indicate carotid arteries (Ca), heart (H), liver (L), spleen (S), pelvis (P) and femur (Fm).

ROIs were drawn over the spleen, right femur and heart and radiotracer uptake (measured in %ID/g) analysed over time (see Figure 4.3). A rapid drop in blood pool was detected by heart uptake falling from 51.2 %ID/g at 0 min to 19.1 %ID/g at 65 min, at which point activity decreased more steadily to 18.2 %ID/g at 115 min. Similarly both the spleen and femur exhibited rapid uptake from 0 min to 65 min (8.8 to 61.9 %ID/g for spleen, 1.8 to 36.1 %ID/g for right femur) which increased less rapidly afterwards (63.9 and 36.3 %ID/g at 115 min for spleen and femur, respectively).

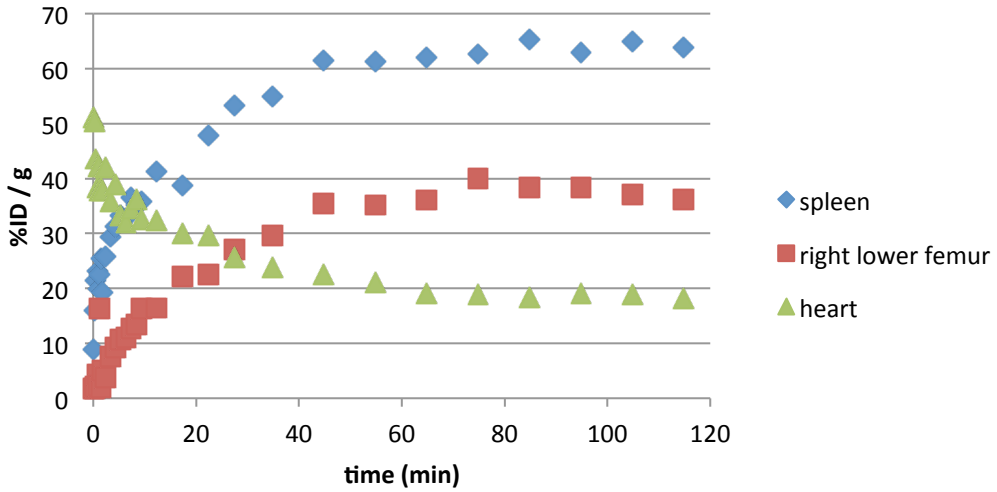

Figure 4.3 Region of interest (ROI) analysis of ^{64}Cu-SER4 Genesys^{4} dynamic scan (n = 1). Mouse injected IV via a tail vein cannula with ~3.5 MBq ^{64}Cu-SER4 and imaged continuously over 2 hr. ROI were drawn over the spleen (blue diamond), right femur (red square) and heart (green triangle). Activity was expressed as % injected dose per gram (%ID/g).

4.3.3 Localised Irradiation

Mice were irradiated on the right hind leg and allowed to recover for either 2 or 7 days, imaged with ^{64}Cu-SER4 then culled and biodistributions performed. Irradiated mice were additionally split in to two groups, either treated with or without CSF1R inhibitor for the period between irradiation and imaging.

Biodistributions for non-tumour bearing mice were performed at 4 hr post injection, whereas for tumour bearing mice they were performed at 20 hr post injection. Data was presented as % injected dose per gram (%ID/g) of the tissue collected. As group sizes were limited to n = 2 or n = 3, only a descriptive analysis is performed.

Flow cytometry was performed on samples taken from one mouse per group, and as such data is not analysed statistically.

4.3.3.1 Day 2 Post Irradiation

At day 2 post irradiation, whole body imaging of non-treated (NT) mice showed probe distribution comparable to normal mice (see Figure 4.4 A) with uptake in the spleen, liver and femur (see Figure 4.4 A). At this time point, treated mice (CSFR1) showed a

similar uptake pattern (see Figure 4.4 B), although slightly higher blood pool was observed as visualised by greater detection of the heart.

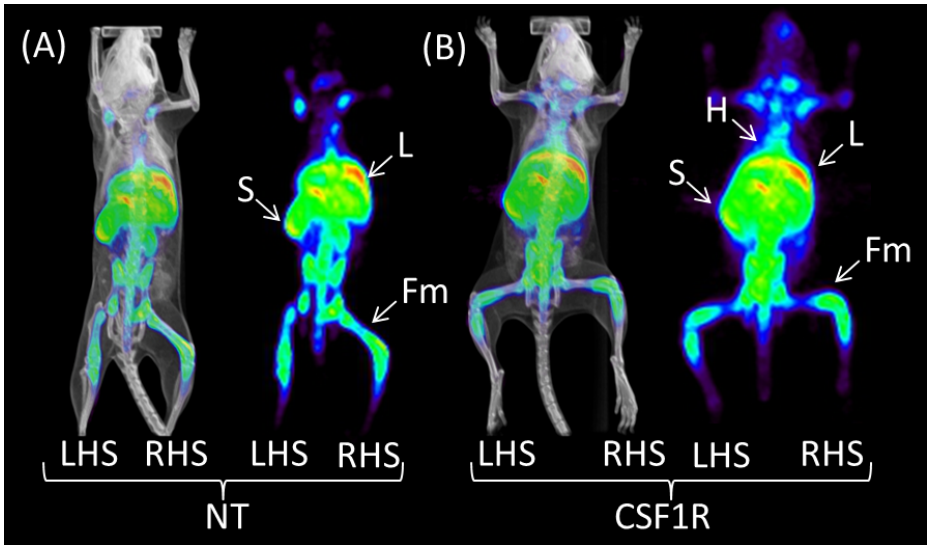

Figure 4.4 Inveon and microCT imaging of ^{64}Cu-SER4 in mice after 2 days recovery following localised irradiation and CSF1R treatment. Mice were shielded on the left side (LHS) and irradiated on right femur (RHS) with 10Gy and received either no treatment (NT) or CSF1 inhibitor treatment (CSF1R) until the date of imaging(A and B, respectively). Mice were injected with ~3.5 MBq ^{64}Cu-SER4 and images were acquired at 4 hours post injection. Arrows indicate heart (H), liver (L), spleen (S), femur (Fm) and tumour (T). LHS = Left hand side; RHS = Right hand side.

For the NT group biodistributions (see Figure 4.5), the spleen exhibited the highest uptake (> 155 %ID/g), followed by the liver and femurs, with the irradiated femurs recording at least 10 %ID/g greater uptake than the non-irradiated. The spleen and liver uptake values after treatment (CSF1R) were all less than the NT group, with > 10 %ID/g difference in splenic uptake. Similar uptake was observed in irradiated and non-irradiated femurs in the CSF1R group.

A:

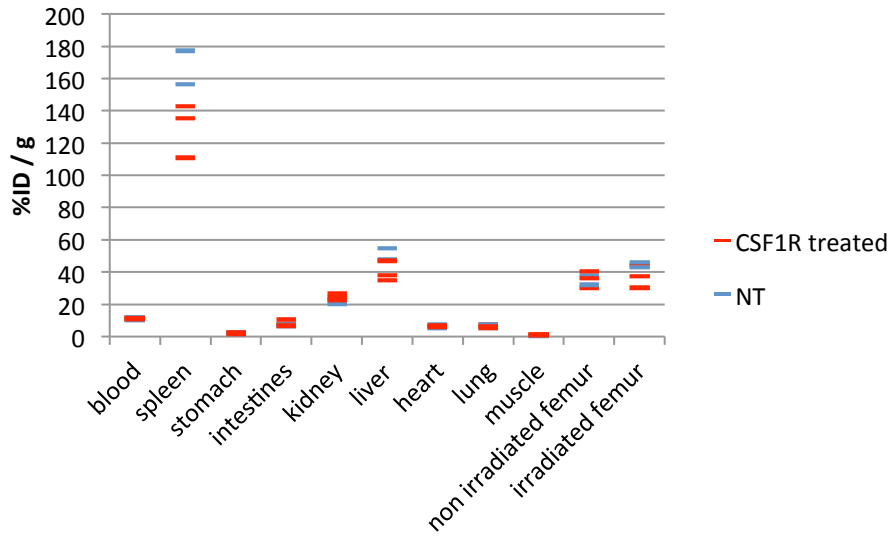

B:

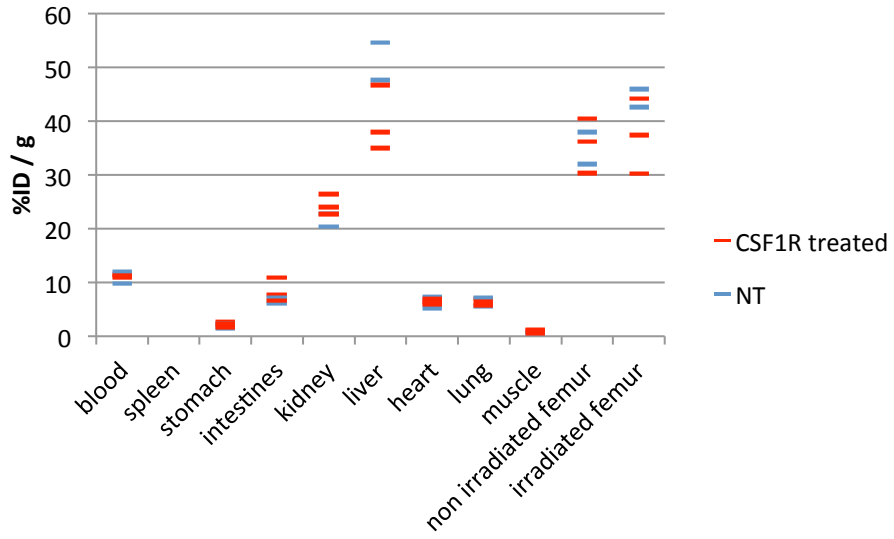

Figure 4.5Biodistribution of ^{64}Cu-SER4 in C57BL6 mice after 2 days recovery following localised irradiation with and without CSF1R treatment (n = 2 to 3 per group). Mice were irradiated locally with 10Gy then received either no treatment (NT – blue dash) or CSF1 inhibitor (CSF1R – red dash) for 2 days post irradiation. Mice were injected IV into the tail vein with ~3.5 MBq ^{64}Cu-SER4 and culled at 4 hr, then organs harvested, weighed and gamma counted. Each dash represents data from one mouse. Radioactive uptake in organs is presented as the percentage-injected dose per gram organ (%ID/g). A: full biodistribution, B: zoom of biodistribution to view low activity organs.

Femurs were excised and bone marrow flushed using PBS, filtered then stained for CD11b, Gr-1 and Sn. Live cells were gated by forward scatter (FSC) and side scatter

(SSC) to eliminate small, granulous cells (see Figure 4.6 A to C). Live cell populations were then assessed for % Sn expression using a threshold set at < 1% expression for unstained cells (see Figure 4.7 and Table 4.1). Comparison of irradiated to non-irradiated femur % Sn expression of whole cell and MDSC subpopulations (identified by CD11b and Gr-1 expression – see Figure 4.6 D) shows in both NT and CSF1R groups expression is relatively less in the irradiated femur than the non irradiated, with the CSF1R group exhibiting the least expression (see Figure 4.7 and Table 4.1).

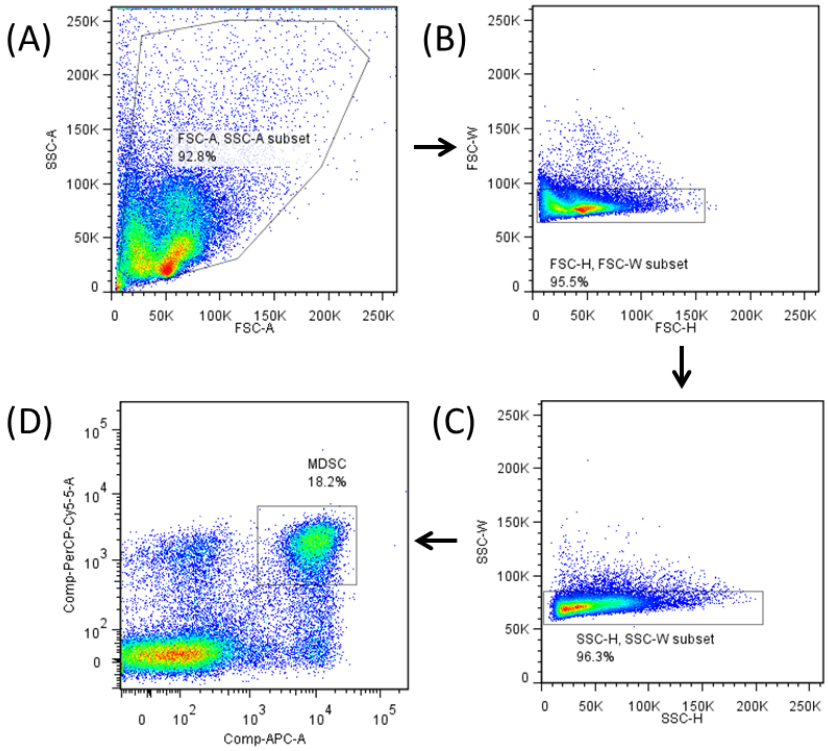

Figure 4.6 Gating of live and myeloid derived suppressor cell (MDSC) populations from bone marrow (n = 1). Filtered bone marrow aspirates were analysed by flow cytometry (A) and live cells identified by gating on forward scatter (FSC) and side scatter (A to C) to identify live cells. MDSC sub-population (D) was identified by expression of Gr-1 (PerCP-Cy5) and CD11b (APC).

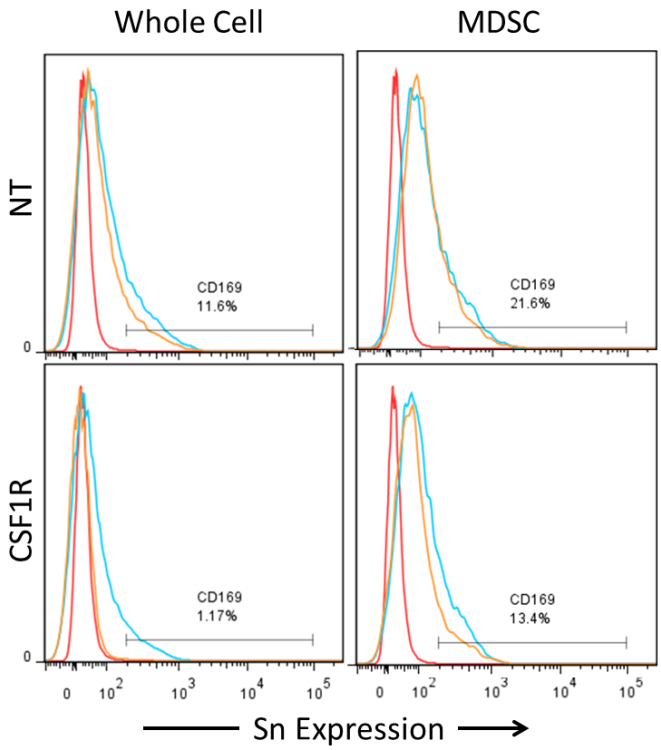

Figure 4.7 Day 2 post irradiation bone marrow Sn expression of whole cell and MDSC subpopulations (n = 1). Live cells and MDSC from day 2 post irradiation femurs, without treatment (NT) or with CSF1R treatment (CSF1R) were analysed for Sn expression (FITC). Blue = non-irradiated femur; Orange = irradiated femur; Red = unstained.

	Irradiated to Non-irradiated Ratio Whole cell	Irradiated to Non-irradiated Ratio MDSC
Day 2 NT	0.68	0.92
Day 2 CSF1R	0.13	0.68

Table 4.1 Day 2 irradiated to non-irradiated Sn expression ratio of whole cells and MDSC subpopulations from bone marrow aspirates. Ratio between irradiated and non-irradiated femur Sn expression levels of whole cell and MDSC subpopulations from Figure 4.10. Values < 1 correspond to less Sn expression in irradiated bone marrow compared to non-irradiated.

4.3.3.2 Day 7 Post Irradiation

Mice were locally irradiated and allowed to recover for 7 days, the imaged. From whole body imaging, the NT group (see Figure 4.8 A) demonstrated expected splenic and liver uptake. However asymmetric uptake was observed in the hind legs, with the irradiated limb exhibiting higher signal than the non-irradiated limb. The CSF1R set (see Figure 4.8 B) showed splenic and liver targeting, but they also exhibited

symmetrical hind limb uptake as well as increased blood pool, as visualised by the heart, compared to NT mice.

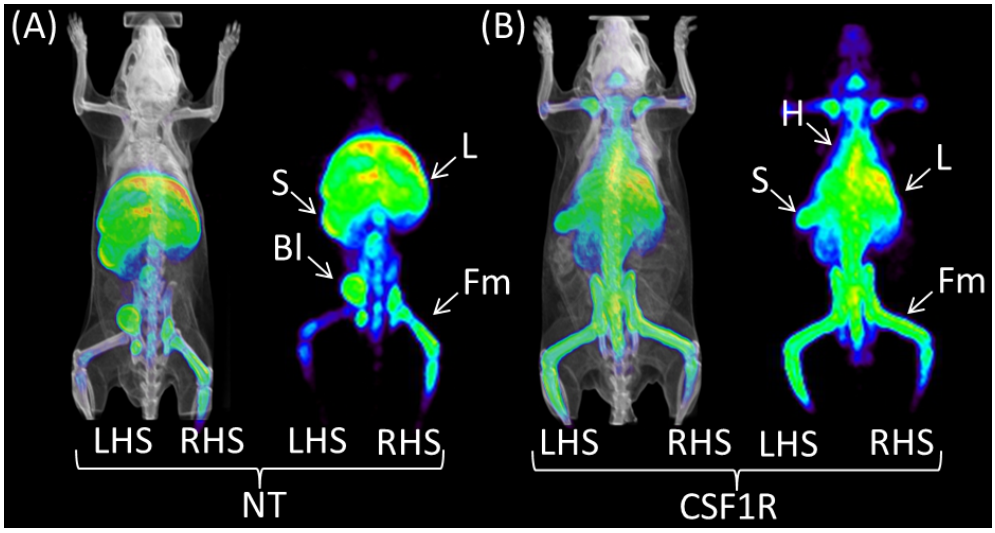

Figure 4.8 Inveon and microCT imaging of ^{64}Cu-SER4 in mice after 7 days recovery following localised irradiation and CSF1R treatment. Mice were shielded on the left side (LHS) and irradiated on right femur (RHS) with 10Gy and received either no treatment (NT) or CSF1 inhibitor treatment (CSF1R) until the date of imaging (A and B, respectively). Mice were injected with ~3.5 MBq ^{64}Cu-SER4 and images were acquired at 4 hours post injection. Arrows indicate heart (H), liver (L), spleen (S), femur (Fm) and tumour (T). LHS = Left hand side; RHS = Right hand side.

In the biodistribution studies, NT mice showed highest uptake in the spleen followed by liver and femurs (see Figure 4.9). No uptake bias was observed between irradiated and non-irradiated NT femurs, with a wide range of uptake values recorded between mice (almost 20 %ID/g difference in non-irradiated femur uptake between NT mice). The CSF1R group displayed reduced splenic (greater than 20 %ID/g between the lowest NT and highest CSF1R values) and liver uptake, whilst more blood (> 5 %ID/g), heart and lung uptake was observed as compared to the NT group. The CSF1R irradiated femurs all showed lower uptake than the non-irradiated femurs (> 5 %ID/g) and CSF1R non-irradiated femurs displayed higher uptake than NT non-irradiated femurs (> 10 %ID/g).

A:

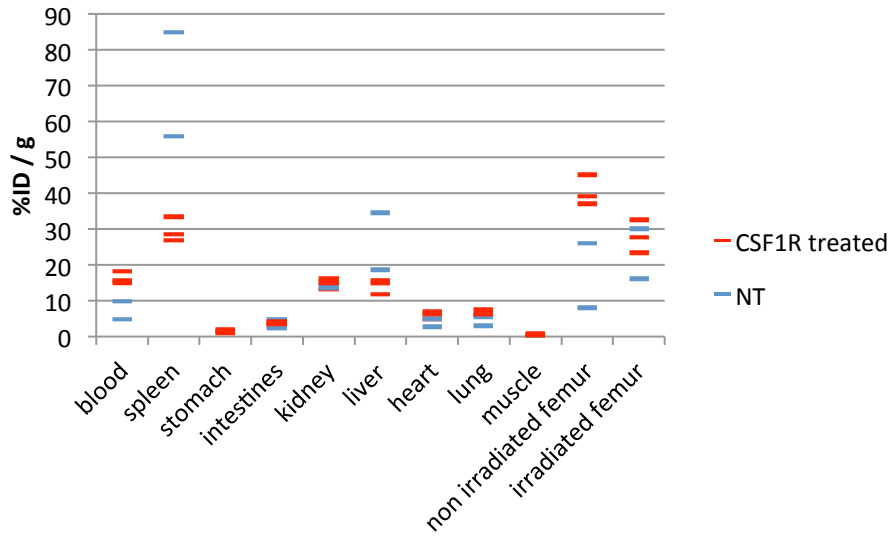

B:

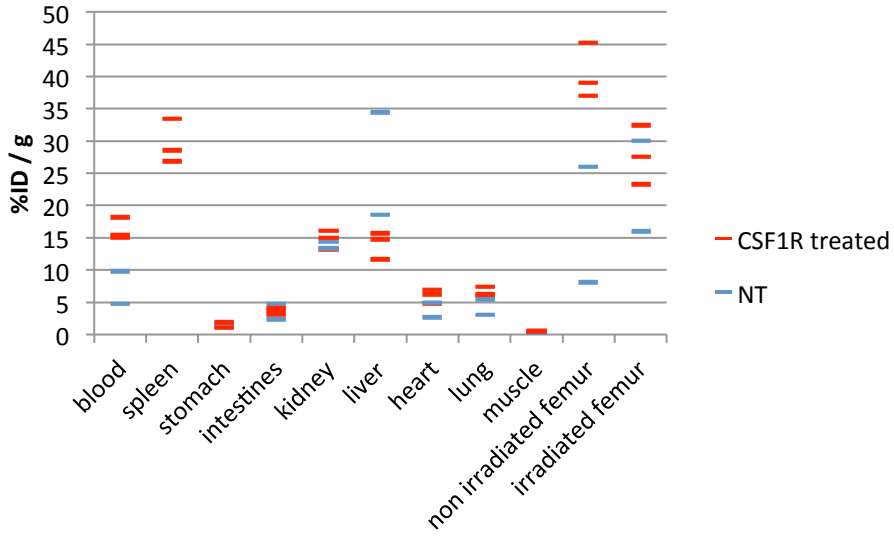

Figure 4.9 Biodistribution of ^{64}Cu-SER4 in C57Bl6 mice after 7 days recovery following localised irradiation with and without CSF1R treatment (n = 2 to 3 per group). Mice were irradiated locally with 10Gy then received either no treatment (NT – blue dash) or CSF1 inhibitor (CSF1R – red dash) for 2 days post irradiation. Mice were injected IV into the tail vein with ~3.5 MBq ^{64}Cu-SER4 and culled at 4 hr, then organs harvested, weighed and gamma counted. Each dash represents data from one mouse. Radioactive uptake in organs is presented as the percentage-injected dose per gram organ (%ID/g). A: full biodistribution, B: zoom of biodistribution to view low activity organs.

Flow cytometry shows the CSF1R irradiated limb to display approximately 50 % Sn expression of the non-irradiated limb (see Figure 4.10 and Table 4.2). However this relationship is reversed in the NT group where the irradiated femur expresses > 5 fold increase in Sn to that of the non-irradiated as measured by whole cell and MDSC subset expression (see Table 4.2).

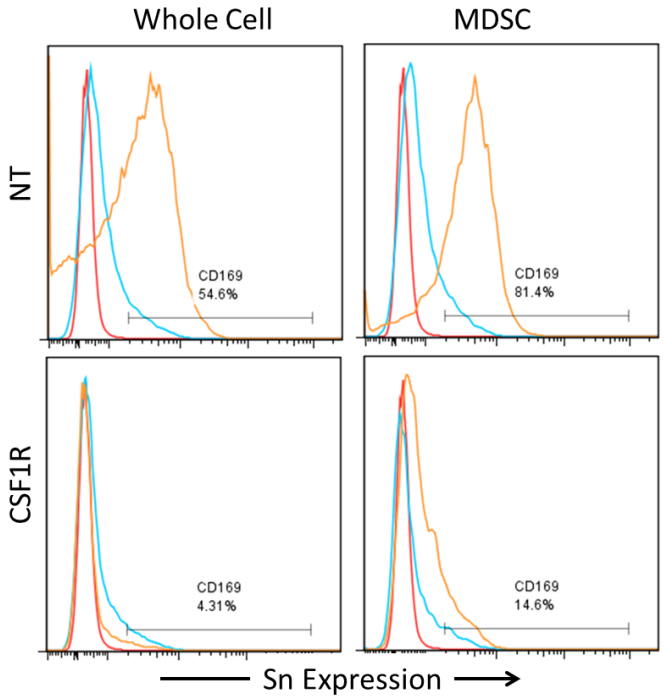

Figure 4.10 Day 7 post irradiation bone marrow Sn expression of whole cell and MDSC subpopulations (n = 1). Live cells and MDSC from day 7 post irradiation femurs, without treatment (NT) or with CSF1R treatment (CSF1R) were analysed for Sn expression (FITC). Blue = non-irradiated femur; Orange = irradiated femur; Red = unstained.

	Irradiated to Non-irradiated Ratio Whole cell	Irradiated to Non-irradiated Ratio MDSC
Day 7 NT	5.30	7.54
Day 7 CSF1R	0.54	0.56

Table 4.2 Day 7 irradiated to non-irradiated Sn expression ratio of whole cells and MDSC subpopulations from bone marrow aspirates. Ratio between irradiated and non-irradiated femur Sn expression levels of whole cell and MDSC subpopulations from Figure 4.10. Values < 1 correspond to less Sn expression in irradiated bone marrow compared to non-irradiated, values > 1 correspond to greater expression in irradiated bone marrow.

4.3.3.3 Tumour Bearing Mice

A further set of mice were given bilateral tumour implants in their thighs then irradiated at 7 days post implantation on the right hind limb. The mice were allowed to recover for 7 days with or without CSF1R treatment then imaged with ^{64}Cu-SER4 (see Figure 4.11). Both sets of mice (NT and CSF1R) exhibited splenic and liver targeting, but once again only the NT group showed asymmetric right hind limb uptake. Additionally, the CSF1R group showed increased blood pool as well visualisation of the non-irradiated tumour.

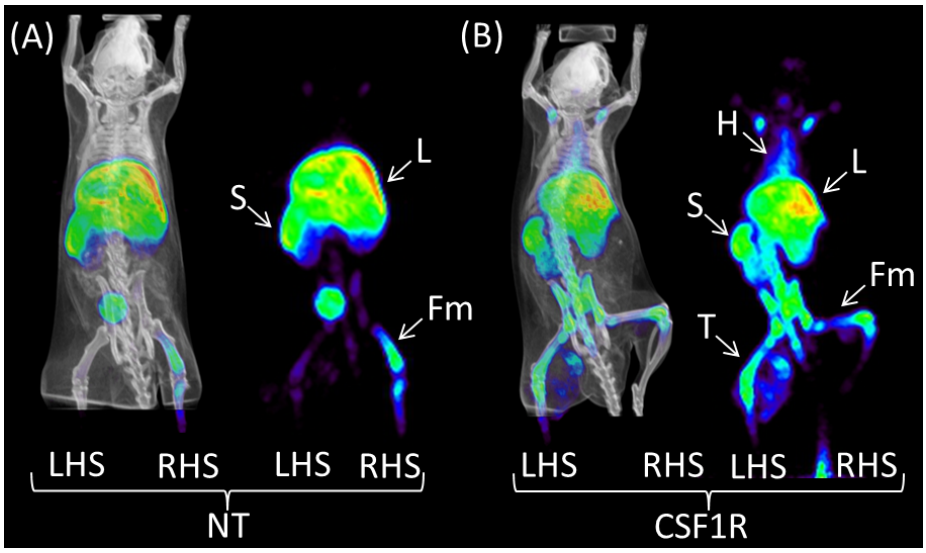

Figure 4.11 Inveon and microCT imaging of ^{64}Cu-SER4 in tumour-bearing mice after 7 days recovery following localised irradiation and CSF1R treatment. Mice bearing bilateral tumours were shielded on the left side (LHS) and irradiated on right femur (RHS) with 10Gy and received either no treatment (NT) or CSF1 inhibitor treatment (CSF1R) until the date of imaging(A and B, respectively). Mice were injected with ~3.5 MBq ^{64}Cu-SER4 and images were acquired at 4 hours post injection. Arrows indicate heart (H), liver (L), spleen (S), bladder (Bl), femur (Fm) and tumour (T). LHS = Left hand side; RHS = Right hand side.

The tumour bearing NT and CSF1R group exhibited highest uptake in the spleen (22 to 31 %ID/g) and liver (19 to 28 %ID/g) (see Figure 4.12). The NT irradiated femurs all displayed greater uptake than the non-irradiated, as did the irradiated versus non-irradiated tumours. The CSF1R group showed higher blood, heart and lung uptake values as compared to the NT group. CSF1R femurs showed greater uptake than their respective NT counterparts, however neither irradiated nor non-irradiated CSF1R femurs exhibited any discernible relationship. Similarly, CSF1R tumours had higher

uptake than NT tumours but no such pattern was observed between CSF1R irradiated and non-irradiated tumours.

A:

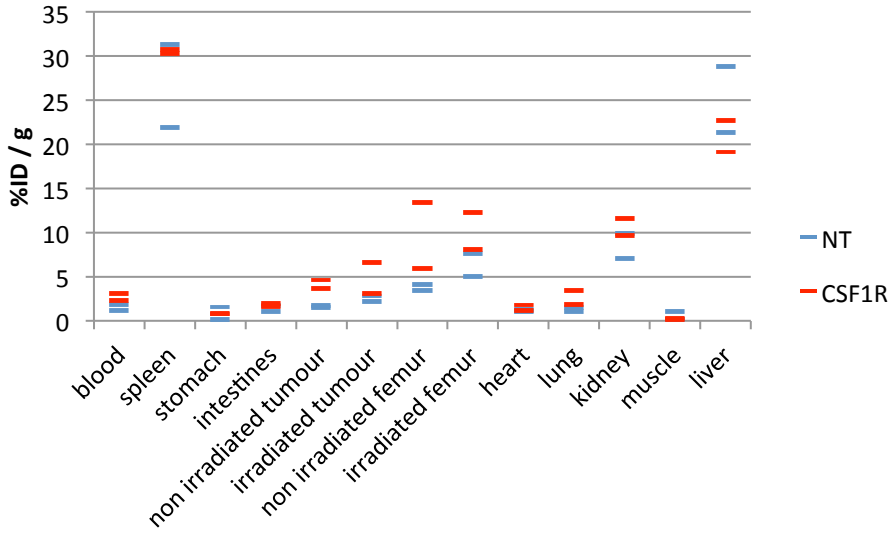

B:

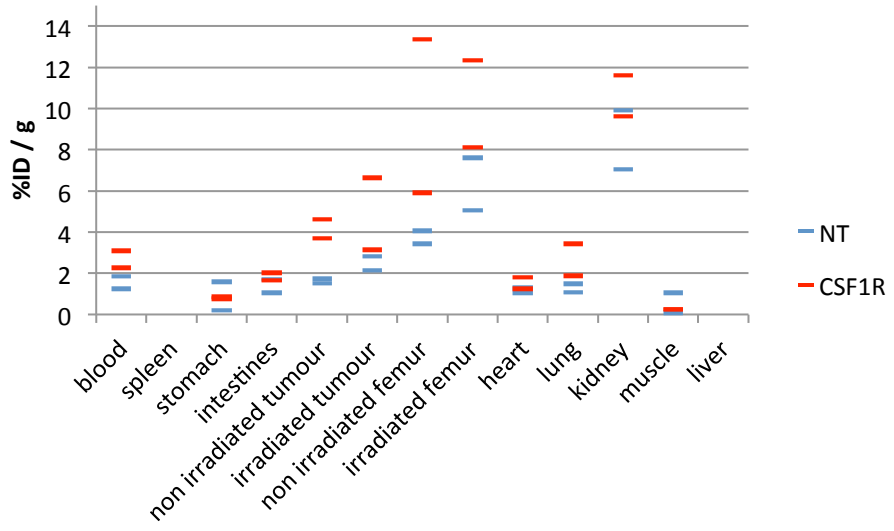

Figure 4.12 Biodistribution of ^{64}Cu-SER4 in tumour bearing C57BL6 mice after 7 days recovery following localised irradiation with and without CSF1R treatment (n = 2 to 3 per group). Bilateral tumour bearing mice were irradiated locally with 10Gy then received either no treatment (NT – blue dash) or CSF1 inhibitor (CSF1R – red dash) for 2 days post irradiation. Mice were injected IV into the tail vein with ~3.5 MBq ^{64}Cu-SER4 and culled at 20 hr, then organs harvested, weighed and gamma counted. Each dash represents data from one mouse. Radioactive uptake in organs is presented as the percentage-injected dose per gram organ (%ID/g).). A: full biodistribution, B: zoom of biodistribution to view low activity organs.

Tumours were excised and digested in collagenase, filtered then stained for CD11b, Gr-1, F4/80 and Sn. Live cells were gated by forward scatter (FSC) and side scatter (SSC) to eliminate small, granulous cells (see Figure 4.13 A to D). Whole live cell populations were then assessed for % Sn expression using a threshold set at < 1% expression for unstained cells (see Figure 4.14 and Table 4.3). Comparison of expression from irradiated and non-irradiated tumours in the NT group shows an increase following irradiation of greater than 2 fold.

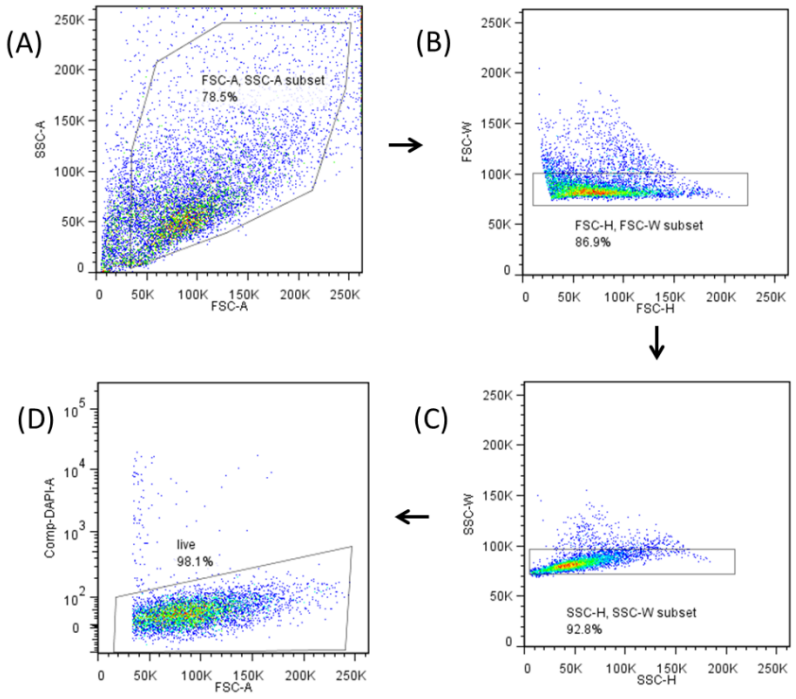

Figure 4.13 Gating of live cell population from tumours. Filtered, de-collagenised tumours were analysed by flow cytometry (A) and live cells identified by gating on forward scatter (FSC), side scatter and DAPI (B to D) to identify live cells.

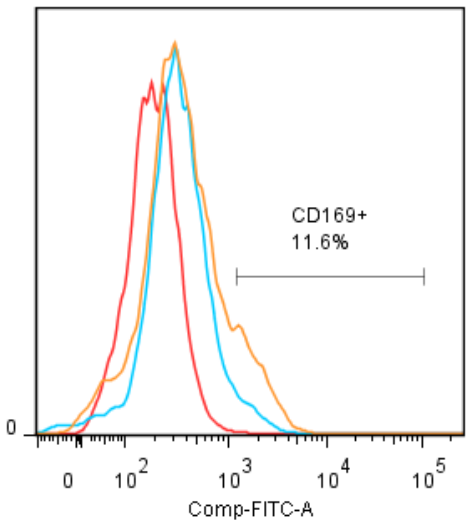

Figure 4.14 Sn expression of live cell population. Live cells from day 7 post tumours, without treatment were analysed for Sn expression (FITC). Blue = left femur; Orange = right femur; Red = unstained.

	Unstained Tumour (%)	Non-irradiate Tumour (%)	Irradiated Tumour (%)	Irradiated to Non-irradiated Ratio
Tumour NT	0.194	4.44	11.6	2.61

Table 4.3 Percentage Sn expression of whole live cells tumours. Data presented from Figure 4.18 with Sn expression gate set using unstained control.

The TAM subset was identified by expression of F4/80 and CD11b. TAM and MDSC subsets were analysed for Sn expression (see Figure 4.15 A and C). TAM expressing Sn increased by 74% following irradiation whilst Sn expression levels increased in MSDC following irradiation, with 15.7% of the irradiated tumour population exhibiting Sn as compared to 0% for the non-irradiated tumour (see Figure 4.15 B and D and Table 4.4)

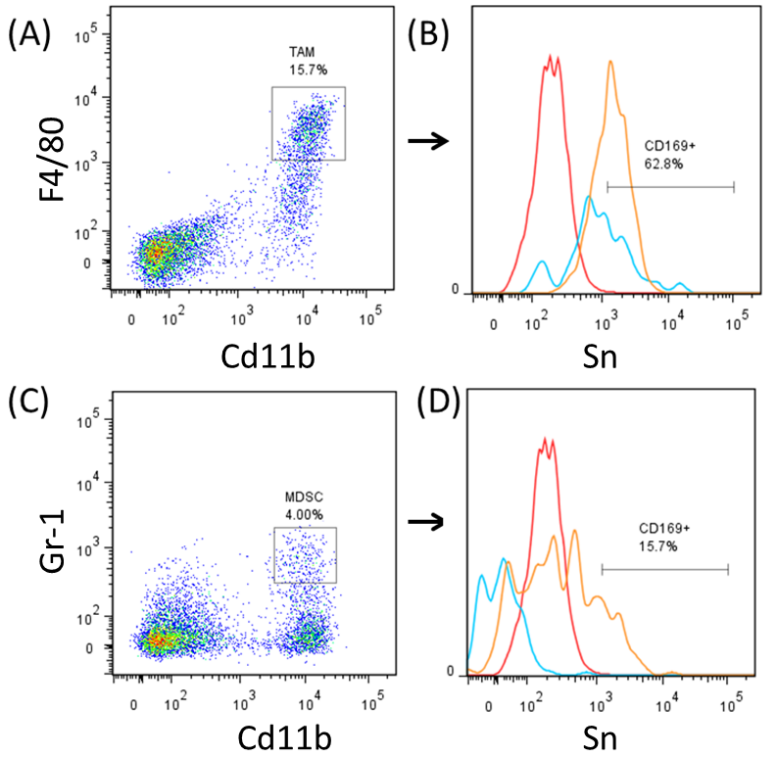

Figure 4.15 Sn expression of tumour associated Mϕ (TAM) and myeloid derived suppressor cell (MSDC) populations. Live cells from tumours (Figure 4.13 D) were stained for TAM subpopulations (A)– F4/80 and CD11b – and MDSC subpopulations (C) - Gr-1 and CD11b. Gated cells were then analysed for Sn expression (B and D for TAM and MDSC, respectively). Red = left femur; Blue = right femur; Red = unstained control.

	Irradiated to Non-irradiated TAM Ratio	Irradiated MDSC (% expression)
Tumour NT	1.74	15.7

Table 4.4 Sn expression of of tumour associated Mϕ (TAM) and myeloid derived suppressor cell (MSDC) populations. Data from figure 4.15 expressed as irradiated to non-irradiated ratio (TAM) or as % expression (MDSC). Gated cells were then analysed for Sn expression with Sn expression gate set using unstained control.

4.3.3.4 Relative Uptake Values

Relative uptake values were determined between the irradiated and non-irradiated bones (see Figure 4.16), such that a value > 1 indicates increased uptake in the irradiated limb as compared to the non-irradiated. Relative uptake values calculated by biodistribution showed all NT mice to have increased uptake in the irradiated limb, whilst Day 7 CSF1R treated group all showed decreased uptake in the irradiated limb.

For day 7 and tumour-bearing groups, NT mice displayed greater uptake than their respective CSF1R counterparts. No uptake bias was observed between day 2 CSF1R and NT mice.

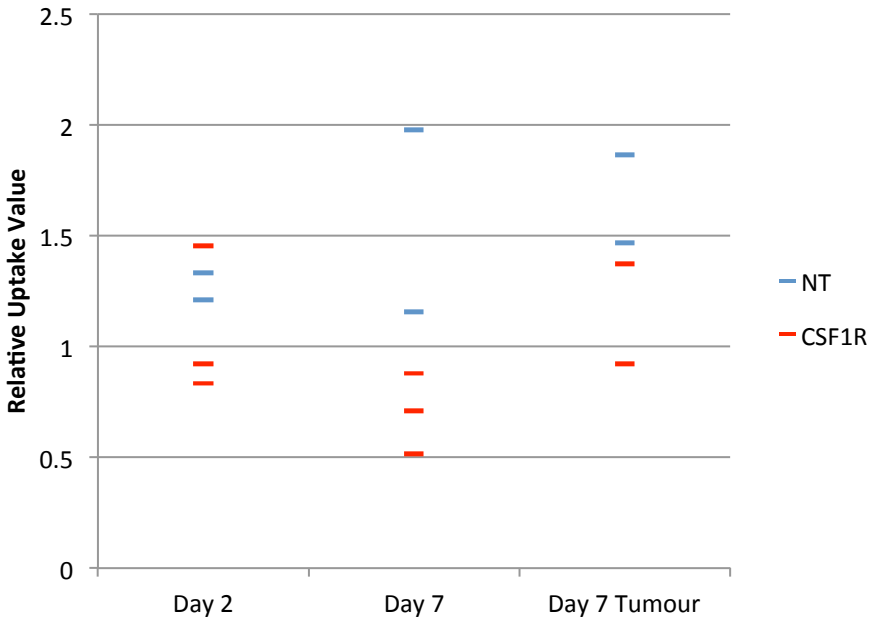

Figure 4.16 Irradiated and non-irradiated femur relative uptake values from biodistribution (n = 2 to 3 per group). Tumour bearing and non-tumour bearing mice (n = 2 to 3 per group) receiving localised irradiation with treatment (NT – blue dash) or CSF1 inhibitor (CSF1R – red dash) were injected with ~3.5 MBq ^{64}Cu-SER4. Non-tumour bearing mice were culled at 2 days and 7 days post irradiation, and tumour bearing mice culled at 7 days post irradiation. Each dash represents data from one mouse. Relative uptake is presented as a ratio between percentage injected dose per gram (%ID/g) of the irradiated (right) femur to that of the non-irradiated (left) femur. Values > 1 indicate an increase in uptake to the irradiated limb versus the non-irradiated, whilst < 1 indicate decrease in irradiated limb uptake relative to non-irradiated.

Comparison of the activity between the irradiated and non-irradiated femurs was also performed by ROI analysis (see Figure 4.17). ROI defined by the bone marrow cavity was compared to produce relative uptake values. The NT groups of day 7 and tumour-bearing mice all showed greater uptake in the irradiated limb than the CSF1R groups. Additionally, tumour mice recorded higher relative uptake values than day 7 mice for both NT and CSF1R groups respectively, with NT tumour bearing mice exhibiting the highest relative uptake values of all groups. No uptake pattern was observed between mice from day 2 NT and CSF1R groups.

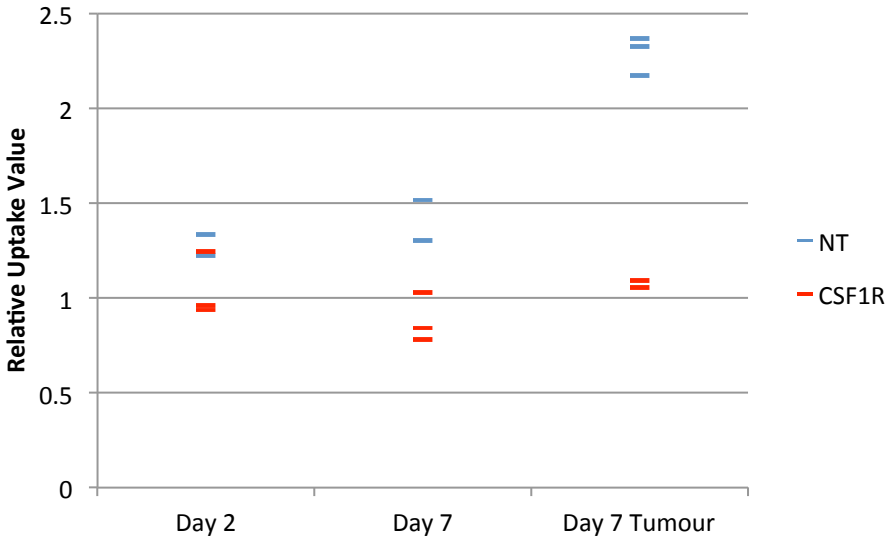

Figure 4.17 13 Irradiated to non-irradiated bone marrow relative uptake values from ^{64}Cu-SER4 imaging in tumour and non-tumour bearing mice post localised irradiation and CSF1R treatment (n = 2 to 3 per group). Mice received localised irradiation either no treatment (NT – blue dash) or CSF1 inhibitor treatment (CSF1R – red dash) until the date of imaging. Non-tumour bearing mice were imaged at 2 days and 7 days post irradiation. Mice bearing bilateral tumours were imaged at 7 days post irradiation. Mice were injected with ~3.5 MBq ^{64}Cu-SER4 and images were acquired at 4 hours post injection. Regions of interest (ROI) of bone marrow were defined by the internal cavity of bone using CT. Comparison of the signal from the irradiated to the non-irradiated ROI was used to generate relative uptake values. Each dash represents data from one mouse. Values > 1 indicate an increase in uptake to the irradiated limb versus the non-irradiated, whilst < 1 indicate decrease in irradiated limb uptake relative to non-irradiated.

4.3.3.5 Comparison of Selected Organ Uptake

For day 2 and day 7 groups (see Figure 4.18), blood activity varied with a range > 10 %ID/g. In day 7 group, CSF1R mice had higher blood uptake values than NT mice, whilst spleen and liver for all mice showed lower uptake values in the CSF1R group compared to its respective NT group. No bias was observed between blood uptake for day 2 NT and CSF1R groups, however as with day 7, liver and spleen all recorded lower uptake values in the day 2 CSF1R group versus NT group.

Day 2 and Day 7 CSF1R groups contained n = 3 data, permitting statistical analysis. CSF1R mice from showed significantly lower splenic ($p = 0.033$, decreasing by 77.2% by percentage injected dose per gram) and liver ($p = 0.011$, decreasing by 64.8% by

percentage injected dose per gram) uptake in day 7 compared to day 2 groups, as shown by Student's T test. Additionally, significantly higher blood activity ($p = 0.033$, increasing by 44.0% by percentage injected dose per gram) was recorded in CSF1R treated day 7 mice as compared to day 2.

A:

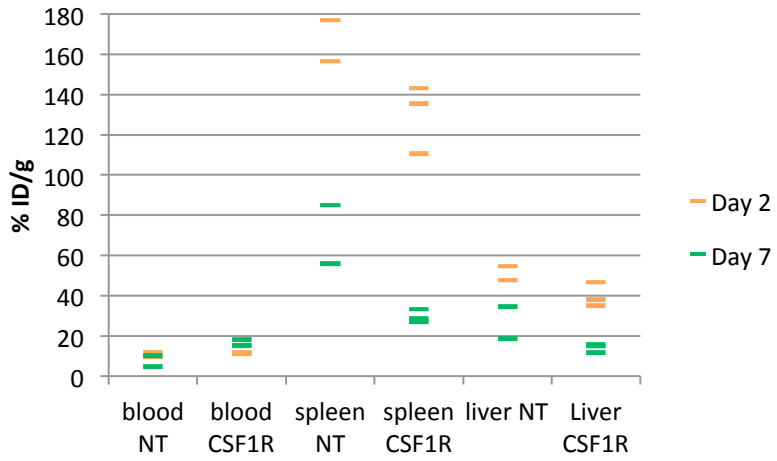

B:

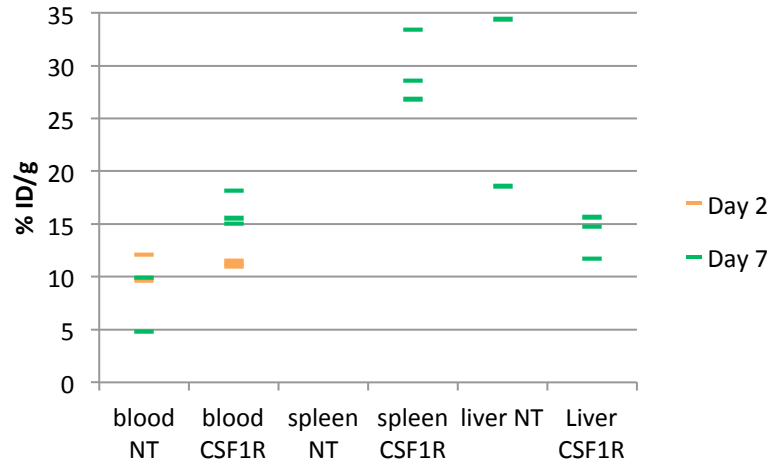

Figure 4.18 Selected organ uptake of ^{64}Cu-SER4 in C57BL6 mice after 2 and 7 days recovery following localised irradiation with and without CSF1R treatment (n = 2 to 3 per group). Non-tumour bearing mice receiving localised irradiation with no treatment (NT)and CSF1 inhibition (CSF1R) were injected with ~3.5 MBq ^{64}Cu-SER4 at 2 days (yellow dash) and 7 days (green dash) post irradiation, culled at 4 hr post injection then organs harvested, weighed and gamma counted. Each dash represents data from one mouse. Radioactive uptake in blood, spleen and liver is represented as percentage injected dose per gram (%ID/g).). A: full biodistribution, B: zoom of biodistribution to view low activity organs.

4.4 Discussion

The preparation and radiolabelling of NOTA-conjugates for labelling with ^{64}Cu is a routine procedure, affording immunoconjugates with fast labelling speed in ambient conditions with a high degree of *in vivo* stability (Cooper, Sabbah et al. 2006; Cooper, Ma et al. 2012). SER4-NOTA exemplified this process and provided consistent radiolabelling that was resistant to EDTA challenge, indicating incorporation of copper into the chelator. Due to time constraints of project in UCLA, *in vitro* characterisation of the ^{64}Cu-SER4 such as serum stability, number of chelators per antibody and binding to recombinant Sn was not carried out (see chapter 3 for recombinant Sn binding and serum stability assays performed with ^{99m}Tc-SER4). As stability of copper-labelled NOTA conjugates is well established, the binding of ^{64}Cu-SER4 to recombinant Sn was a desirable assay to determine whether specificity of the parent antibody had been retained for the immunoconjugate (for a description of this assay see chapter 2). Given time constraints an effective *in vivo* binding assay was decided upon using uptake in endogenous Sn expressing tissues (such as the spleen) as indication of binding. Unfortunately this technique doesn't permit quantification of binding, and so it will be necessary to conduct *in vitro* binding assays to determine immunoreactivity of ^{64}Cu-SER4.

Dynamic scanning was performed on one mouse and hence is not statistically analysed or significant; however it indicated rapid accumulation of ^{64}Cu-SER4 to target organs. As observed with the tracer ^{99m}Tc-SER4, the highest uptake of the antibody is in the spleen, followed by the liver and bone marrow. Once again, the rate at which the tracer accumulates is unique amongst intact IgG, which traditionally have much longer residence times (see chapter 3). Where targeting to the spleen results from antigen expression, liver uptake is a combination of antigen targeting and non-specific copper uptake. Macrocyclic structures such as DOTA conjugated to peptides and proteins have been noted for their high liver uptake (Smith 2004). Although the mechanism has yet be elucidated, *in vivo* transchelation of copper-64 to copper binding proteins is thought to participate in this uptake. Further on, the selection of BFC has been shown to influence the biodistribution of a tracer, such that NOTA is thus far identified as the

commercially available conjugate that affords the least non-specific liver uptake (Dearling, Voss et al. 2011; Cooper, Ma et al. 2012). The selection of NOTA-SCN reflected this favourable *in vivo* property, as well as its fast labelling kinetics.

From the kinetic data presented in the dynamic study, the rate of blood clearance and tissue uptake appears to undergo two phases: an initial rapid change in which blood activity is seen to half in approximately 20 min post injection, which adjusts to a slower rate of change from approximately 1 hr post injection onwards, suggesting two processes are taking place. A possible explanation is that in the first period the antigen sink is in excess, as such the rate of tissue accumulation/blood clearance is determined by antigen access and hence is rapid in the highly perfused organs where the antigen resides at the point of contact with the blood. The transition to a slower rate of blood clearance may result from antigen saturation, thus the probe is in approximate equilibrium and further blood clearance results from antigen internalisation and/or radiotracer metabolism. Whether or not antigen sink is the determinant of the first phase could be investigated by kinetic studies of the radiotracer in combination with excess cold antibody to block antigen sink. In the instance that antigen sink is in excess but becomes saturated with time, addition of excess cold SER4 would reduce organ uptake/blood clearance. Such a methodology has been applied to the imaging of non-Hodgkin lymphoma using anti-CD20 IgG, in which unlabelled antibody is administered before radiotracer to block endogenous antigen and thereby extend blood residence of the tracer (Sharkey, Karacay et al. 2009). Alternatively, the transition from rapid uptake to slow uptake/plateau may represent the complete uptake of targeting antibody and remaining non-targeting immune-conjugate (which has lost binding through the process of radiotracer development) presenting as non-specific signal. The amount of non-binding tracer could be ascertained by an immunoreactivity assay using recombinant antigen (see Chapter 2).

As the data is limited to one mouse, determining whether tissue uptake is occurring or a plateau has been reached is not possible. However there is the suggestion that splenic uptake is slowly increasing, possibly representing antigen internalising and residualising of the tracer. This effect could be probed by comparison of kinetic data from ^{64}Cu-SER4 with iodinated-SER4 to determine/confirm whether the antigen is

internalising. This is based upon Cu presenting as a residualising radioisotope that after internalisation is trapped intracellularly, whereas iodine is readily cleaved from the radiotracer in the acidic environment of the phagolysosome and then exported out of the cell (Olafsen and Wu 2010). Establishing whether or not an antigen is internalising has implications for both imaging and therapy (Nielsen and Marks 2000).

The localised irradiation model was performed on groups of n = 2 or n = 3, hence the discussion does not include statistically significant conclusions unless specifically mentioned. At day 2 post irradiation, correlation between Sn expression and tracer uptake was not observed. For the NT group, decreased Sn expression was seen by flow cytometry in the irradiated limb as compared to the non-irradiated, whereas biodistribution and ROI analysis all indicated higher uptake. This disparity may arise from subject variability and be addressed by greater sample numbers. Alternatively, lower Sn expression may result from radioablation of Sn expressing cells, whilst the increased uptake could be accounted for by non-specific uptake of the tracer. Administered to the whole body, 10 Gy is lethal however localised irradiation of a femur results in the collapse of the resident cell population which is then steadily repopulated (Werts, Gibson et al. 1980). Radiation induced break down of the bone marrow sinusoidal structure can cause blood pooling (Higashi, Fisher et al. 2000) which may lead to enhanced non-specific retention of the tracer. Flow data indicates that CSF1R mice exhibit less Sn expression between irradiated and non-irradiated limbs than NT mice, so larger group sizes would allow for the statistical comparison of whether Sn expression influences the uptake at day 2 post irradiation.

A striking asymmetrical tracer uptake was seen on Day 7 mice between irradiated and non-irradiated limbs of the NT group. Whole body imaging showed more uptake in the irradiated femur, which was confirmed by relative uptake values determined from both biodistribution and ROI analysis. Asymmetrical uptake was not seen directly in the biodistribution data, as irradiated femurs did not display uniformly greater uptake than non-irradiated femurs. However the femurs showed a wide range of values between mice, which may in part be due to recording the mass and activity of the entire bone rather than the bone marrow. Additionally, it has been previously reported that when examining the response of bone marrow to localised irradiation,

considerable intersubject variation of bone marrow cellularity can comparison of variations in absolute cell numbers during the response (Elnaggar, Hanna et al. 1980). As such, comparison of relative activity of the non-irradiated femur to the irradiated more accurately reflects the response to localised irradiation between subjects, and confirmed the increased uptake observed by imaging. A possible explanation regarding the increased Mϕ burden is that following irradiation, a rapid influx of neutrophils is observed (Higashi, Fisher et al. 2000) which would require clearance during the resolution of inflammation, a process that is conducted by tissue Mϕ. Another explanation is based on the recently finding that bone marrow Mϕ are directly implicated in the retention of HSCs (Winkler, Sims et al. 2010), in which specific ablation of Sn positive Mϕ results in increased levels of circulating HSCs (Chow, Lucas et al. 2011). This raises the possibility that alongside a scavenging role, the presence of increased numbers of Sn positive Mϕ may be part of the host response in restoring the haematopoietic environment through increased restriction of HSC efflux.

Furthermore, relative uptake values from ROI indicated higher uptake following 7 day recovery to irradiation in the presence of a tumour. This suggests that the tumoural environment, or its response to irradiation, has a local effect upon the bone marrow. Flow cytometry of day 7 mice showed that Sn expression was relatively increased in the irradiated bone marrow, and in particular on a subset of cells expressing CD11b and Gr-1, which are sometimes characterised as MDSC (Ribechini, Greifenberg et al. 2010). This result indicates Sn expression is present upon an immature myeloid cell type resident in the bone marrow, which poses questions as to the identity of this cell type (are they MDSC) and the purpose/function of Sn expression upon them. The possibility arises that following irradiation tumours may enrich MDSC bone marrow populations expressing Sn, which may then traffic to the tumour and contribute to increased MDSC recruitment. To further investigate this, Sn expression in irradiated bone marrow from tumour bearing mice should be compared to non-tumour bearing mice.

For tumour and non-tumour bearing mice at day 7 post irradiation, CSF1R groups all showed lower relative uptake values than their NT counterparts. In this instance, CSF1R inhibition may be delaying the recruitment of monocyte/Mϕ to the irradiated

tissue, a strategy which has been used for blocking Mϕ recruitment to tumours (MacDonald, Palmer et al. 2010; Coniglio, Eugenin et al. 2012). Alternatively, disruption of CSF-1 may be inhibiting maturation signals that allow for Sn expression. It is tempting to speculate that as the degree of structural damage arising from irradiation is likely to be independent of Mϕ recruitment, and thus non-specific uptake to be the same in both NT and CSF1R groups, that the increased relative uptake between NT and CSF1R represents specific uptake. This may be probed by comparison of uptake using a labelled isotype control or by using Sn KO mice (see Chapter 3).

In the tumour-bearing group, whole body imaging also delineated the non-irradiated tumour more clearly than the irradiated. On inspection the irradiated tumour was significantly smaller than the non-irradiated (approximately 10 times less mass recorded during biodistribution). Additionally the non-irradiated contained a substantial necrotic core, and as such produced far more non-specific tracer uptake due to enhanced permeabilisation which contributed to better visualisation of the non-irradiate tumour. Irradiation of solid tumours frequently results in the enhanced recruitment of myeloid cells which can enhance tumour growth (Ahn, Tseng et al. 2010; Kozin, Kamoun et al. 2010) and the flow cytometry data from the tumours revealed the upregulation of Sn following irradiation, agreeing with biodistribution data. When cellular subsets were analysed, it could also be seen that Sn expression by TAM increased following irradiation, and that the cell population defined as MDSC showed upregulation of Sn. Though inconclusive, this data may reveal the target cell type to be not exclusively mature Mϕ but to include other cells of the myeloid lineage. The subject of MDSC in tumour proliferation is an active area of research as this class of cell are thought to contribute to the immunosuppressive environment that allows permits tumour growth (Ochando and Chen 2012). The data shows that Sn expressing myeloid cells are part of the tumoural infiltrate in response to irradiation, and hence may be an important cellular subset during this process. The preliminary biodistribution data also indicates that higher uptake of tracer was observed in tumours with higher target expression. Future studies may be performed with tumour implantation of the non-irradiated occurring after implantation of the irradiated so as

to be able to image tumours that are approximately of equivalent size and thus reduce the impact of necrosis.

Day 7 CSF1R mice showed higher blood uptake than day 7 NT mice and significantly higher blood uptake than day 2 CSF1R mice, suggesting CSF1R treatment and duration influenced blood kinetics. All CSF1R treated mice also recorded lower splenic uptake than their NT counterpart, suggesting that uptake decreases with CSF1R exposure. Additionally, Day 7 CSF1R mice show significantly less splenic uptake than day 2 CSF1R mice suggesting that uptake decreases with CSF1R treatment duration. This apparent inverse relationship between splenic uptake and blood pool may be connected, whereby reduced Sn levels in the spleen serve to decrease the antigen sink and hence increase the amount of circulating ^{64}Cu-SER4. This direct relationship between CSF1R and Sn expression is in agreement with the recent finding that treatment with anti-CSF1R mAb results in down regulation of Sn expression in the MZM (Hashimoto, Chow et al. 2011). However the day 2 NT mice also exhibit higher splenic uptake values than day 7 NT mice so it can't be ruled out that this drop the CSF1R treated group may reflect some overall change in Sn expression following irradiation. Radiation exposure results in the release of cytokines, in particular IL-6 (Haveman, Geerdink et al. 1998; Van der Meeren, Monti et al. 2001) which can induce systemic effects, such as increased haematopoiesis (Mouthon, Vandamme et al. 2001). In this way the influence of irradiation may be realised by the release of soluble factors that influence splenic populations of Mϕ, upregulating Sn. However, the day 2 mice were on average 2 weeks younger than the day 7 and tumour groups, hence it cannot be eliminated that this observed change in splenic uptake between day 2 and day 7 groups may be attributable to developmental regulation of Sn. To address this, the selection of age matched mice could establish whether Sn upregulation is an early, systemic response to localised irradiation.

4.5 Summary

In this chapter the preparation and preliminary data concerning the *in vivo* functioning of the novel Mϕ-specific PET imaging agent ^{64}Cu-SER4 was described. ^{64}Cu-SER4 demonstrated rapid binding to endogenous populations of Sn positive Mϕ. In a model of localised bone marrow irradiation, ^{64}Cu-SER4 indicated increased Sn expression during recovery which was increased further in the presence of an irradiated tumour. Inhibition of CSF1 signalling blocked increased uptake following irradiation, and also diminished endogenous Sn expression. ^{64}Cu-SER4 may also have revealed transient elevation in splenic Sn expression resulting from localised irradiation. Future studies require greater subject numbers to establish significance, however at present the data reports the first specific myeloid response to radiation recovery which may provide insights for bone marrow transplantation. Furthermore, identification of Sn expressing myeloid infiltrates in tumour confirms indicates the potential of imaging this class of cell type following irradiation induced recruitment, however preliminary data indicates the significance of endogenous Sn-expressing Mϕ populations obscuring this population.

Chapter 5:

Dual Isotope Imaging of ED2-DTPA-^{111}In and ^{99m}Tc-ED3

5.1 Introduction

Mϕs display considerable plasticity of phenotype and often it is considered the balance between phenotypes that determines the outcome of disease processes. In this way tumour progression is often considered the transition of an inflammatory M1 phenotype to an immuno-suppressive M2 phenotype (see Chapter 1). Therefore detecting the relative levels of these populations *in vivo* has important implications for predicting disease progression and treatment. Given the promising results of anti-Sn imaging in mice as an M1 marker (see Chapter 3) we sought to compare the behaviour of such an M1 probe with an M2 probe in the rat. SPECT imaging technology is able to detect gamma emissions at different energies and consequently allows for the simultaneous imaging of different tracers. In this chapter we aim to produce two radiotracers using anti-Mϕ antibodies ED2 and ED3 with orthogonal radioisotopes and evaluate their feasibility for imaging of different endogenous Mϕ populations using SPECT/CT.

5.1.1 ED2 and ED3

The ED hybridoma series were originally prepared by immunising mice with rat spleen cells, then selecting clones on the basis of splenic tissue staining. ED2 and ED3 emerged as antibodies identifying different Mϕ subpopulations which exhibited distinct localisation patterns in the lymphoid tissue (Dijkstra, Dopp et al. 1985). ED3 was shown to have binding properties and tissue distribution similar to antibodies recognising murine Sn leading to its assignment as an anti-Sn antibody (Damoiseaux, Huitinga et al. 1992) and often cited as a marker of inflammatory/M1 Mϕs (see Chapter 1). ED2 was more recently shown to recognise the antigen CD163, the so called haemoglobin-haptoglobin scavenger receptor (SR), and has routinely been used

to characterise mature tissue Mϕ (Polfliet, Fabriek et al. 2006) and is a putative marker for M2 Mϕs (see below).

5.1.2 Scavenger Receptor CD163

The SR family is a class of proteins defined by their ability to recognise polyanionic structures, and originally identified by their mediation of modified low-density lipoprotein uptake by Mϕ (Fabriek, van Bruggen et al. 2009). CD163 is a myeloid-restricted antigen belonging to the SR family which exhibits scavenging as well as immunomodulatory behaviour (Van Gorp, Delputte et al. 2010).

CD163 is composed of nine extracellular scavenger receptor cysteine rich (SRCR) domains, a transmembrane domain, and a cytoplasmic domain containing a variety of phosphorylation sites as well as an internalising motif (Van Gorp, Delputte et al. 2010). Low levels of expression are found on circulating monocytes (in humans), with levels significantly increased on tissue resident Mϕs (such as Kupffer cells and red pulp Mϕs) suggesting its use as a maturation marker. Additionally, significant levels of soluble CD163 are found in serum (approximately 2 mg/L) which can be further elevated during diseased states (Moller, Peterslund et al. 2002). Expression of CD163 in human monocytes can be increased by exposure to glucocorticoids and anti-inflammatory cytokines IL-6 and IL-10, whilst inflammatory cytokines such as IFN-γ and TNF-α have been shown to decrease expression. However, ligation of toll-like receptors (TLRs) has been shown to increase expression whilst no modulation occurs in the presence of the anti-inflammatory cytokines IL-4 and IL-13, qualifying expression as broadly anti-inflammatory (Van Gorp, Delputte et al. 2010). Similarly, expression in rodent Mϕs has been shown to be induced by glucocorticoid exposure and enhanced by co-incubation with IL-4, whilst a range of other cytokines have failed to exhibit regulation properties (Polfliet, Fabriek et al. 2006).

The most characterised function for CD163 is as the haemoglobin SR, in which it removes haemoglobin-haptoglobin (Hb-Hp) complexes from the circulation via endocytosis (Kristiansen, Graversen et al. 2001). Additionally CD163 has been shown to be an erythroblast adhesion receptor (Fabriek, Polfliet et al. 2007) and act as a

bacterial sensor (Fabriek, van Bruggen et al. 2009) which has been exploited by some pathogens for entry into Mϕs (Van Gorp, Delputte et al. 2010). Down regulation of CD163 by exposure to IFN-γ and TNF-α and induction from glucocorticoids, IL-6 and IL-10 implies its expression relates to Mϕ subsets known as "alternatively activated" (or M2) (Van Gorp, Delputte et al. 2010) rather than "classically activated" (M1) Mϕs (see Chapter 1). In accordance with this, IL-10 secretion resulting from CD163-mediated internalisation of Hb-Hp indicates an anti-inflammatory role for CD163 (Philippidis, Mason et al. 2004). However, antibody-mediated cross-linking of CD163 as well as bacterial ligation have been shown to induce secretion of pro-inflammatory cytokines (Polfliet, Fabriek et al. 2006; Fabriek, van Bruggen et al. 2009). These data point to CD163 exerting both pro- and anti-inflammatory functions *in vivo*.

With constitutive expression on monocytes making CD163 not a strictly Mϕ-restricted antigen, it can be argued that its targeting permits the tracking of myeloid cells. However, the significant upregulation of it in mature Mϕs as compared to circulating monocytes may not preclude it from functioning as essentially a Mϕ-specific antigen. Where clinically CD163 Mϕs have been identified in a variety of pathologies, including atherosclerotic plaques (Johnson and Newby 2009), multiple sclerotic lesions (Zhang, Zhang et al. 2011) as well as present on TAMs (Pettersen, Fuentes-Duculan et al. 2011), there is clearly an imperative for assessing Mϕ presence using this marker.

5.2 Materials and Methods

5.2.1 ED2 Hybridoma

Anti-rat Sn ED2 antibody was isolated as previously described using the ED2 hybridoma (Dijkstra, Dopp et al. 1985) which was acquired from HPACC (UK). Cells were grown in 1640 RPMI (Sigma, Poole, UK) supplemented with pen/strep (Invitrogen) and IgG depleted FBS (Source Bioscience UK Ltd, Nottingham, UK). 8 x 10^6 cells were suspended in 5 then transferred to a Celline CL350 flask (Integra Biosciences AG). Cells were pelleted every 7 days, the supernatant harvested with the pellet resuspended 1:4 in media and returned to the CL350 flask (see Figure 2.4).

5.2.2 ED2 and ED3 Purification

ED3 ascites was a gift from C.D. Dijkstra (VU University Medical Centre, Amsterdam, Netherlands). Excess lipoprotein was removed from ascites by dextran sulphate precipitation in the presence Ca^{2+} ions to prevent column degradation (Amersham Handbook of Protein Purification). 0.32 mL of 10% dextran sulphate solution (Sigma, Gillingham, UK) and 8 mL of 1 M CaCl2 (Sigma, Gillingham, UK) were added to 8 mL of ED3 ascites and left for 15 min. The mixture was centrifuged at 10,000 x g for 10 min and the supernatant collected.

5 mL of supernatant from ED2 hybridoma or lipoprotein-depleted ED3 ascites was diluted in 5 mL binding buffer (20 mM sodium phosphate, pH 7.0) and passed through a 0.22 µm filter. Filtrate was loaded on to a 5 mL HiTrap Protein G HP column (GE, Amersham, UK) then washed with 10 column volumes of binding buffer. Antibody was eluted with 0.1 M glycine-HCl, pH 2.7, collected in 2.5 mL fractions and neutralised with 200 µL of 1 M Tris.HCl, pH 9.0. Protein concentration was determined by measuring OD_{280} using a Biophotometer (Eppendorf, Cambridge, UK). Protein fractions were transferred to dialysis cassettes (Thermofisher, Loughborough, UK) and dialysed in PBS with 3 buffer exchanges. Antibody was then concentrated using Vivaspin columns (Sartorius Stedim, Epsom, UK) to 10 mg/mL. Protein fractions were then analysed by reduced and non-reduced SDS PAGE gel (200 V, 120 A, 50 min) Gels were then stained with SimplyBlue Safe Stain (Invitrogen, Paisley, UK) for 45 minutes followed by 3 washes with deionised water.

5.2.3 Immunohistochemistry

Spleens from 8 week old male Wistar rats were harvested, embedded in OCT (RA Lamb Ltd, Eastbourne, UK) and snap frozen in liquid nitrogen. Tissue was then cut at 5 µm using a Brightwater Cryostat (Bright Instruments, Huntingdon, UK) and mounted onto polylysine slides (Thermofisher, Loughborough, UK). Sections were air dried overnight, transferred to 50 mL falcon tubes (BD Biosciences) then stored at – 80°C until staining. For staining, sections were taken from freezer and left at room temperature for 10 min before removing from falcon tube. Sections were immersed in chilled acetone for 5 min and then left to air dry for 15 min. Sections were rehydrated in PBS, then

incubated overnight with either ED2 or ED3 (1 μg/mL), followed by anti-mouse Fc AlexaFluor-480 (1:200, 1 h, AbD Serotec, Oxon, UK). Slides were washed then mounted in VectaShield with DAPI (Vector Labs). Images were captured using a Leica Leitz DMRB research microscope and ExiBlue camera. Images were analysed with Image-Pro Plus 7.0 software from Media Cybernetics and Photoshop.

5.2.4 Preparation of ED2-CHX-A''-DTPA

Ethylenediaminetetraacetic acid (EDTA, 50 mM, 25 μL) was added to ED2 antibody (3 mg) in PBS (250 μL) and incubated at room temperature for 30 min. The solution was transferred to an ultracentrifugation tube (Vivaspin 2, 30,000 MWCO, PES membrane) and the buffer exchanged to 0.1 M HEPES buffer, pH 8.9 by washing three times with HEPES buffer.

N-[(R)-2-Amino-3-(*p*-isothiocyanato-phenyl) propyl]-*trans*-(*S,S*)- cyclohexane-1,2-diamine-*N,N,N',N'',N''*-pentaacetic acid (CHX-A''-DTPA) (0.4 mg) in DMSO (40 μL) was added to the ED2 solution (400 μL) and the conjugation allowed to proceed at room temperature for 3 h then overnight at 4°C. Buffer exchange was then performed with 0.1 M ammonium acetate, pH 6 and the final solution concentrated (5 mg/mL). Conjugation was assisted by Dr. MS Cooper.

5.2.5 Radiolabelling ED2-CHX-A''-DTPA

$^{111}InCl_3$ in 0.05 M HCl (Covidien, Petten, Netherlands) was added (47 MBq, 114 μL) to ED2-CHX-A''-DTPA in ammonium acetate (120 μL, 2 mg/mL) and incubated at room temperature for 20 min. The radiolabelled antibody was analysed by size exclusion HPLC by size exclusion HPLC using a BioSep SEC-S-2000 column (Phenomenex, Macclesfield, UK) with an isocratic mobile phase of 0.1 M phosphate buffer containing 2 mM EDTA, pH 7 and a flow rate of 1 mL/min. The retention time of the radioimmunoconjugate was typically 7 min and that of the unbound ^{111}In impurities was approximately 11 min.

5.2.6 Preparation of ^{99m}Tc-ED3

200 µL of protein G-purified ED3 (10 mg/mL, PBS) was incubated with 2µL of 14.3 M 2-mercaptoethanol (Sigma Aldrich, Poole, UK) for 30 min at room temperature. The solution was transferred to a PD MiniTrap G-10 column (GE, Chalfont St. Giles, UK) and eluted with degassed PBS. 0.2 mL fractions were collected and OD_{280} determined using a BioPhotometer (Eppendorf, Cambridge, UK). Fractions with an OD_{280} >5 mg/mL were pooled, aliquoted into 20 µL fractions, snap-frozen in liquid nitrogen and stored at -80C until further use.

For radiolabelling, 5 µL of a reconstituted MDP kit (Medronate Draximage, Draxis, USA) was added to 20 µL of freshly thawed reduced ED3, followed by 200 MBq of sodium pertechnetate Tc-99m in between 20 to 40 µL saline (kindly provided by Department of Nuclear Medicine at Guys Hospital UK) then incubated at room temperature for 15 min. Labelling efficiency was measured using thin layer chromatography strips (ITLC-SA) (Varian Medical Systems UK, Ltd., Crawley, UK) with a mobile phase of 0.1 M citrate buffer, pH 5 and analysed using a gamma-ray TLC scanner (Lablogic, UK). Labelling efficiency was assessed also by HPLC-SEC using a BioSep SEC-300 column (Phenomenex, Macclesfield, UK) with an isocratic mobile phase of 100 mM phosphate buffer, pH 7.0, at a flow rate of 1 mL/min and in-line gamma detector (Lablogic, UK).

5.2.7 ED2-DTPA-^{111}In and ^{99m}Tc-ED3 Serum Stability

10 MBq of ED2-DTPA-^{111}In and 50 MBq of ^{99m}Tc labelled ED3 were added to AB type human serum (Sigma) or PBS (Gibco) at 1:4 v/v and incubated at 37 °C for 20 h. Samples were analysed at 0, 3, 6 and 20h by HPLC-SEC using a BioSep SEC-300 column (Phenomenex, Macclesfield, UK) with an isocratic mobile phase of 100 mM phosphate buffer, pH 7.0, at a flow rate of 1 mL/min and in-line gamma detector (Lablogic, UK). Serum stability was calculated as the area under the antibody-bound activity peaks as a fraction of total eluted activity.

5.2.8 *In vivo* Imaging and Biodistribution of ED2-DTPA-^{111}In and ^{99m}Tc-ED3

Imaging was performed using a nanoSPECT/CT small animal scanner (Bioscan Inc., Washington, USA) SPECT images were obtained using a 4-head scanner with 1 mm pinhole collimators. Helical acquisitions were performed with 24 projections with the time per projection adjusted so as to make overall scan time equal to 45 min. CT images were obtained using 45 KVp X-ray source, set with a 500 ms exposure time in 180 projections lasting approximately 10 min. Images were reconstructed using proprietary BioScan InVivoScope (IVS) software.

Adult male rats (Wistar, 8 – 10 weeks) were injected IV under anaesthesia (isoflurane, VetOne, UK) with approximately 2MBq ED2-DTPA-^{111}In and 50MBq ^{99m}Tc-ED3 in 500 µL (approx. 1 mg/mL; n = 3). Each was recovered, culled at 3 h then imaged immediately. After imaging standard biodistributions were performed.

Syringes (25G X 16mm, Terumo) were weighed before and after injection, and serial dilutions of 1:4 were performed with a starting 100 µL stock solution (containing both ED2-DTPA-^{111}In and ^{99m}Tc-ED3). After culling according to schedule 1, the animals were dissected and the following organs harvested: intestines, stomach, spleen, liver, kidney, heart, lungs, blood (20 µL), muscle, bone and tail. The tissue samples were weighed and radioactivity counted using a gamma counter (LKB Wallac, Finland) alongside standards. Both In-111 emission windows (110-155, 170-185) were measured at day 1 and at day 4 post-experiment. Contribution of In-111 signal to Tc-99m emission was back calculated from day 4 counts and used to correct Tc-99m signal at day 1. Injected dose was then calculated for each isotope from total activity in each injected syringe minus activity counted in tail, and presented as the percentage of injected dose per gram (%ID/g) of each tissue sample.

5.2.9 Statistics

Uptake values were analysed for significance using a paired, 2-tail Student's T test, where p values < 0.05 were reported as significant.

5.3 Results

5.3.1 ED2 and ED3 Purification

ED2 and ED3 antibodies (against antigens CD163 and Sn, respectively) were purified via Protein G from culture supernatant of ED2 hybridoma grown in IgG depleted media and ED3 ascites. Purified protein was of approximately 150 kDa (lanes 2 and 4) and following reduction showed fragmentation pattern characteristic of IgG with 75 kDa, 50 kDa, 25 kDa bands (see Figure 5.1). For ED2 hybridoma, yields of between 9 – 12 mg/L of unsupplemented media were recovered, whilst of 8 mL ED3 ascites 2 mg of antibody was recovered.

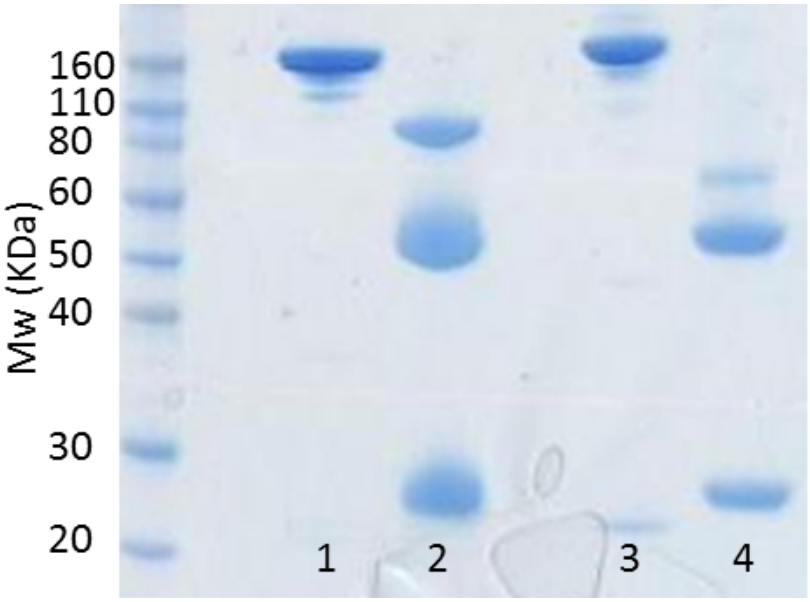

Figure 5.1 Reduced and non-reduced Protein G purified ED2 and ED3. Antibody was isolated from hybridoma supernatant (ED2) and ascites (ED3) using a Protein G column. Purified antibodies were run as non-reduced (ED2 lane 1; ED3 lane 3) and reduced (ED2 lane 2; ED3 lane 4) on SDS-PAGE.

5.3.2 Immunohistochemistry

Purified antibodies were assayed for functioning by staining endogenously Sn and CD163-expressing splenic tissue. ED2 heavily stained the red pulp (as distinguished from the white pulp by less cell numbers/nuclearity evidenced by DAPI – see Figure 5.2 A) whereas ED3 localised with cells lining the periphery of the white and red pulp with sporadic staining of the red pulp (see Figure 5.2).

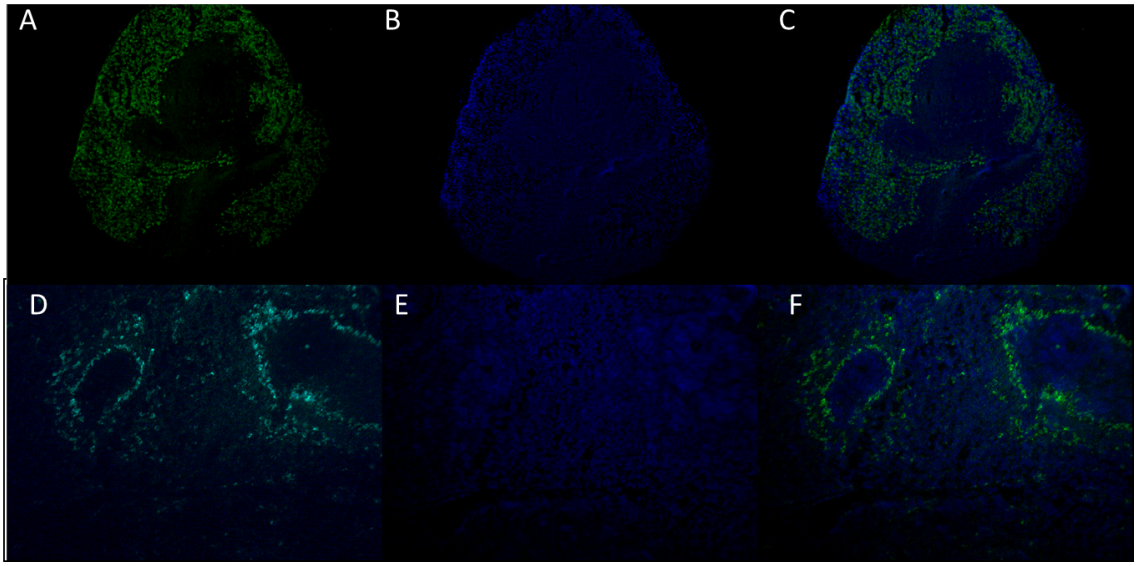

Figure 5.2 ED2 and ED3 staining of spleen. Rat spleens were incubated with ED2 and ED3 overnight, followed by a fluorescent secondary (A and D for ED2 and ED3, respectively) and mounted with DAPI mountant (B and E for ED2 and ED3, respectively). ED2 antibody stains Mϕs heavily in the red pulp which can be distinguished from white pulp by less cell numbers/nuclearity (identified by DAPI). ED3 antibody identifies Mϕs bordering the red and white pulp regions, forming characteristic elliptical structures in the spleen. Merged fluorophore and DAPI images are presented in panels C and F (ED2 and ED3, respectively). Magnification of 50x for A to C, 100x for D to F.

5.3.3 Preparation of ED2-CHX-A''-DTPA-^{111}In

ED2 was reacted with CHX-A''-DTPA and radiolabelling of the resulting immunoconjugate assessed by SEC radioHPLC. After 20 min incubation with $^{111}InCl_3$ 100% of radioactivity is found associated with the antibody as shown by single peak in radioHPLC chromatogram with a retention time of 7 min 20s (see Figure 5.3). The column was inspected for residual activity using a geiger counter (900 Series, Thermo Fisher Scientific, UK) to assay qualitatively any activity trapped on the column. Column activity did not significantly exceed background. A specific activity of 196 MBq/mg was routinely achieved

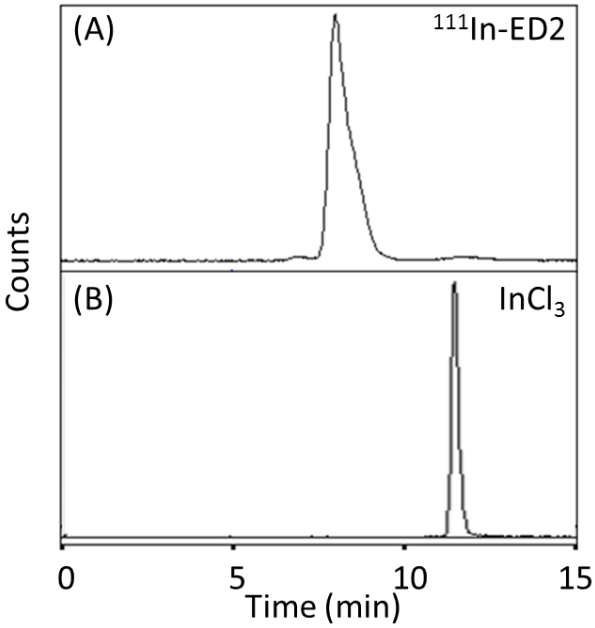

Figure 5.3 Radiolabelling ED2-CHX-A''-DTPA. The immunoconjugateED2- CHX-A''-DTPA was labelled with ^{111}In and analysed by SEC radioHPLC. All activity was associated with antibody (t = 7 min 20s – (A)) and $^{111}InCl_3$ signal absent (t = 11 min 30 sec - (B)).

5.3.4 Preparation of ^{99m}Tc-ED3

ED3 was partially reduced by incubation with 2-mercaptoethanol, stored in frozen aliquots then radiolabelling performed by addition of pertechnetate with freshly reconstituted MDP kit. Radiolabelling was assessed by SEC radioHPLC with PBS as eluent and ITLC using citrate buffer (pH 5, 0.1 M). SEC radioHPLC recorded three peaks with 97% of activity eluted at 7 min 20 sec, corresponding to antibody fraction, 2% activity eluted at 10 min 45 sec (representing either radiolabelled antibody fragment or 2-ME chelated activity), and 1% activity at 17 min 20 sec, corresponding to free pertechnetate (see Figure 5.4 A). ITLC shows 98% activity associated with protein (Rf = 0) and 2% as unbound (either free or colloidal – see Figure 5.4 B), corresponding to a specific activity of c. 2 GBq/mg

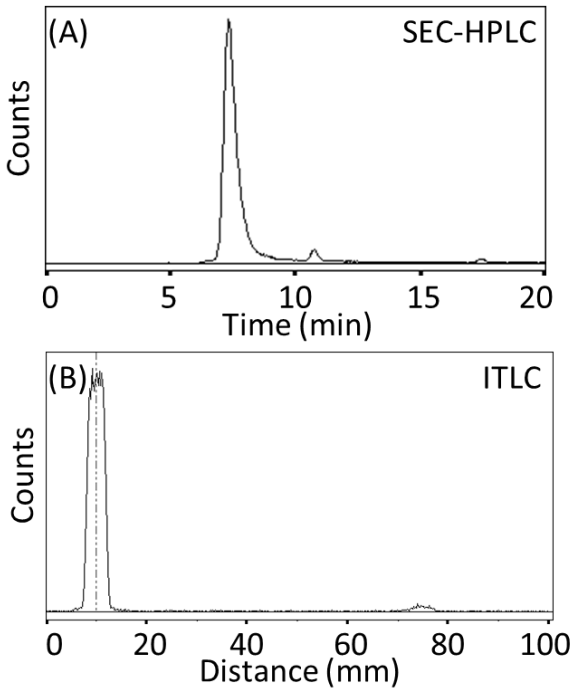

Figure 5.4 Direct labelling of ED3. Following disulphide reduction, ED3 was labelled with ^{99m}Tc. Samples were injected on a) SEC radioHPLC showing elution of majority activity with the antibody (t = 7 min 20 sec, 97%) and two minor peaks (t = 10 min 45 sec, 2%; t = 17 min 20 sec, 1%). B) ITLC showed the presence of radiolabelled protein (Rf = 0, 98%) and free pertechnetate (Rf=1, 2%).

5.3.5 ^{111}In-CHX-A''-DTPA-ED2 and ^{99m}Tc-ED3 Serum Stability

^{99m}Tc-ED3 was incubated in the presence of serum or PBS overnight and stability assayed by SEC radioHPLC. In the presence of PBS alone, ED2-CHX-A''-DTPA-^{111}In shows increased dissociation over time (from 96% to 86% labelled protein over 20 h), however not as markedly as directly labelled ED3 (from 90% to 75% labelled protein over 20 h - see Table 5.5) indicating the greater stability of the immunoconjugate. Both radiolabelled antibodies demonstrate similar stability in the presence of serum. Example traces of both antibodies at 20 h in the presence of serum or PBS are provided (see Figure 5.6).

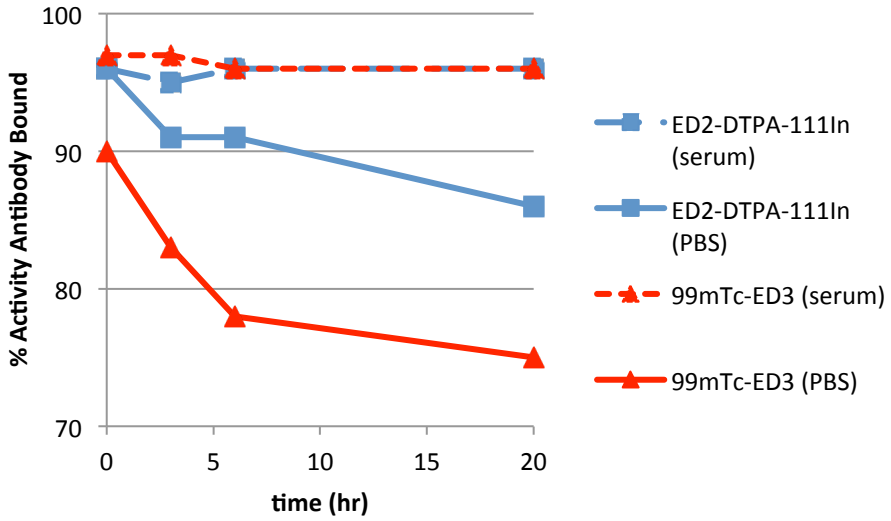

Figure 5.5 Serum stability of ED2-DTPA-^{111}In and ^{99m}Tc-ED3. Antibodies were labelled according to 2.3.3, incubated in either mouse serum or PBS and stability assessed by SEC radioHPLC. Percentage bound was assessed by comparison of bound activity to that of free activity peaks.

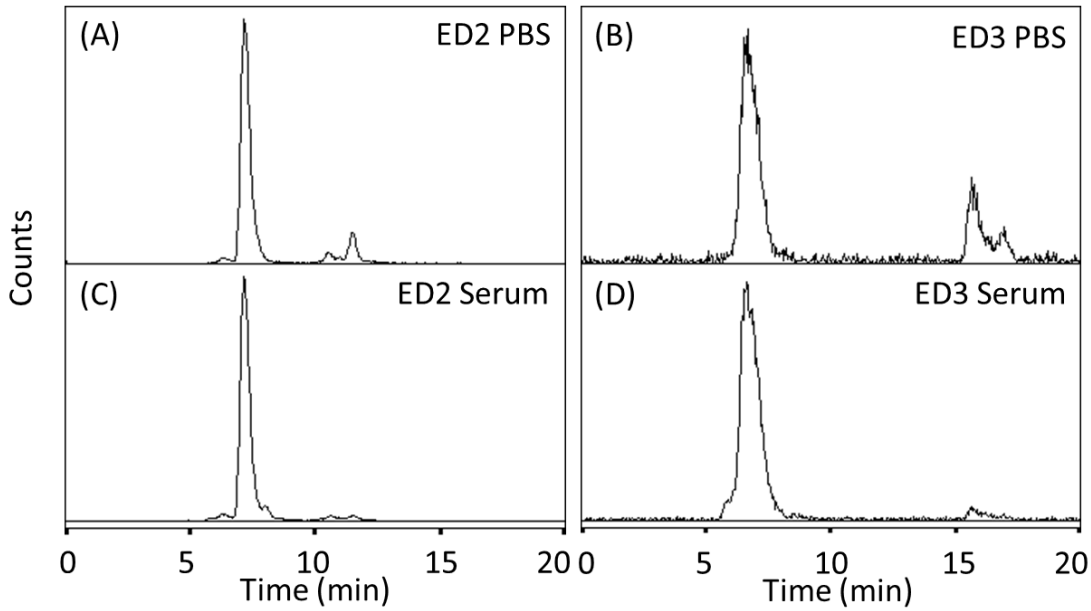

Figure 5.6 SEC radioHPLC analysis of ED2-DTPA-^{111}In and ^{99m}Tc-ED3 serum stability at 20 h. Both antibodies were incubated in the presence of PBS (^{99m}Tc-ED3 = A; ED2-DTPA-^{111}In = B) or serum (^{99m}Tc-ED3 = C; ED2-DTPA-^{111}In = D) for 20 h at 37°C then injected into SEC radioHPLC system. Percentage bound was assessed by comparison of bound activity (integral of 7 min 10 sec and 6 min 45 sec peaks for ED2 and ED3, respectively) to that of free activity (integral of 10 min 30 sec to 11 min 30 sec, and 15 min 20 sec to 16 min 05 sec peaks for ED2 and ED3, respectively).

5.3.6 *In vivo* ED2-CHX-A''-DTPA-^{111}In and ^{99m}Tc-ED3

Rats were culled 3 h post injection of ED2-CHX-A''-DTPA-^{111}In and ^{99m}Tc-ED3 followed by whole body imaging performed using nanoSPECT/CT. Imaging revealed co-localisation of ED2 and ED3 in the spleen and liver, with ED2 additionally accumulating in the bone. ^{99m}Tc was also observed in the bladder (see Figure 5.7).

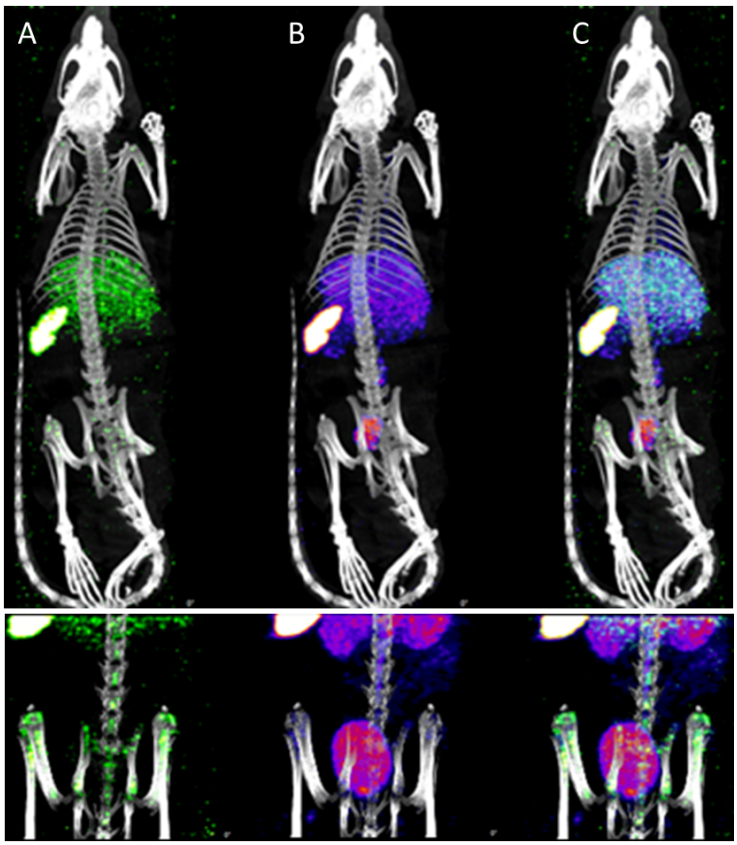

Figure 5.7 Simultaneous nanoSPECT/CT imaging of ED2-CHX-A''-DTPA-111In and 99mTc-ED3 in a wistar rat. Rat injected IV with ~2 MBq ED2-CHX-A''-DTPA-^{111}In and ~50 MBq ^{99m}Tc-ED3 then imaged at 3 h post injection. (A) ED2-CHX-A''-DTPA-^{111}In signal; (B) ^{99m}Tc-ED3 signal; (C) Fused ED2-CHX-A''-DTPA-^{111}In and ^{99m}Tc-ED3 signal. Upper panel: whole body acquisition, lower panel: pelvis acquisition.

Biodistributions were performed on animals culled at 3 h post injection of ED2-CHX-A''-DTPA-^{111}*In* and ^{99m}Tc-ED3 (see Figure 5.8). Both ^{111}In and ^{99m}Tc showed comparable accumulation in the spleen, liver, bone and heart. ^{99m}Tc additionally showed significantly higher accumulation in the kidney ($p < 0.001$), lungs ($p = 0.013$), urine ($p = 0.012$) and blood ($p = 0.019$) as compared to ^{111}In.

A:

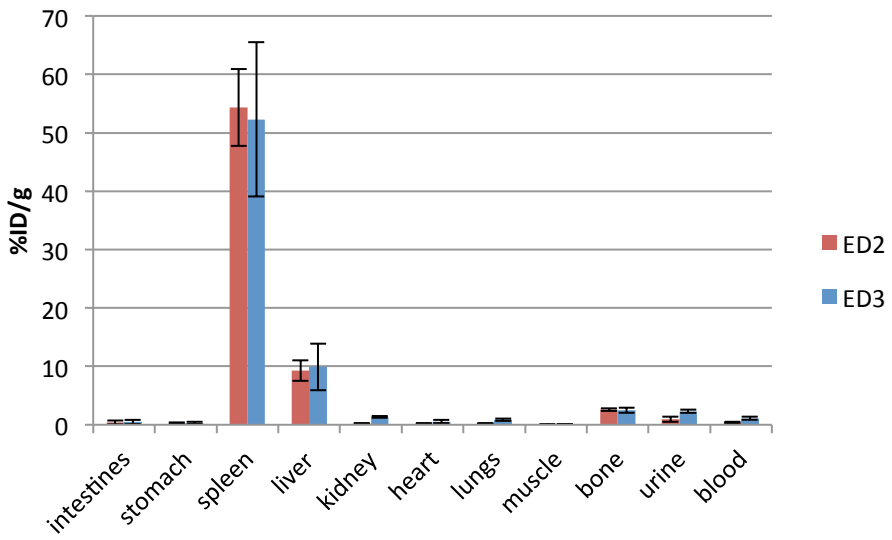

B:

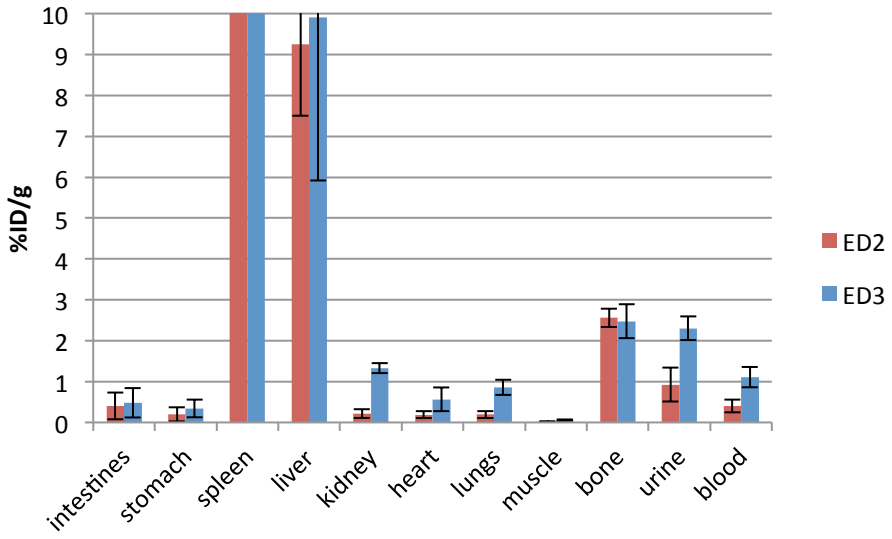

Figure 5.8 Biodistribution of ED2-CHX-A''-DTPA-111In and 99mTc-ED3 in 8 week old wistar rats (n=3). Rats were injected IV into the tail vein with ~2 MBq ED2-CHX-A''-DTPA-^{111}In and ~50 MBq ^{99m}Tc-ED3 then culled at 3 h post injection. Organs harvested, weighed and gamma counted. Radioactive uptake in organs is presented as the percentage-injected dose per gram per organ. **A:** Full biodistribution. **B:** Rescaled to a max of 10 %ID/g of A to see biodistribution of lower activity organs (error represents a standard deviation of n = 3)

Organ-to-blood ratios (see Figure 5.9) showed significantly elevated uptake of ED2 in spleen ($p = 0.030$) and bone ($p = 0.041$) as compared to ED3 and higher, albeit not significantly, liver uptake of ED2.

A:

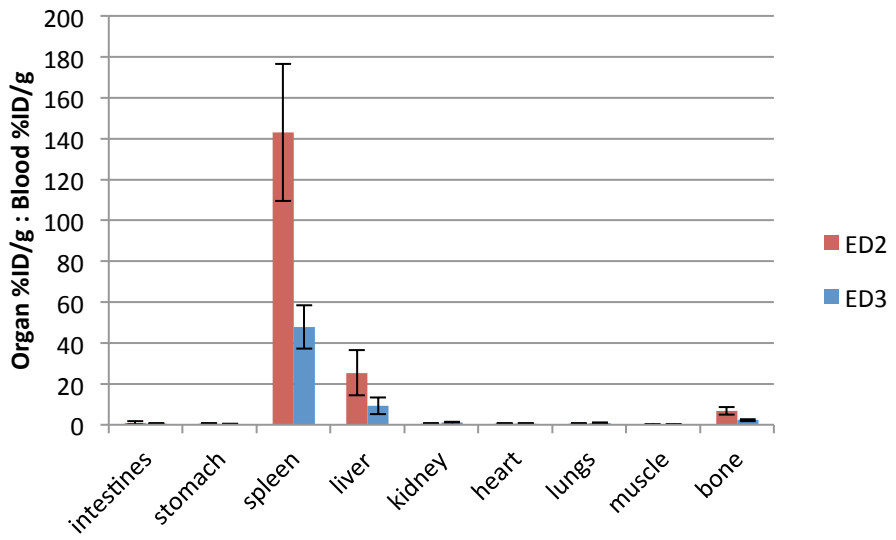

B:

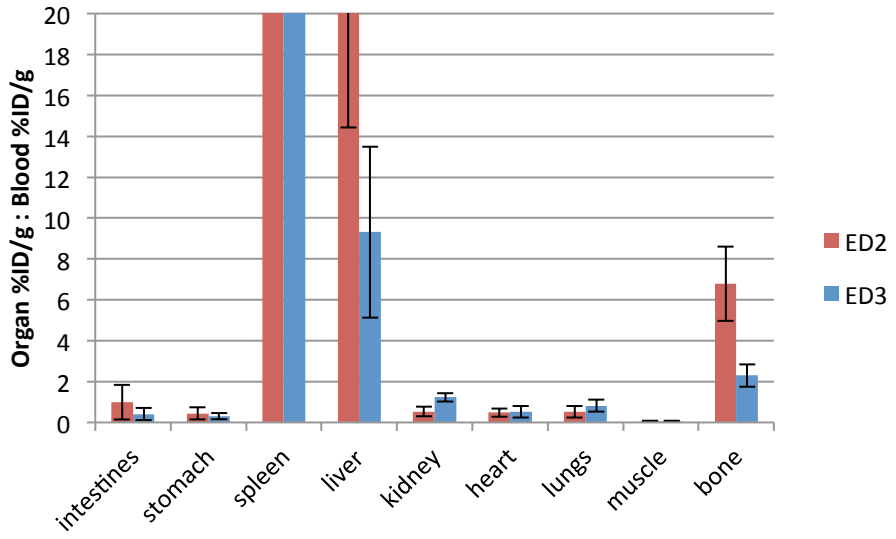

Figure 5.9 Organ-to-blood ratio of ED2-CHX-A''-DTPA-111In and 99mTc-ED3 in 8 week old wistar rats (n=3). Representation of biodistribution data from figure 6.7 as organ-to-blood ratio. A: full biodistribution, B: zoom of biodistribution to view low activity organs.

5.4 Discussion

ED2 hybridoma was grown using the Celline CL350 system followed by Protein G extraction resulted in yields comparable to the SER4 hybridoma (see chapter 2), whilst ED3 ascites yielded sufficient antibody for direct labelling procedure. Antibody

function was assayed in vitro by immunohistochemistry, which confirmed binding to discrete Mϕ subpopulations in the spleen identified as red pulp Mϕs and marginal metallophilic Mϕs for ED2 and ED3, respectively (Dijkstra, Dopp et al. 1985).

When deciding upon the radioisotope to label ED2 with it was taken into account that although endogenous CD163 could provide an antigen sink for circulating ED2, allowing imaging at a relatively earlier time point for an intact antibody (as with anti-CD169 SER4 antibody in mice – see chapter 3) significant amounts of soluble CD163 (sCD163) could bind to ED2 in the circulation and eliminate the endogenous sink effect (Moller, Peterslund et al. 2002). The preparation of ^{111}In-labelled ED2 permitted imaging over several days so as to allow blood clearance of any sCD163-bound ED2 and offered the chance to image ^{99m}Tc-labelled ED3 simultaneously. Additionally, the availability of established protocols in immunoconjugate production made preparation routine (Cooper, Sabbah et al. 2006).

The development of *in vitro* radiolabelling assays for ED2 and ED3 was obstructed by the availability of rat ED2 antigen (CD163) as well as the limited resource of ED3 antibody. As yet no recombinant form of rat CD163 is available, nor has a cell type been induced to express CD163. Preparation of affinity purified CD163 using sepharose column functionalised with ED2 has been performed, however a low recovery of approximately 100 μg antigen from 60 spleens was reported (Fabriek, Polfliet et al. 2007). Induction of ED3 antigen (CD169) has been shown using the Mϕ cell line R2 after incubation with dexamethasone and various cytokines (vandenBerg, vanDie et al. 1996). Due to limited amounts of ED3 available it was decided to not pursue this cell based assay. Based upon the behaviour of SER4 in mice (see chapter 3) it was determined that an *in vivo* based assay could be performed, wherein uptake to endogenous populations of Mϕs (particularly in the spleen) would indicate functioning of radiolabelled ED2 and ED3.

Whole body imaging revealed antibody uptake as expected from histological data (Dijkstra, Dopp et al. 1985). ED2 showed tracking to the spleen, liver and bone marrow due to CD163 expression by red pulp Mϕs, Kupffer cells and RBMMs as the target cell type in each of these organs, respectively. Organ expression of Sn in rats differs to that

of mice (and humans) in that it is not endogenously expressed by RBMMs. Thus ED3 showed only uptake to the spleen and liver. In this way whole body imaging of ED2 more resembled the distribution pattern of SER4 in mice than ED3 in rats. To our surprise, ED2-DTPA-^{111}In did not display prolonged circulation time of conventional radiolabelled IgG but instead exhibited rapid blood clearance similar to that of anti-Sn antibodies (i.e. ED3 and SER4). The levels of circulating sCD163 in rats has not been determined, so this effect may represent an absence of circulating sCD163 or alternatively it may be that ED2 is raised to an epitope outside of sCD163 structure but instead located on the membrane bound, extracellular portion of CD163.

Additionally the choice of radiolabel can influence targeting properties and distribution of activity. Non-specific hepatic uptake by of immunoconjugates is a clinically relevant feature that limits the use of radiolabelled antibodies in imaging disease processes involving the liver (Bander, Trabulsi et al. 2003; Bhattacharyya and Dixit 2011). Although the exact nature of this uptake has yet to be elucidated, both antibody (Morris, Divgi et al. 2005) and radioisotope-specific (Vallabhajosula, Kuji et al. 2005) effects have been shown to influence this uptake. In this way, ED2-DTPA-^{111}In imaging exhibits non-specific as well as specific uptake (mediated by the radiolabel and target antigen on Kupffer cells, respectively) to the liver, confounding the amount of specific uptake in this organ. Use of a directly labelled antibody, as with ED3, would avoid this uptake and instead result in accumulation of activity in the bladder. This effect is thought to be due to transchelation to cysteine in the bladder, which has the benefit of decreasing blood pool activity (see Chapter 3), and is observed in the imaging of ^{99m}Tc-ED3.

The distribution patterns of ED2 and ED3 in the liver indicate apparent heterogenous localisation of their respective Mϕ populations, as illustrated by ^{99m}Tc-ED3 signal observed from regions absent from ED2-DTPA-^{111}In. Similarly, faint ^{99m}Tc-ED3 can be seen in the femoral and tibial space, whereas distinct signal is observed from ED2-DTPA-^{111}In in these regions. This is consistent with the presence and absence of ED2 and ED3 positive Mϕs (respectively) from the bone marrow (see above) but also with the same pattern observed in synovial lining of the joint space (Verschure, Vannoorden et al. 1989).

Biodistribution data reproduced the expected distribution pattern with highest %ID/g for spleen then liver for both ED2-DTPA-^{111}In and ^{99m}Tc-ED3. Raw %ID/g values were similar for both ED2-DTPA-^{111}In and ^{99m}Tc-ED3 in the spleen. With ED3 absent from this compartment coupled with imaging data that indicated no specific uptake in the bone marrow by ^{99m}Tc-ED3 whereas ED2-DTPA-^{111}In showed definite uptake, the influence of contaminating blood pool was taken into consideration. With approximately a two fold increase of blood pool for ^{99m}Tc-ED3 compared to ED2-DTPA-^{111}In (in line with greater antigen sink for ED2) it was reasoned more perfused organs (such as spleen, liver and bone marrow) would exhibit higher levels of non-specific uptake due to contaminating blood pool signal. Representing biodistribution data as organ-to-blood ratios revealed significantly higher specific uptake of ED2-DTPA-^{111}In compared to ^{99m}Tc-ED3 in the spleen, which is in line with the relative abundances of CD163 and Sn positive Mϕs in the spleen (Dijkstra, Dopp et al. 1985). Additionally, organ-to-blood ratios identified the significantly higher uptake of ED2-DTPA-^{111}In in the bone, which is expected because of expression of CD163 but not Sn in rat bone marrow Mϕs.

5.5 Summary

In this chapter the development of two anti-Mϕ imaging agents based upon the antibodies ED2 (anti-CD163) and ED3 (anti-CD169, Sn) was reported. The imaging agents were designed to include orthogonal isotopes to permit the simultaneous imaging of two different Mϕ cell populations simultaneously. Due to time constraints and resources *in vitro* characterisation of both radiotracers was limited, with binding validated by *in vivo* tracking to target organs. Both antibodies displayed extravasation corresponding to degree of antigen sink, in which ED2 showed the more rapid clearance, and with each agent permitting early imaging time point for an intact antibody. The data are encouraging and supports the pursuit of *in vitro* characterisation of both agents, and warrant their application in the study of disease processes in which Mϕ balance is critical, such as rheumatoid arthritis and cancer.

Chapter 6

Summary

This thesis proposed that radiolabelled anti-Sn antibody could be used to image Mϕ *in vivo*. To this end, we have shown that a radiotracer based on the direct labelling of the anti-Sn antibody SER4 with ^{99m}Tc was able to bind to recombinant target antigen *in vitro* using a radioHPLC assay, and that *in vivo* the tracer tracked to the expected tissues in which endogenous Sn is expressed. Using a model of transplant rejection, we demonstrated that it was possible to image the recruitment of Sn positive Mϕ in an acutely rejecting transplant as compared to a tolerated transplant. The specific identity of these Mϕ was not identified and future studies should seek to characterise these, which could be achieved by flow cytometry analysis based on a panel of known phenotypic markers. From a basic science point of view, it is of interest to know if Sn is a functional participant in these Mϕ populations, which has been shown previous adaptive immune responses, or if Sn is simply a passive marker for inflammatory Mϕ. Whether Sn is functional could be investigated by conducting transplants onto Sn KO background mice, or via blocking Sn with antibody, however neither approach would determine if the influence of Sn is exerted locally in the rejected heart or systemically in lymphoid tissue. From a more clinical perspective, identifying if Sn has a functional role in rejection may provide a therapeutic strategy for treating this disease. When also considering imaging, the ability of the probe to measure the response to treatment would be informative upon the possibility of Sn imaging as a clinical tool. Further on, although acute graft rejection events represent a significant outcome for transplant recipients, it is the monitoring of chronic rejection that will have the greatest impact as this is the chief cause of transplant rejection. Therefore, imaging of Sn in a chronic transplant rejection model is a natural step from from these results.

The preliminary data collected during residence in the Wu Lab using a PET isotope labelled anti-Sn antibody generated the novel result that bone marrow Sn expression is upregulated following response to localised irradiation, and that this could be imaged. With scant data related to the roles of this particular Mϕ subset, this represents some tantalising data with a great deal of scope to explore. Regarding the functional

significance of this result, establishing whether Sn upregulation relates to Mϕ recruited for the clearance of the debris resulting from irradiation or, more speculatively, whether these Mϕ are re-establishing the haemopoietic niche, of which they are critical components, in order to resume haematopoiesis. With the finding that inhibition of CSF-1 signalling was able to abrogate this response then subsequent investigation could seek to examine the cellular constituents of treated and non-treated mice and relate whether clearance is impeded. Simultaneously, the levels of HSC colony forming units could be used to determine whether HSC are being retained or released systemically in response to irradiation, and then this data may be correlated with levels of Sn expression in the irradiated tissue. However, this would not ascribe whether increased HSC retention is occurring specifically in the irradiated tissue.

Sn expression was also found on a population of cells expressing markers of MDSC. Although the possibility that Sn may include MDSC confounds its use as a Mϕ-restricted marker, it also suggests another avenue for its function *in vivo*. Following the observation that MDSC are recruited to the tumour environment following localised irradiation and that these cells assist in tumour development (personal communication, Lily Wu), as well as the enrichment of bone marrow Sn in the proximity of an irradiated tumour that also express MDSC markers suggests an origin for these infiltrating cells. Where MDSC are characterised by considerable heterogeneity, the identification of Sn as a cell surface marker may represent the identification of a specific subset with tumour promoting capacity. The significance of this finding needs to be established but at present points to a novel cellular expression of Sn.

We finally showed the feasibility of using antibodies targeted to different Mϕ-specific antigens for simultaneous imaging of two different macrophage populations in rats. Leading on from this a study examining the relative merits of these antibodies in imaging Mϕ recruitment during various disease models would be a logical next step. With previous research comparing macrophages expressing these antigens during

arthritic induction using histological examination, repetition of this work with whole body imaging would be a suitable experiment to assess the validity of this approach.

Apart from addressing the questions raised by the specific studies performed during this thesis, the initial data supports the investigation of Sn targeting for imaging Mϕ in man. With the availability of anti-human Sn antibody (HSN-1), the next stage would be the humanisation of this mouse background protein and production of it in GMP facilities. With Sn expression identified on circulating monocytes the utility of strategy may be restricted to binding to this cell population and subsequent imaging after their extravasation from the vascular system. In this manner it would present as a similar agent to Leukoscan, a radiolabelled antibody targeted to granulocytes. However the different trafficking properties of the target cells, namely granulocytes tracking to acute inflammation versus monocyte trafficking to chronic inflammation, could be especially informative, for example in conditions such as atherosclerosis. If levels of Sn on circulating monocytes were not found to be significant then anti-human Sn imaging could be a means of targeting inflammatory Mϕ as observed in the preclinical findings recorded here.

Future work focussed on preclinical studies may also involve the development of engineered antibody fragments. The advantages of such proteins are often found with site specific labelling to be able to produce uniform, reproducible imaging agents but also for increasing antibody clearance and thus reducing imaging time points. Although SER4 showed exceptionally high clearance for an intact antibody, blood activities were still relatively high during imaging. By dropping this further, the influence of blood pool could be reduced whilst keeping the time between injection and imaging short.

In conclusion, this thesis has proposed anti-Sn imaging as a means of identifying by whole body imaging Mϕ populations *in vivo*, and with the potential to track their appearance during disease processes. By showing targeting to Sn Mϕ in wild type animals and during different disease models the validity of Sn targeting for *in vivo* imaging has been established. Along with future studies examining the role of Sn expressing cells in the specific systems that were covered during the course of this research, our findings indicate the utility of pursuing Sn imaging for humans.

Publications and Posters

7.1 Publications

A.S.G. O'Neill, T.K. van den Berg, G.E.D. Mullen; Sialoadhesin – A Macrophage-Restricted Marker of Immunoregulation and Inflammation, Immunology

7.2 Posters

A.S.G. O'Neill et al "Radiolabelled SER-4 Antibody Detects Increased Bone Marrow Sialoadhesin Expression During Recovery to Radioablation of Prostate Tumour", World Molecular Imaging Congress, 2012

A.S.G. O'Neill et al "Simultaneous Imaging of M1 and M2 Macrophages", World Molecular Imaging Congress, 2012

A.S.G. O'Neill et al "Imaging Immunoregulatory Macrophages in Transplantation", World Molecular Imaging Congress, 2011

References

Ahn, G. O., D. Tseng, et al. (2010). "Inhibition of Mac-1 (CD11b/CD18) enhances tumor response to radiation by reducing myeloid cell recruitment." Proceedings of the National Academy of Sciences of the United States of America **107**(18): 8363-8368.

Aparicio-Vergara, M., R. Shiri-Sverdlov, et al. (2010). "Bone marrow transplantation in mice as a tool for studying the role of hematopoietic cells in metabolic and cardiovascular diseases." Atherosclerosis **213**(2): 335-344.

Asano, K., A. Nabeyama, et al. (2011). "CD169-Positive Macrophages Dominate Antitumor Immunity by Crosspresenting Dead Cell-Associated Antigens." Immunity **34**(1): 85-95.

Ayala-Lopez, W., W. Xia, et al. (2010). "Imaging of Atherosclerosis in Apoliprotein E Knockout Mice: Targeting of a Folate-Conjugated Radiopharmaceutical to Activated Macrophages." Journal of Nuclear Medicine **51**(5): 768-774.

Backer, R., T. Schwandt, et al. (2010). "Effective collaboration between marginal metallophilic macrophages and CD8(+) dendritic cells in the generation of cytotoxic T cells." Proceedings of the National Academy of Sciences of the United States of America **107**(1): 216-221.

Ballou, B., G. Levine, et al. (1979). "Tumor location detected with radioactively labeled monoclonal antibody and external scintigraphy." Science **206**(4420): 844-847.

Bander, N. H., E. J. Trabulsi, et al. (2003). "Targeting metastatic prostate cancer with radiolabeled monoclonal antibody J591 to the extracellular domain of prostate specific membrane antigen." Journal of Urology **170**(5): 1717-1721.

Barral, P., P. Polzella, et al. (2010). "CD169(+) macrophages present lipid antigens to mediate early activation of iNKT cells in lymph nodes." Nature Immunology **11**(4): 303-U348.

Beckmann, N., C. Cannet, et al. (2006). "Macrophage infiltration detected at MR imaging in rat kidney allografts: Early marker of chronic rejection?" Radiology **240**(3): 717-724.

Berney, C., S. Herren, et al. (1999). "A member of the dendritic cell family that enters B cell follicles and stimulates primary antibody responses identified by a mannose receptor fusion protein." Journal of Experimental Medicine **190**(6): 851-860.

Bhattacharyya, S. and M. Dixit (2011). "Metallic radionuclides in the development of diagnostic and therapeutic radiopharmaceuticals." Dalton Transactions **40**(23): 6112-6128.

Biesen, R., C. Demir, et al. (2008). "Sialic acid-binding Ig-like lectin I expression in inflammatory and resident monocytes is a potential biomarker for monitoring disease activity and success of therapy in systemic lupus erythematosus." Arthritis and Rheumatism **58**(4): 1136-1145.

Bingle, L., N. J. Brown, et al. (2002). "The role of tumour-associated macrophages in tumour progression: implications for new anticancer therapies." Journal of Pathology **196**(3): 254-265.

Blixt, O., B. E. Collins, et al. (2003). "Sialoside specificity of the siglec family assessed using novel multivalent probes - Identification of potent inhibitors of myelin-associated glycoprotein." Journal of Biological Chemistry **278**(33): 31007-31019.

Boswell, C. A. and M. W. Brechbiel (2007). "Development of radioimmunotherapeutic and diagnostic antibodies: an inside-out view." Nuclear Medicine and Biology **34**(7): 757-778.

Brinkman-Van der Linden, E. C. M., E. R. Sjoberg, et al. (2000). "Loss of N-glycolylneuraminic acid in human evolution - Implications for sialic acid recognition by siglecs." Journal of Biological Chemistry **275**(12): 8633-8640.

Carol, M., C. Pelegri, et al. (2000). "Immunohistochemical study of lymphoid tissues in adjuvant arthritis (AA) by image analysis; relationship with synovial lesions." Clinical and Experimental Immunology **120**(1): 200-208.

Carter, P. J. (2006). "Potent antibody therapeutics by design." Nature Reviews Immunology **6**(5): 343-357.

Chakrabarti, M. C., N. Le, et al. (1996). "Prevention of radiolysis of monoclonal antibody during labeling." Journal of Nuclear Medicine **37**(8): 1384-1388.

Chasis, J. A. and N. Mohandas (2008). "Erythroblastic islands: niches for erythropoiesis." Blood **112**(3): 470-478.

Chou, R. C., X. L. Dong, et al. (1998). "Adrenergic regulation of macrophage-derived tumor necrosis factor-alpha generation during a chronic polyarthritis pain model." Journal of Neuroimmunology **82**(2): 140-148.

Chow, A., D. Lucas, et al. (2011). "Bone marrow CD169(+) macrophages promote the retention of hematopoietic stem and progenitor cells in the mesenchymal stem cell niche." Journal of Experimental Medicine **208**(2): 261-271.

Christen, T., K. Shimizu, et al. (2010). "Advances in Imaging of Cardiac Allograft Rejection." Current Cardiovascular Imaging Reports **3**(2): 6.

Chtanova, T., S.-J. Han, et al. (2009). "Dynamics of T Cell, Antigen-Presenting Cell, and Pathogen Interactions during Recall Responses in the Lymph Node." Immunity **31**(2): 342-355.

Cochran, A. J., R.-R. Huang, et al. (2006). "Tumour immunology - Tumour-induced immune modulation of sentinel lymph nodes." Nature Reviews Immunology **6**(9): 659-670.

Coniglio, S. J., E. Eugenin, et al. (2012). "Microglial Stimulation of Glioblastoma Invasion Involves Epidermal Growth Factor Receptor (EGFR) and Colony Stimulating Factor 1 Receptor (CSF-1R) Signaling." Molecular Medicine **18**(3): 519-527.

Cook, H. T., S. J. Singh, et al. (1999). "Interleukin-4 ameliorates crescentic glomerulonephritis in Wistar Kyoto rats." Kidney International **55**(4): 1319-1326.

Cooper, M. S., M. T. Ma, et al. (2012). "Comparison of Cu-64-Complexing Bifunctional Chelators for Radioimmunoconjugation: Labeling Efficiency, Specific Activity, and in Vitro/in Vivo Stability." Bioconjugate Chemistry **23**(5): 1029-1039.

Cooper, M. S., E. Sabbah, et al. (2006). "Conjugation of chelating agents to proteins and radiolabeling with trivalent metallic isotopes." Nature Protocols **1**(1): 314-317.

Copelan, E. A. (2006). "Medical progress: Hematopoietic stem-cell transplantation." New England Journal of Medicine **354**(17): 1813-1826.

Cormode, D. P., R. Chandrasekar, et al. (2009). "Comparison of Synthetic High Density Lipoprotein (HDL) Contrast Agents for MR Imaging of Atherosclerosis." Bioconjugate Chemistry **20**(5): 937-943.

Crocker, P. R., S. Freeman, et al. (1995). "Sialoadhesin binds preferentially to cells of the granulocytic lineage." Journal of Clinical Investigation **95**(2): 635-643.

Crocker, P. R. and S. Gordon (1985). "Isolation and characterization of resident stromal macrophages and hematopoietic-cell clusters from mouse bone-marrow." Journal of Experimental Medicine **162**(3): 993-1014.

Crocker, P. R. and S. Gordon (1986). "Properties and distribution of a lectin-like hemagglutinin differentially expressed by murine stromal tissue macrophages." Journal of Experimental Medicine **164**(6): 1862-1875.

Crocker, P. R. and S. Gordon (1989). "Mouse macrophage hemagglutinin (sheep erythrocyte receptor) with specificity for sialylated glycoconjugates characterized by a monoclonal-antibody." Journal of Experimental Medicine **169**(4): 1333-1346.

Crocker, P. R., A. Hartnell, et al. (1997). "The potential role of sialoadhesin as a macrophage recognition molecule in health and disease." Glycoconjugate Journal **14**(5): 601-609.

Crocker, P. R., M. Hill, et al. (1988). "Regulation of a murine macrophage hemagglutinin (sheep erythrocyte receptor) by a species-restricted serum factor." Immunology **65**(4): 515-522.

Crocker, P. R., S. Kelm, et al. (1991). "Purification and properties of sialoadhesin, a sialic acid-binding receptor of murine tissue macrophages." Embo Journal **10**(7): 1661-1669.

Crocker, P. R., S. Mucklow, et al. (1994). "Sialoadhesin, a macrophage sialic-acid binding-receptor for hematopoietic-cells with 17 immunoglobulin-like domains." Embo Journal **13**(19): 4490-4503.

Crocker, P. R., J. C. Paulson, et al. (2007). "Siglecs and their roles in the immune system." Nature Reviews Immunology **7**(4): 255-266.

Crocker, P. R. and P. Redelinghuys (2008). "Siglecs as positive and negative regulators of the immune system." Biochemical Society Transactions **36**: 1467-1471.

Dainiak, N. (2002). "Hematologic consequences of exposure to ionizing radiation." Experimental Hematology **30**(6): 513-528.

Daldrup-Link, H., D. Golovko, et al. (2011). "MRI of tumor-associated macrophages with clinically applicable iron oxide nanoparticles." (1078-0432 (Print)).

Daldrup-Link, H. E., T. Henning, et al. (2007). "MR imaging of therapy-induced changes of bone marrow." European Radiology **17**(3): 743-761.

Damoiseaux, J., E. A. Dopp, et al. (1989). "Rat bone-marrow and monocyte cultures - Influence of culture time and lymphokines on the expression of macrophage differentiation antigens." Journal of Leukocyte Biology **46**(3): 246-253.

Damoiseaux, J., I. Huitinga, et al. (1992). "Expression of the ED3 antigen on rat macrophages in relation to experimental autoimmune diseases." Immunobiology **184**(4-5): 311-320.

de Roos, A. (2012). "Science to Practice: Why Follow the Track of Macrophages in Obesity?" Radiology **263**(3): 623-625.

Dearling, J. L. J., S. D. Voss, et al. (2011). "Imaging cancer using PET - the effect of the bifunctional chelator on the biodistribution of a Cu-64-labeled antibody." Nuclear Medicine and Biology **38**(1): 29-38.

Delputte, P. L., W. Van Breedam, et al. (2007). "IFN-alpha treatment enhances porcine Arterivirus infection of monocytes via upregulation of the porcine Arterivirus receptor sialoadhesin." Journal of Interferon and Cytokine Research **27**(9): 757-766.

Delputte, P. L., H. Van Gorp, et al. (2011). "Porcine Sialoadhesin (CD169/Siglec-1) Is an Endocytic Receptor that Allows Targeted Delivery of Toxins and Antigens to Macrophages." Plos One **6**(2).

den Haan, J. M. and G. Kraal (2012). "Innate Immune Functions of Macrophage Subpopulations in the Spleen." J Innate Immun.

Dijkstra, C. D., E. A. Dopp, et al. (1985). "The heterogeneity of mononuclear phagocytes in lymphoid organs - distinct macrophage subpopulations in the rat recognised by the monoclonal antibody-ED1, antibody-ED2 and antibody-ED3." Immunology **54**(3): 589-599.

Dijkstra, C. D., E. A. Dopp, et al. (1987). "Macrophages and dendritic cells in antigen-induced arthritis - an immunohistochemical study using cryostat sections of the whole knee-joint of rat." Scandinavian Journal of Immunology **26**(5): 513-523.

Ducreux, J., P. R. Crocker, et al. (2009). "Analysis of sialoadhesin expression on mouse alveolar macrophages." Immunology Letters **124**(2): 77-80.

Elnaggar, A. M., I. R. A. Hanna, et al. (1980). "Bone marrow changes after localized acute and fractionated X irradiation." Radiation Research **84**(1): 46-52.

Erwig, L. P. and A. J. Rees (1999). "Macrophage activation and programming and its role for macrophage function in glomerular inflammation." Kidney & Blood Pressure Research **22**(1-2): 21-25.

Fabriek, B. O., M. M. J. Polfliet, et al. (2007). "The macrophage CD163 surface glycoprotein is an erythroblast adhesion receptor." Blood **109**(12): 5223-5229.

Fabriek, B. O., R. van Bruggen, et al. (2009). "The macrophage scavenger receptor CD163 functions as an innate immune sensor for bacteria." Blood **113**(4): 887-892.

Fischer, C. R., C. Mueller, et al. (2012). "F-18 Fluoro-Deoxy-Glucose Folate: A Novel PET Radiotracer with Improved in Vivo Properties for Folate Receptor Targeting." Bioconjugate Chemistry **23**(4): 805-813.

Fliedner, T. M., D. Graessle, et al. (2002). "Structure and function of bone marrow hemopoiesis: Mechanisms of response to ionizing radiation exposure." Cancer Biotherapy and Radiopharmaceuticals **17**(4): 405-426.

Gabrilovich, D. I. and S. Nagaraj (2009). "Myeloid-derived suppressor cells as regulators of the immune system." Nature Reviews Immunology **9**(3): 162-174.

Garcia, E. V. (2012). "Physical attributes, limitations, and future potential for PET and SPECT." Journal of nuclear cardiology : official publication of the American Society of Nuclear Cardiology **19 Suppl 1**: S19-29.

Geissmann, F., M. G. Manz, et al. (2010). "Development of Monocytes, Macrophages, and Dendritic Cells." Science **327**(5966): 656-661.

Gessl, A., G. Boltznitulescu, et al. (1989). "Expression of a binding structure for sialic acid-containing glycoconjugates on rat bone marrow-derived macrophages and its modulation by IFN, TNF-alpha, and dexamethasone." Journal of Immunology **142**(12): 4372-4377.

Glaudemans, A. W. J. M., R. A. J. Dierckx, et al. (2010). "The role of radiolabelled anti-TNF alpha monoclonal antibodies for diagnostic purposes and therapy evaluation." Quarterly Journal of Nuclear Medicine and Molecular Imaging **54**(6): 639-653.

Gmeiner Stopar, T., J. Fettich, et al. (2008). "99mTc-labelled rituximab, a new non-Hodgkin's lymphoma imaging agent: first clinical experience." Nuclear medicine communications **29**(12): 1059-1065.

Goldenberg, D., D. F. Preston, et al. (1974). "Photoscan localization of GW-39 tumors in hamsters using radiolabeled anticarcinoembryonic antigen immunoglobulin G." Cancer Research **34**(1): 1-9.

Goldsmith, S. J. and A. Signore (2010). "An overview of the diagnostic and therapeutic use of monoclonal antibodies in medicine." Quarterly Journal of Nuclear Medicine and Molecular Imaging **54**(6): 574-581.

Gordon, S. and P. R. Taylor (2005). "Monocyte and macrophage heterogeneity." Nature Reviews Immunology **5**(12): 953-964.

Hamilton, J. (2011). "Colony stimulating factors and macrophage heterogeneity." Inflammation and Regeneration **31**(3): 9.

Hartnell, A., J. Steel, et al. (2001). "Characterization of human sialoadhesin, a sialic acid binding receptor expressed by resident and inflammatory macrophage populations." Blood **97**(1): 288-296.

Hashimoto, D., A. Chow, et al. (2011). "Pretransplant CSF-1 therapy expands recipient macrophages and ameliorates GVHD after allogeneic hematopoietic cell transplantation." Journal of Experimental Medicine **208**(5): 1069-1082.

Hashimoto, Y., M. Suzuki, et al. (1998). "A streptavidin-based neoglycoprotein carrying more than 140 GT1b oligosaccharides: Quantitative estimation of the binding specificity of murine sialoadhesin expressed on CHO cells." Journal of Biochemistry **123**(3): 468-478.

Haveman, J., A. G. Geerdink, et al. (1998). "TNF, IL-1 and IL-6 in circulating blood after total-body and localized irradiation in rats." Oncology Reports **5**(3): 679-683.

Heikema, A. P., M. P. Bergman, et al. (2010). "Characterization of the Specific Interaction between Sialoadhesin and Sialylated Campylobacter jejuni Lipooligosaccharides." Infection and Immunity **78**(7): 3237-3246.

Henne, W. A., R. Rothenbuhler, et al. (2012). "Imaging Sites of Infection Using a Tc-99m-Labeled Folate Conjugate Targeted to Folate Receptor Positive Macrophages." Molecular Pharmaceutics **9**(5): 1435-1440.

Heuff, G., M. B. Vanderende, et al. (1993). "Macrophage populations in different stages of induced hepatic metastases in rats - an immunohistochemical analysis." Scandinavian Journal of Immunology **38**(1): 10-16.

Higashi, T., S. J. Fisher, et al. (2000). "Evaluation of the early effect of local irradiation on normal rodent bone marrow metabolism using FDG: Preclinical PET studies." Journal of Nuclear Medicine **41**(12): 2026-2035.

Histed, S. N., M. L. Lindenberg, et al. (2012). "Review of functional/anatomical imaging in oncology." Nuclear medicine communications **33**(4): 349-361.

Hitchens, T. K., Q. Ye, et al. (2011). "F-19 MRI Detection of Acute Allograft Rejection with In Vivo Perfluorocarbon Labeling of Immune Cells." Magnetic Resonance in Medicine **65**(4): 1145-1154.

Hnatowich, D. J., G. Mardirossian, et al. (1993). "Directly and indirectly technetium-99m-labeled antibodies- A comparison of in vitro and animal in vivo properties." Journal of Nuclear Medicine **34**(1): 109-119.

Holt, P. G., D. H. Strickland, et al. (2008). "Regulation of immunological homeostasis in the respiratory tract." Nature Reviews Immunology **8**(2): 142-152.

Honke, N., N. Shaabani, et al. (2012). "Enforced viral replication activates adaptive immunity and is essential for the control of a cytopathic virus." Nature Immunology **13**(1): 51-U131.

Hume, D. A. and K. P. A. MacDonald (2012). "Therapeutic applications of macrophage colony-stimulating factor-1 (CSF-1) and antagonists of CSF-1 receptor (CSF-1R) signaling." Blood **119**(8): 1810-1820.

Iannacone, M., E. A. Moseman, et al. (2010). "Subcapsular sinus macrophages prevent CNS invasion on peripheral infection with a neurotropic virus." Nature **465**(7301): 1079-U1143.

Ikezumi, Y., T. Suzuki, et al. (2005). "The sialoadhesin (CD169) expressing a macrophage subset in human proliferative glomerulonephritis." Nephrology Dialysis Transplantation **20**(12): 2704-2713.

Ip, C. W., A. Kroner, et al. (2007). "Sialoadhesin deficiency ameliorates myelin degeneration and axonopathic changes in the CNS of PLP overexpressing mice." Neurobiology of Disease **25**(1): 105-111.

Jain, M., G. Venkatraman, et al. (2007). "Optimization of Radioimmunotherapy of solid tumors: Biological impediments and their modulation." Clinical Cancer Research **13**(5): 1374-1382.

James, M. L. and S. S. Gambhir (2012). "A molecular imaging primer: modalities, imaging agents, and applications." Physiological reviews **92**(2): 897-965.

Jiang, H. R., L. Hwenda, et al. (2006). "Sialoadhesin promotes the inflammatory response in experimental autoimmune uveoretinitis." Journal of Immunology **177**(4): 2258-2264.

Johnson, J. L. and A. C. Newby (2009). "Macrophage heterogeneity in atherosclerotic plaques." Current Opinion in Lipidology **20**(5): 370-378.

Jones, C., M. Virji, et al. (2003). "Recognition of sialylated meningococcal lipopolysaccharide by siglecs expressed on myeloid cells leads to enhanced bacterial uptake." Molecular Microbiology **49**(5): 1213-1225.

Junt, T., E. A. Moseman, et al. (2007). "Subcapsular sinus macrophages in lymph nodes clear lymph-borne viruses and present them to antiviral B cells." Nature **450**(7166): 110-+.

Karacay, H., G. L. Ong, et al. (1998). "Intracellular processing of Tc-99(m)-antibody conjugates." Nuclear medicine communications **19**(10): 971-979.

Karkar, A. M., J. Smith, et al. (1997). "Abrogation of glomerular injury in nephrotoxic nephritis by continuous infusion of interleukin-6." Kidney International **52**(5): 1313-1320.

Kaur, S., G. Venktaraman, et al. (2012). "Recent trends in antibody-based oncologic imaging." Cancer Letters **315**(2): 97-111.

Kelm, S., A. Pelz, et al. (1994). "Sialoadhesin, myelin-associated glycoprotein and CD22 define a new family of sialic acid-dependent adhesion molecules of the immunoglobulin superfamily." Current Biology **4**(11): 965-972.

Kelm, S., R. Schauer, et al. (1994). "Modifications of cell-surface sialic acids modulate cell-adhesion mediated by sialoadhesin and CD22." Glycoconjugate Journal **11**(6): 576-585.

Kinne, R. W., B. Stuhlmueller, et al. (2007). "Cells of the synovium in rheumatoid arthritis - Macrophages." Arthritis Research & Therapy **9**(6).

Kirchberger, S., O. Majdic, et al. (2005). "Human rhinoviruses inhibit the accessory function of dendritic cells by inducing sialoadhesin and B7-H1 expression." Journal of Immunology **175**(2): 1145-1152.

Kitchens, W. H., C. M. Chase, et al. (2007). "Macrophage depletion suppresses cardiac allograft vasculopathy in mice." American Journal of Transplantation **7**(12): 2675-2682.

Klaas, M. and P. R. Crocker (2012). "Sialoadhesin in recognition of self and non-self." (1863-2300 (Electronic)).

Kluth, D. C., L. P. Erwig, et al. (2004). "Multiple facets of macrophages in renal injury." Kidney International **66**(2): 542-557.

Knospe, W. H., J. Blom, et al. (1966). "Regeneration of locally irradiated bone marrow. 1. Dose dependent long-term changes in rat with particular emphasis upon vascular and stromal reaction." Blood-the Journal of Hematology **28**(3): 398-&.

Kobsar, I., C. Oetke, et al. (2006). "Attenuated demyelination in the absence of the macrophage-restricted adhesion molecule sialoadhesin (Siglec-1) in mice heterozygously deficient in P0." Molecular and Cellular Neuroscience **31**(4): 685-691.

Kohler, G. and C. Milstein (1975). "CONTINUOUS CULTURES OF FUSED CELLS SECRETING ANTIBODY OF PREDEFINED SPECIFICITY." Nature **256**(5517): 495-497.

Kool, J., M. Y. Gerritsboeye, et al. (1992). "Immunohistology of joint inflammation induced in rats by cell-wall fragments of eubacterium-aerofaciens." Scandinavian Journal of Immunology **36**(3): 497-506.

Kozin, S., W. S. Kamoun, et al. (2010). "Recruitment of myeloid but not endothelial precursor cells facilitates tumor regrowth after local irradiation." (1538-7445 (Electronic)).

Kraal, G. and R. Mebius (2006). "Now insights into the cell biology of the marginal zone of the spleen." International Review of Cytology - a Survey of Cell Biology, Vol 250 **250**: 175-+.

Kristiansen, M., J. H. Graversen, et al. (2001). "Identification of the haemoglobin scavenger receptor." Nature **409**(6817): 198-201.

Kumamoto, Y., N. Higashi, et al. (2004). "Identification of sialoadhesin as a dominant lymph node counter-receptor for mouse macrophage galactose-type C-type lectin 1." Journal of Biological Chemistry **279**(47): 49274-49280.

Labarrere, C. A. and B. R. Jaeger (2012). "Biomarkers of heart transplant rejection: the good, the bad, and the ugly!" Translational Research **159**(4): 238-251.

Lai, P. C., H. T. Cook, et al. (2001). "Interleukin-11 attenuates nephrotoxic nephritis in Wistar Kyoto rats." Journal of the American Society of Nephrology **12**(11): 2310-2320.

Lan, H. Y., D. J. Nikolicpaterson, et al. (1993). "Trafficking of inflammatory macrophages from the kidney to draining lymph-nodes during experimental glomerulonephritis." Clinical and Experimental Immunology **92**(2): 336-341.

Lan, H. Y., D. J. Nikolicpaterson, et al. (1995). "Local macrophage proliferation in the progression of glomerular and tubulointerstitial injury in rat anti-GBM glomerulonephritis." Kidney International **48**(3): 753-760.

Landstrom, M. and K. Funa (1997). "Apoptosis in rat prostatic adenocarcinoma is associated with rapid infiltration of cytotoxic T-cells and activated macrophages." International Journal of Cancer **71**(3): 451-455.

Laoui, D., E. Van Overmeire, et al. (2011). "Mononuclear phagocyte heterogeneity in cancer: Different subsets and activation states reaching out at the tumor site." Immunobiology **216**(11): 1192-1202.

Laskin, D. L., V. R. Sunil, et al. (2011). Macrophages and Tissue Injury: Agents of Defense or Destruction? Annual Review of Pharmacology and Toxicology, Vol 51, 2011. A. K. Cho. **51:** 267-288.

Lenzo, J. C., A. L. Turner, et al. (2012). "Control of macrophage lineage populations by CSF-1 receptor and GM-CSF in homeostasis and inflammation." Immunology and Cell Biology **90**(4): 429-440.

Lerouxel, E., A. Moreau, et al. (2009). "Effects of high doses of ionising radiation on bone in rats: A new model for evaluation of bone engineering." British Journal of Oral & Maxillofacial Surgery **47**(8): 602-607.

Li, X. C. (2010). "The Significance of Non-T-Cell Pathways in Graft Rejection: Implications for Transplant Tolerance." Transplantation **90**(10): 1043-1047.

Liu, S. (2008). "Bifunctional coupling agents for radiolabeling of biornolecules and target-specific delivery of metallic radionuclides." Advanced Drug Delivery Reviews **60**(12): 1347-1370.

Loening, A. M. and S. S. Gambhir (2003). "AMIDE: a free software tool for multimodality medical image analysis." Molecular imaging **2**(3): 131-137.

Low, P. S., W. A. Henne, et al. (2008). "Discovery and development of folic-acid-based receptor targeting for Imaging and therapy of cancer and inflammatory diseases." Accounts of Chemical Research **41**(1): 120-129.

Lunov, O., V. Zablotskii, et al. (2011). "Modeling receptor-mediated endocytosis of polymer-functionalized iron oxide nanoparticles by human macrophages." Biomaterials **32**(2): 547-555.

MacDonald, K. P. A., J. S. Palmer, et al. (2010). "An antibody against the colony-stimulating factor 1 receptor depletes the resident subset of monocytes and tissue- and tumor-associated macrophages but does not inhibit inflammation." Blood **116**(19): 3955-3963.

Mach, J. P., S. Carrel, et al. (1974). "In vivo localisation of radiolabelled antibodies to carcinoembryonic antigen in human colon carcinoma grafted into nude mice." Nature **248**(5450): 704-706.

Malviya, G., E. F. J. de Vries, et al. (2011). "Synthesis and Evaluation of Tc-99m-Labelled Monoclonal Antibody 1D09C3 for Molecular Imaging of Major Histocompatibility Complex Class II Protein Expression." Molecular Imaging and Biology **13**(5): 930-939.

Malviya, G., F. Galli, et al. (2010). "Targeting T and B lymphocytes with radiolabelled antibodies for diagnostic and therapeutic applications." Quarterly Journal of Nuclear Medicine and Molecular Imaging **54**(6): 654-676.

Mannon, R. B. (2012). "Macrophages: contributors to allograft dysfunction, repair, or innocent bystanders?" Current Opinion in Organ Transplantation **17**(1): 20-25.

Mantovani, A., P. Allavena, et al. (2008). "Cancer-related inflammation." Nature **454**(7203): 436-444.

Mantovani, A. and A. Sica (2010). "Macrophages, innate immunity and cancer: balance, tolerance, and diversity." Current Opinion in Immunology **22**(2): 231-237.

Marmey, M., C. Boix, et al. (2006). "CD14 and CD169 expression in human lymph nodes and spleen: specific expansion of CD14(+)CD169(-) monocyte-derived cells in diffuse large B-cell lymphomas." Human Pathology **37**(1): 68-77.

Martinez-Pomares, L., P. R. Crocker, et al. (1999). "Cell-specific glycoforms of sialoadhesin and CD45 are counter-receptors for the cysteine-rich domain of the mannose receptor." Journal of Biological Chemistry **274**(49): 35211-35218.

Massoud, T. F. and S. S. Gambhir (2003). "Molecular imaging in living subjects: seeing fundamental biological processes in a new light." Genes & Development **17**(5): 545-580.

Mather, S. J. and D. Ellison (1990). "Reduction-mediated Tc-99m labeling of monoclonal antibodies." Journal of Nuclear Medicine **31**(5): 692-697.

May, A. P., R. C. Robinson, et al. (1998). "Crystal structure of the N-terminal domain of sialoadhesin in complex with 3 ' sialyllactose at 1.85 angstrom resolution." Molecular Cell **1**(5): 719-728.

McGaha, T. L., Y. Chen, et al. (2011). "Marginal zone macrophages suppress innate and adaptive immunity to apoptotic cells in the spleen." Blood **117**(20): 5403-5412.

McWilliam, A. S., P. Tree, et al. (1992). "Interleukin-4 regulates induction of sialoadhesin, the macrophage sialic acid-specific receptor." Proceedings of the National Academy of Sciences of the United States of America **89**(21): 10522-10526.

Mebius, R. E., H. R. Hendriks, et al. (1990). "Macrophages and the activity of high endothelial venules - the effect of interferon-gamma." European Journal of Immunology **20**(7): 1615-1618.

Mebius, R. E. and G. Kraal (2005). "Structure and function of the spleen." Nature Reviews Immunology **5**(8): 606-616.

Miyake, Y., K. Asano, et al. (2007). "Critical role of macrophages in the marginal zone in the suppression of immune responses to apoptotic cell-associated antigens." Journal of Clinical Investigation **117**(8): 2268-2278.

Moller, H. J., N. A. Peterslund, et al. (2002). "Identification of the hemoglobin scavenger receptor/CD 163 as a natural soluble protein in plasma." Blood **99**(1): 378-380.

Monteiro, V. G., C. S. S. Lobato, et al. (2005). "Increased association of Trypanosoma cruzi with sialoadhesin positive mice macrophages." Parasitology Research **97**(5): 380-385.

Moore, A., R. Weissleder, et al. (1997). "Uptake of dextran-coated monocrystalline iron oxides in tumor cells and macrophages." Jmri-Journal of Magnetic Resonance Imaging **7**(6): 1140-1145.

Morris, M. J., C. R. Divgi, et al. (2005). "Pilot trial of unlabeled and indium-111-labeled anti-prostate-specific membrane antigen antibody J591 for castrate metastatic prostate cancer." Clinical Cancer Research **11**(20): 7454-7461.

Mosser, D. M. and J. P. Edwards (2008). "Exploring the full spectrum of macrophage activation." Nature Reviews Immunology **8**(12): 958-969.

Mouthon, M., M. Vandamme, et al. (2001). "Inflammatory response to abdominal irradiation stimulates hemopoiesis." (0955-3002 (Print)).

Mueller, C. and R. Schibli (2011). "Folic Acid Conjugates for Nuclear Imaging of Folate Receptor-Positive Cancer." Journal of Nuclear Medicine **52**(1): 1-4.

Muerkoster, S., J. D. Laman, et al. (2000). "Functional and in situ evidence for nitric oxide production driven by CD40-CD40L interactions in graft-versus-leukemia reactivity." Clin Cancer Res **6**(5): 1988-1996.

Muerkoster, S., M. Rocha, et al. (1999). "Sialoadhesin-positive host macrophages play an essential role in graft-versus-leukemia reactivity in mice." Blood **93**(12): 4375-4386.

Muerkoster, S., O. Wachowski, et al. (1998). "Graft-versus-leukemia reactivity involves cluster formation between superantigen-reactive donor T lymphocytes and host macrophages." Clin Cancer Res **4**(12): 3095-3106.

Murray, P. J. and T. A. Wynn (2011). "Protective and pathogenic functions of macrophage subsets." Nature Reviews Immunology **11**(11): 723-737.

Nakamura, K., T. Yamaji, et al. (2002). "Lymph node macrophages, but not spleen macrophages, express high levels of unmasked sialoadhesin: implication for the adhesive properties of macrophages in vivo." Glycobiology **12**(3): 209-216.

Narula, J., E. R. Acio, et al. (2001). "Annexin-V imaging for noninvasive detection of cardiac allograft rejection." Nature Medicine **7**(12): 1347-1352.

Nath, D., A. Hartnell, et al. (1999). "Macrophage-tumour cell interactions: identification of MUC1 on breast cancer cells as a potential counter-receptor for the macrophage-restricted receptor, sialoadhesin." Immunology **98**(2): 213-219.

Nath, D., P. A. Vandermerwe, et al. (1995). "The amino-terminal immunoglobulin-like domain of sialoadhesin contains the sialic acid-binding site - comparison with CD22." Journal of Biological Chemistry **270**(44): 26184-26191.

Nemeth, E., A. W. Baird, et al. (2009). "Microanatomy of the liver immune system." Seminars in Immunopathology **31**(3): 333-343.

Nielsen, U. B. and J. D. Marks (2000). "Internalizing antibodies and targeted cancer therapy: direct selection from phage display libraries." (1461-5347 (Electronic)).

Nikolic-Paterson, D. J. and R. C. Atkins (2001). "The role of macrophages in glomerulonephritis." Nephrology Dialysis Transplantation **16**: 3-7.

Ochando, J. C. and S. H. Chen (2012). "Myeloid-derived suppressor cells in transplantation and cancer." (1559-0755 (Electronic)).

Oetke, C., M. C. Vinson, et al. (2006). "Sialoadhesin-deficient mice exhibit subtle changes in B- and T-Cell populations and reduced immunoglobulin M levels." Molecular and Cellular Biology **26**(4): 1549-1557.

Olafsen, T. and A. M. Wu (2010). "Antibody Vectors for Imaging." Seminars in Nuclear Medicine **40**(3): 167-181.

Pastula, A. and J. Marcinkiewicz (2011). "Myeloid-derived suppressor cells: a double-edged sword?" International Journal of Experimental Pathology **92**(2): 73-78.

Pello, O. M., C. Silvestre, et al. (2011). "A glimpse on the phenomenon of macrophage polarization during atherosclerosis." Immunobiology **216**(11): 1172-1176.

Perry, V. H., P. R. Crocker, et al. (1992). "The blood-brain-barrier regulates the expression of a macrophage sialic acid-binding receptor on microglia." Journal of Cell Science **101**: 201-207.

Pettersen, J. S., J. Fuentes-Duculan, et al. (2011). "Tumor-Associated Macrophages in the Cutaneous SCC Microenvironment Are Heterogeneously Activated." Journal of Investigative Dermatology **131**(6): 1322-1330.

Phan, T. G., J. A. Green, et al. (2009). "Immune complex relay by subcapsular sinus macrophages and noncognate B cells drives antibody affinity maturation." Nature Immunology **10**(7): 786-U153.

Philippidis, P., J. C. Mason, et al. (2004). "Hemoglobin scavenger receptor CD163 mediates interleukin-10 release and heme oxygenase-1 synthesis - Antiinflammatory monocyte-macrophage responses in vitro, in resolving skin blisters in vivo, and after cardiopulmonary bypass surgery." Circulation Research **94**(1): 119-126.

Poderoso, T., P. Martinez, et al. (2011). "Delivery of antigen to sialoadhesin or CD163 improves the specific immune response in pigs." Vaccine **29**(29-30): 4813-4820.

Polfliet, M. M. J., B. O. Fabriek, et al. (2006). "The rat macrophage scavenger receptor CD163: Expression, regulation and role in inflammatory mediator production." Immunobiology **211**(6-8): 419-425.

Pollard, J. W. (2009). "Trophic macrophages in development and disease." Nature Reviews Immunology **9**(4): 259-270.

Polman, C. H., C. D. Dijkstra, et al. (1986). "Immunohistological analysis of macrophages in the central-nervous-system of Lewis rats with acute experimental allergic encephalomyelitis." Journal of Neuroimmunology **11**(3): 215-222.

Pressman, D. and G. Keighley (1948). "The zone of activity of antibodies as determined by the use of radioactive tracers: the zone of activity of nephritoxic antikidney serum." Journal of Immunology **59**(2): 141-146.

Pulliam, L., B. Sun, et al. (2004). "Invasive chronic inflammatory monocyte phenotype in subjects with high HIV-1 viral load." Journal of Neuroimmunology **157**(1-2): 93-98.

Qualls, J. E. and P. J. Murray (2010). "A double agent in cancer: Stopping macrophages wounds tumors." Nature Medicine **16**(8): 863-864.

Quillard, T., K. Croce, et al. (2011). "Molecular imaging of macrophage protease activity in cardiovascular inflammation in vivo." Thrombosis and Haemostasis **105**(5): 828-836.

Rempel, H., C. Calosing, et al. (2008). "Sialoadhesin Expressed on IFN-Induced Monocytes Binds HIV-1 and Enhances Infectivity." Plos One **3**(4).

Revilla, C., T. Poderoso, et al. (2009). "Targeting to porcine sialoadhesin receptor improves antigen presentation to T cells." Veterinary Research **40**(3).

Ribechini, E., V. Greifenberg, et al. (2010). "Subsets, expansion and activation of myeloid-derived suppressor cells." Medical Microbiology and Immunology **199**(3): 273-281.

Ricardo, S. D., H. van Goor, et al. (2008). "Macrophage diversity in renal injury and repair." Journal of Clinical Investigation **118**(11): 3522-3530.

Richards, P. J., A. S. Williams, et al. (1999). "Liposomal clodronate eliminates synovial macrophages, reduces inflammation and ameliorates joint destruction in antigen-induced arthritis." Rheumatology **38**(9): 818-825.

Rocha, M., V. Umansky, et al. (1997). "Differences between graft-versus-leukemia and graft-versus-host reactivity .1. Interaction of donor immune T cells with tumor and/or host cells." Blood **89**(6): 2189-2202.

Roopenian, D. C. and S. Akilesh (2007). "FcRn: the neonatal Fc receptor comes of age." Nature Reviews Immunology **7**(9): 715-725.

Sawitzki, B., S. Schlickeiser, et al. (2011). "Monitoring tolerance and rejection in organ transplant recipients." Biomarkers **16**: S42-S50.

Segers, F. M. E., H. Yu, et al. (2012). "Design and Validation of a Specific Scavenger Receptor Class AI Binding Peptide for Targeting the Inflammatory Atherosclerotic Plaque." Arteriosclerosis Thrombosis and Vascular Biology **32**(4): 971-U285.

Seyer, M., S. Kirchberger, et al. (2010). "Human rhinoviruses induce IL-35-producing Treg via induction of B7-H1 (CD274) and sialoadhesin (CD169) on DC." European Journal of Immunology **40**(2): 321-329.

Sharkey, R., H. Karacay, et al. (2009). "Improving the treatment of non-Hodgkin lymphoma with antibody-targeted radionuclides." (0008-543X (Print)).

Shih, Y.-Y. I., Y.-H. Hsu, et al. (2011). "Longitudinal study of tumor-associated macrophages during tumor expansion using MRI." Nmr in Biomedicine **24**(10): 1353-1360.

Sica, A. and A. Mantovani (2012). "Macrophage plasticity and polarization: in vivo veritas." Journal of Clinical Investigation **122**(3): 787-795.

Smith, S. V. (2004). "Molecular imaging with copper-64." Journal of Inorganic Biochemistry **98**(11): 1874-1901.

Srour, E. F., A. Jetmore, et al. (2001). "Homing, cell cycle kinetics and fate of transplanted hematopoietic stem cells." Leukemia **15**(11): 1681-1684.

Stefater, J. A., III, S. Ren, et al. (2011). "Metchnikoff's policemen: macrophages in development, homeostasis and regeneration." Trends in Molecular Medicine **17**(12): 743-752.

Stehlik, J., L. B. Edwards, et al. (2010). "The Registry of the International Society for Heart and Lung Transplantation: Twenty-seventh official adult heart transplant report-2010." Journal of Heart and Lung Transplantation **29**(10): 1089-1103.

Steiniger, B., P. Barth, et al. (1997). "The species-specific structure of microanatomical compartments in the human spleen: strongly sialoadhesin-positive macrophages occur in the perifollicular zone, but not in the marginal zone." Immunology **92**(2): 307-316.

Stout, R. D., C. C. Jiang, et al. (2005). "Macrophages sequentially change their functional phenotype in response to changes in microenvironmental influences." Journal of Immunology **175**(1): 342-349.

Tang, T. Y., K. H. Muller, et al. (2009). "Iron Oxide Particles for Atheroma Imaging." Arteriosclerosis Thrombosis and Vascular Biology **29**(7): 1001-1008.

Taylor, P. R., L. Martinez-Pomares, et al. (2005). Macrophage receptors and immune recognition. Annual Review of Immunology. **23:** 901-944.

Temme, S., F. Boenner, et al. (2012). "19F magnetic resonance imaging of endogenous macrophages in inflammation." Wiley Interdisciplinary Reviews-Nanomedicine and Nanobiotechnology **4**(3): 329-343.

Umansky, V., P. Beckhove, et al. (1996). "A role for sialoadhesin-positive tissue macrophages in host resistance to lymphoma metastasis in vivo." Immunology **87**(2): 303-309.

Vallabhajosula, S., I. Kuji, et al. (2005). "Pharmacokinetics and biodistribution of In-111-Lu-177-labeled J591 antibody specific for prostate-specific membrane antigen: Prediction of Y-90-J591 radiation dosimetry based on In-111 or Lu-177?" Journal of Nuclear Medicine **46**(4): 634-641.

van den Berg, T. K., D. Nath, et al. (2001). "Cutting edge: CD43 functions as a T cell counterreceptor for the macrophage adhesion receptor sialoadhesin (Siglec-1)." Journal of Immunology **166**(6): 3637-3640.

Van der Meeren, A., P. Monti, et al. (2001). "Characterization of the acute inflammatory response after irradiation in mice and its regulation by interleukin 4 (114)." Radiation Research **155**(6): 858-865.

Van Gorp, H., P. L. Delputte, et al. (2010). "Scavenger receptor CD163, a Jack-of-all-trades and potential target for cell-directed therapy." Molecular Immunology **47**(7-8): 1650-1660.

vandenBerg, T., I. vanDie, et al. (1996). "Regulation of sialoadhesin expression on rat macrophages - Induction by glucocorticoids and enhancement by IFN-beta, IFN-gamma, IL-4, and lipopolysaccharide." Journal of Immunology **157**(7): 3130-3138.

Vandenberg, T. K., J. J. P. Breve, et al. (1992). "Sialoadhesin on macrophages - its identification as a lymphocyte adhesion molecule." Journal of Experimental Medicine **176**(3): 647-655.

Vanderheijden, N., P. L. Delputte, et al. (2003). "Involvement of sialoadhesin in entry of porcine reproductive and respiratory syndrome virus into porcine alveolar macrophages." Journal of Virology **77**(15): 8207-8215.

Verschure, P. J., C. J. F. Vannoorden, et al. (1989). "Macrophages and dendritic cells during the early stages of antigen-induced arthritis in rats - immunohistochemical analysis of cryostat sections of the whole knee-joint." Scandinavian Journal of Immunology **29**(3): 371-381.

von Gunten, S. and B. S. Bochner (2008). "Basic and Clinical Immunology of Siglecs." Year in Immunology 2008 **1143**: 61-82.

Werts, E. D., D. P. Gibson, et al. (1980). "Stromal cell-migration precedes hematopoietic repopulation of the bone marrow after irradiation." Radiation Research **81**(1): 20-30.

Winkler, I. G., N. A. Sims, et al. (2010). "Bone marrow macrophages maintain hematopoietic stem cell (HSC) niches and their depletion mobilizes HSCs." Blood **116**(23): 4815-4828.

Wu, C., U. Rauch, et al. (2009). "Sialoadhesin-Positive Macrophages Bind Regulatory T Cells, Negatively Controlling Their Expansion and Autoimmune Disease Progression." Journal of Immunology **182**(10): 6508-6516.

Wu, Y. L., Q. Ye, et al. (2011). "Cellular and Functional Imaging of Cardiac Transplant Rejection." (1941-9074 (Electronic)).

Xia, W., A. R. Hilgenbrink, et al. (2009). "A functional folate receptor is induced during macrophage activation and can be used to target drugs to activated macrophages." Blood **113**(2): 438-446.

Xiong, Y. S., Y. H. Zhou, et al. (2009). "Siglec-1 on monocytes is a potential risk marker for monitoring disease severity in coronary artery disease." Clinical Biochemistry **42**(10-11): 1057-1063.

Yamashiro, S., M. Takeya, et al. (1998). "Intradermal injection of monocyte chemoattractant protein-1 induces emigration and differentiation of blood monocytes in rat skin." International Archives of Allergy and Immunology **115**(1): 15-23.

Yamashiro, S., M. Takeya, et al. (1994). "Tumor-derived monocyte chemoattractant protein-1 induces intratumoral infiltration of monocyte-derived macrophage subpopulation in transplanted rat-tumors." American Journal of Pathology **145**(4): 856-867.

Yamate, J., Y. Machida, et al. (2004). "Effects of lipopolysaccharide on the appearance of macrophage populations and fibrogenesis in cisplatin-induced rat renal injury." Experimental and Toxicologic Pathology **56**(1-2): 13-24.

York, M. R., T. Nagai, et al. (2007). "A macrophage marker, Siglec-1, is increased on circulating monocytes in patients with systemic sclerosis and induced by type I Interferons and Toll-like receptor agonists." Arthritis and Rheumatism **56**(3): 1010-1020.

Zhang, Z., Z.-Y. Zhang, et al. (2011). "Parenchymal accumulation of CD163(+) macrophages/microglia in multiple sclerosis brains." Journal of Neuroimmunology **237**(1-2): 73-79.

Zola, H., B. Swart, et al. (2007). Leukocyte and stromal cell molecules: the CD markers. Hoboken, N.J., Wiley-Liss.